

FIBEC File Copy

AFFDL-TR-79-3148

ADA 083978

F-4 SERVICE LIFE TRACKING PROGRAM (CRACK GROWTH GAGES)

C.R. Saff

McDonnell Douglas Corporation
McDonnell Aircraft Company
P.O. Box 516
St. Louis, Missouri 63166

December 1979

Technical Report AFFDL-TR-79-3148
Final Report
February 1978 - September 1979

20081006 199

Approved for public release; distribution unlimited.


Air Force Flight Dynamics Laboratory
Air Force Wright Aeronautical Laboratories
Air Force Systems Command
Wright-Patterson Air Force Base, Ohio 45433

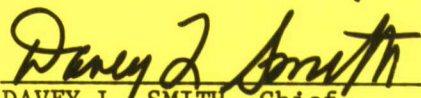
NOTICE

When Government drawings, specifications, or other data are used for any purpose other than in connection with a definitely related Government procurement operation, the United States Government thereby incurs no responsibility nor any obligation whatsoever; and the fact that the government may have formulated, furnished, or in any way supplied the said drawings, specifications, or other data, is not to be regarded by implication or otherwise as in any manner licensing the holder or any other person or corporation, or conveying any rights or permission to manufacture, use, or sell any patented invention that may in any way be related thereto.

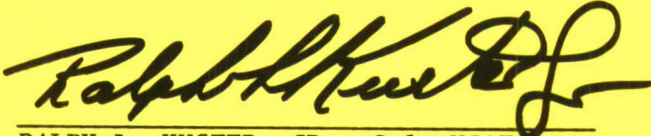
This report has been reviewed by the Information Office (OI) and is releasable to the National Technical Information Service (NTIS). At NTIS, it will be available to the general public, including foreign nations.

This technical report has been reviewed and is approved for publication.


DONALD R. HOLLOWAY, Capt. USAF
Project Engineer


DAVEY L. SMITH, Chief
Structural Integrity Br
Structures and Dynamics Division

FOR THE COMMANDER


RALPH L. KUSTER, JR., Col. USAF
Chief, Structures and Dynamics Division

If your address has changed, if you wish to be removed from our mailing list, or if the addressee is no longer employed by your organization please notify, AFFDL/FBE, W-PAFB, OH 45433 to help us maintain a current mailing list.

Copies of this report should not be returned unless return is required by security considerations, contractual obligations, or notice on a specific document.

REPORT DOCUMENTATION PAGE		READ INSTRUCTIONS BEFORE COMPLETING FORM
1. REPORT NUMBER AFFDL-TR-79-3148	2. GOVT ACCESSION NO.	3. RECIPIENT'S CATALOG NUMBER
4. TITLE (and Subtitle) F-4 SERVICE LIFE TRACKING PROGRAM (CRACK GROWTH GAGES)		5. TYPE OF REPORT & PERIOD COVERED Final Report February 1978-September 1979
		6. PERFORMING ORG. REPORT NUMBER
7. AUTHOR(s) C. R. Saff		8. CONTRACT OR GRANT NUMBER(s) F42600-78-D-0014
9. PERFORMING ORGANIZATION NAME AND ADDRESS McDonnell Aircraft Company P. O. Box 516 St. Louis, Missouri 63166		10. PROGRAM ELEMENT, PROJECT, TASK AREA & WORK UNIT NUMBERS Project 2401 Task 240101 Work Unit 24010109
11. CONTROLLING OFFICE NAME AND ADDRESS Air Force Air Logistics Center Hill Air Force Base Utah 84406		12. REPORT DATE December 1979
		13. NUMBER OF PAGES 123
14. MONITORING AGENCY NAME & ADDRESS (if different from Controlling Office) Air Force Flight Dynamics Laboratory (FBE) Wright-Patterson Air Force Base Ohio 45433		15. SECURITY CLASS. (of this report) Unclassified
		15a. DECLASSIFICATION/DOWNGRADING SCHEDULE
16. DISTRIBUTION STATEMENT (of this Report) Approved for public release: distribution unlimited.		
17. DISTRIBUTION STATEMENT (of this abstract entered in Block 20, if different from Report)		
18. SUPPLEMENTARY NOTES		
19. KEY WORDS (Continue on reverse side if necessary and identify by block number) Crack growth Spectrum loads Crack growth gages Life management Crack growth prediction Service life tracking		
20. ABSTRACT (Continue on reverse side if necessary and identify by block number) The objective of this program was to evaluate the ability of a crack growth gage to monitor potential crack growth damage in fatigue critical locations of F-4C/D aircraft structure. Crack growth gages were designed for use on the lower wing skin of F-4 aircraft. An element test program was performed to verify gage design and provide data for predicting gage behavior when attached to the fatigue test article. Results of those tests prompted performance of a supplemental test program to investigate effects of sheet		

BLOCK #20 (ABSTRACT) continued:

thickness on crack growth retardation. Results from both of these test programs were used to develop procedures to predict crack growth in gages attached to the fatigue test article. Eight gages were bonded to the test article using room temperature cure adhesive after an elevated cure temperature adhesive failed. Results show gage crack growth is predictable. Analysis results demonstrate the monitoring potential of the gage.

FOREWORD

This report was prepared by McDonnell Aircraft Company (MCAIR), St. Louis, Missouri, for both the Ogden Air Logistics Center, Hill Air Force Base, Utah, and the Air Force Flight Dynamics Laboratory, Wright-Patterson Air Force Base, Ohio, under Contract F42600-78-D-0014, Item 0002. The contract was sponsored by the Ogden Air Logistics Center, with technical monitoring provided by the Air Force Flight Dynamics Laboratory. Mr. Ralph Elwell, ALC/MMSRW, was the Air Force Program Manager and Capt. Don Holloway, AFFDL/FBE, was the Air Force Technical Monitor.

The Structural Research Department of McDonnell Aircraft Company was responsible for performance of this program. Principal author of this report is C. R. Saff. K. C. Garland, MCAIR Metallurgical Laboratories, performed the MCAIR test program, and F. L. Wood, MCAIR Non-metallics Laboratories, performed gage bonding.

This report covers work accomplished during the period February 1978 to September 1979.

This report was released by the author in November 1979 for publication.

TABLE OF CONTENTS

<u>Section</u>		<u>Page</u>
I	INTRODUCTION	1
	1. PROGRAM SUMMARY	1
	2. RESULTS AND CONCLUSIONS	2
II	CRACK GROWTH GAGE DESIGN	4
	1. GAGE SIZE CONSIDERATIONS	4
	2. STRESS INTENSITY FACTOR	4
	3. GAGE OPTIMIZATION	17
	4. LOAD TRANSFER ANALYSIS	17
	5. STRENGTH ANALYSIS	23
	6. GAGE CONFIGURATION	25
	7. EFFECTS OF MANUFACTURING TOLERANCES ON GAGE STRESS	25
III	GAGE ATTACHMENT	34
	1. ADHESIVE SELECTION	34
	2. SURFACE PREPARATION	35
	3. GAGE BONDING	36
IV	GAGE SITE SELECTION	44
	1. CRITERIA	44
	2. PRIMARY GAGE SITES	45
	3. ADDITIONAL GAGE SITES	46
	4. OPTIONAL WING SITES	49
	5. OPTIONAL NON-WING SITES	50
V	COMPARISON OF ELEMENT TEST AND ANALYSIS RESULTS . .	53
	1. MECHANICAL PROPERTY AND BASELINE CRACK GROWTH DATA	53
	2. LOAD TRANSFER TESTS	63
	3. GAGE CALIBRATION (CONSTANT AMPLITUDE TESTS) . .	69
	4. EFFECT OF THICKNESS ON CRACK GROWTH RETARDATION	74
	5. GAGE CALIBRATION (SPECTRUM TESTS)	80
	6. GAGE VALIDATION TESTS	86
VI	PREDICTED RESPONSE OF CRACK GROWTH GAGES ON F-4 FATIGUE TEST ARTICLE	97
	1. RELATIONSHIP OF STRESS IN GAGE TO STRESS IN STRUCTURE	97
	2. RELATIONSHIP OF GAGE STRESS TO STRUCTURAL STRESS USED TO PREDICT CRACK GROWTH	102

TABLE OF CONTENTS (Continued)

<u>Section</u>	<u>Page</u>
3. STRESS INTENSITY FACTORS	102
4. CRACK GROWTH ANALYSES	103
5. RELATIONSHIP OF GAGE CRACK GROWTH TO POTENTIAL CRACK GROWTH IN STRUCTURE	103
VII MONITORING POTENTIAL OF CRACK GROWTH GAGE	108
1. GAGE PERFORMANCE ON TEST ARTICLE	108
2. CRACK GROWTH GAGE AS USAGE MONITOR	113
3. LIMITATIONS OF GAGE DESIGN, ADHESIVE BONDING, AND MANUFACTURING TOLERANCES ON MONITORING POTENTIAL	120
REFERENCES	122

LIST OF ILLUSTRATIONS

<u>Figure No.</u>		<u>Page</u>
1	Use of Crack Growth Gage to Monitor Potential Crack Growth in Structure	2
2	Preliminary Crack Growth Gage Configurations .	5
3	Solid Element Model Used to Determine Crack Displacements	6
4	Typical Results from Finite Element Analysis of Uniform Thickness Plate	8
5	Typical Results from Finite Element Analysis of Stepped Thickness Plate	8
6	Comparison of Stress Intensity Factors Determined from Finite Element Analysis and Isida's Factors	9
7	Comparison of Stress Intensity Factors Determined from Finite Element Analysis and Rice's Factors	9
8	Comparison of Finite Element Analysis and Closed Form Solution for Gage 2	10
9	Generalized Gage Dimensions	10
10	Finite Element Analysis Predicts Considerable Bending for Gage 2.	11
11	For Symmetric Gage, Finite Element Analysis Agrees with Closed Form Solution.	12
12	Comparison of Predicted Crack Growth for Candidate Gages with Desired Behavior.	13
13	Effect of Changing Gage Length and Width on Life.	14
14	Effect of Changing Step Length on Life.	15
15	Effect of Changing Thickness Ratio on Life.	15
16	Three Gage Designs Predicted to Give 12,000 Hr Service Life.	16
17	Crack Growth for Gage A Design is Closest to Linear Growth	16

LIST OF ILLUSTRATIONS (Continued)

<u>Figure No.</u>		<u>Page</u>
18	Finite Element Results Confirm Gage Stress Intensity Factor Computation.	17
19	Gage Stiffness as a Function of Crack Length. .	18
20	Idealization Used for Specimen Compliance Analysis.	19
21	Strain Transfer Idealization of Bonded Gage . .	20
22	Measured and Idealized Shear Stress/Strain Curves.	21
23	Typical Bond Shear Strain Distribution from Strain Transfer Analysis.	22
24	Strain Transmitted to Gage Increases with Gage Crack Length.	22
25	Nominal Relationship of Gage Stress to Stress in Gage Calibration Specimen.	23
26	Impact of Step Length on Joint Strength	24
27	Idealization Used for Buckling Analysis	25
28	Selected Gage Configuration	26
29	Precracking Configuration for Selected Gage . .	26
30	Impact of Free Length and Gage Width Tolerances on Gage Stress.	27
31	Impact of Step Length and Overall Length Tolerances on Gage Stress.	28
32	Impact of Step Thickness and Overall Thickness Tolerances on Gage Stress	29
33	Step Mismatch from Front to Back.	29
34	Impact of Step Mismatch on Gage Stress.	30
35	Impact of Adhesive Properties on Gage Stress to Element Stress Relationship	32
36	Impact of Adhesive Thickness Variations on Gage Stress.	32

LIST OF ILLUSTRATIONS (Continued)

<u>Figure No.</u>		<u>Page</u>
37	Effect of Gage Misalignment with Principal Strain Direction in Structure	33
38	Major Adhesive Systems Give Same Elastic Joint Strengths	35
39	Crack Growth Gage - Thermocouple Locations for Bonding Tests	37
40	Gage Bonding Technique.	38
41	Thermocouple Locations for Third Bonding Test .	41
42	Maximum Temperatures Recorded During Third Bonding Test.	42
43	Fracture Critical Areas of Lower Wing Skin Identified in F-4 ASIP Program.	45
44	Primary Gage Sites.	46
45	Relationship of Primary Gage Sites to Stress Contours on Lower Wing Skin	47
46	Lower Wing Skin Stress Spectra.	47
47	Relationship of Gage Sites to Load Pad Locations on Lower Wing Skin.	48
48	Gage Sites and Thermocouple Locations	48
49	Location of Primary and Additional Gage Sites Relative to Stress Contours on Lower Wing Skin.	49
50	Optional Gage Site Areas Have Limit Stress Levels from 24 to 30 KSI.	50
51	Fatigue Critical Fuselage Areas Identified in F-4 ASIP Program.	51
52	Optional Fuselage Gage Sites Selected from Fracture Critical Areas	52
53	Flat Tensile Specimen	55
54	Round Tensile Specimen.	55
55	Center Crack Panel Specimen	56

LIST OF ILLUSTRATIONS (Continued)

<u>Figure No.</u>		<u>Page</u>
56	Crack Growth Gage Calibration Specimen.	57
57	F-4 BL.44.5 Lower Wing Skin Element Fatigue Specimen.	58
58	Crack Growth Rate for 7075-T6 Crack Growth Gage Sheet R = 0.02	61
59	Crack Growth Rate for 7075-T6 Crack Growth Gage Sheet R = 0.05	62
60	Crack Growth Rate for 7075-T651 F-4 Wing Skin Plate R = 0.02	64
61	Crack Growth Rate for 7075-T651 F-4 Wing Skin Plate R = 0.5	65
62	Load Transfer Test Instrumentation.	66
63	Comparison of Measured and Predicted Strains in Crack Growth Gages.	68
64	Comparison of Measured and Predicted Average Gage Stress	69
65	Predicted and Measured Crack Growth Rates for Gage Calibration Specimen - Test 1.	70
66	Predicted and Measured Crack Growth Rates for Gage Calibration Specimen - Test 2.	71
67	Predicted and Measured Crack Growth Rates for Constant Amplitude Gage Calibration - Test 1.	71
68	Predicted and Measured Crack Growth for Constant Amplitude Gage Calibration - Test 2.	72
69	Predicted and Measured Crack Growth for Constant Amplitude Gage Calibration - Test 3.	73
70	Predicted and Measured Crack Growth for Constant Amplitude Gage Calibration - Test 4.	73
71	Comparison of Predicted and Measured Crack Growth in Gage Under BL 44.5 Lower Wing Spectrum.	74
72	Comparison of Predicted and Measured Crack Growth in Gage Under BL 100 Lower Wing Spectrum.	75

LIST OF ILLUSTRATIONS (Continued)

<u>Figure No.</u>		<u>Page</u>
73	Relationship of Effective Minimum Stress Level to Applied Stress Levels	75
74	Sheet Thickness Tests - Constant Amplitude and Spectrum Test Results	77
75	Comparison of Finite Element Analysis Results with Predicted Boundary Layer Depth	78
76	Relationship of Effective Minimum Stress Level to Boundary Layer Depth	79
77	Effect of Thickness on Constant Amplitude Crack Growth Lives - Comparison of Analysis and Test Results	79
78	Effect of Thickness on Spectrum Crack Growth Lives - Comparison of Analysis and Test Results	80
79	Comparison of Analysis and Test Results for Gage Calibration Test - BL 44.5 Spectrum - Test 1.	81
80	Comparison on Analysis and Test Results for Gage Calibration Test - BL 44.5 Spectrum - Test 2.	81
81	Comparison on Analysis and Test for Gage Calibration Test - BL 44.5 Spectrum - Test 3.	82
82	Comparison of Analysis and Test Results for Gage Calibration Test - BL 44.5 Spectrum - Test 4.	82
83	Comparison of Analysis and Test Results for Gage Calibration Tests - BL 100 Spectrum - Test 1.	83
84	Comparison of Analysis and Test Results for Gage Calibration Tests - BL 100 Spectrum - Test 2.	83
85	Comparison of Analysis and Test Results for Gage Calibration Test - BL 132.5 Spectrum - Test 1.	84

LIST OF ILLUSTRATIONS (Continued)

<u>Figure No.</u>		<u>Page</u>
86	Comparison of Analysis and Test Results for Gage Calibration Test - BL 132.5 Spectrum - Test 2.	84
87	Comparison of Analysis and Test Results for Gage Calibration Test - BL 132.5 Spectrum - Test 3.	85
88	Comparison of Analysis and Test Results for Gage Calibration Test - BL 132.5 Spectrum - Test 4.	85
89	Comparison of Analysis and Test Results for Gage Calibration Test - BL 132.5 Spectrum - Test 5.	86
90	Stress Intensity Correction Factor Used for Analysis of Corner Flaw at Hole	87
91	Predicted and Measured Flaw Shapes for Gage Validation Specimens.	87
92	Crack Growth from Hole-Gage Validation Test Results - BL 44.5 Spectrum at 30 ksi Limit Stress (Test 1)	88
93	Crack Growth from Hole-Gage Validation Test Results - BL 44.5 Spectrum at 30 ksi Limit Stress (Test 2)	89
94	Crack Growth from Hole-Gage Validation Test Results - BL 100 Spectrum at 33 ksi Limit Stress.	89
95	Crack Growth from Hole-Gage Validation Test Results - BL 132.5 Spectrum at 30 ksi Limit Stress.	90
96	Relationship of Gage Stress to Gross Stress Applied to Gage Validation Specimen	90
97	Stress Intensity Factor Correction for Gage Bonded to Gage Validation Specimen.	91
98	Gage Crack Growth - Gage Validation Test Results - BL 44.5 Spectrum at 30 ksi Limit Stress (Test 1)	92

LIST OF ILLUSTRATIONS (Continued)

<u>Figure No.</u>		<u>Page</u>
99	Gage Crack Growth - Gage Validation Test Results - BL 44.5 Spectrum at 30 ksi Limit Stress (Test 2)	93
100	Gage Crack Growth - Gage Validation Test Results - BL 100 Spectrum at 33 ksi Limit Stress.	93
101	Gage Crack Growth - Gage Validation Test Results - BL 132.5 Spectrum at 30 ksi Limit Stress.	94
102	Gage Validation Test Results - BL 44.5 Spectrum at 30 ksi Limit Stress (Test 1). . . .	94
103	Gage Validation Test Results - BL 44.5 Spectrum at 30 ksi Limit Stress (Test 2). . . .	95
104	Gage Validation Test Results - BL 100 Spectrum at 33 ksi Limit Stress	96
105	Gage Validation Test Results - BL 132.5 Spectrum at 30 ksi Limit Stress	96
106	Nominal Relationships of Gage Stress to Stress in Wing Skin.	98
107	Impact of Step Thickness Tolerances on Relationship of Gage Stress to Wing Skin Stress at Site 1.	98
108	Impact of Step Thickness to Tolerances on Relationship of Gage Stress to Wing Stress at Site 3.	99
109	Stress in Gage Due to Bonding Thermal Strains .	101
110	Predicted Crack Growth in Gages on F-4 Fatigue Test Article.	103
111	Predicted Crack Growth in Fatigue Test Article Lower Wing Skin - BL 44.5	104
112	Predicted Crack Growth in Fatigue Test Article Lower Wing Skin at Pylon Hole	105
113	Predicted Crack Growth in Fatigue Test Article Lower Wing Skin at BL 132.5	106

LIST OF ILLUSTRATIONS (Continued)

<u>Figure No.</u>		<u>Page</u>
114	Predicted Relationship of Site 1 Gage Crack Length to Structural Flaw Length in Fatigue Test Article.	106
115	Predicted Relationship of Site 2 Gage Crack Length to Structural Flaw Lengths in Fatigue Test Article.	107
116	Predicted Relationship of Site 3 Gage Crack Length to Structural Flaw Lengths in Fatigue Test Article.	107
117	Comparison of Measured and Predicted Wing Skin Strain at BL 44.5	109
118	Comparison of Measured and Predicted Wing Skin Strain at BL 100.	109
119	Comparison of Measured and Predicted Strains in Wing Skin at BL 132.5.	110
120	Comparison of Predicted Gage Crack Lengths Using Predicted and Measured Strains.	110
121	Comparison of Crack Length Measurements and Predictions for Sites 6 and 7	111
122	Comparison of Crack Length Measurements and Predictions for Sites 1 and 5	111
123	Comparison of Crack Length Measurements and Predictions for Sites 2 and 4	112
124	Comparison of Crack Length Measurements and Predictions for Site 3.	112
125	Comparison of Crack Length Measurements and Predictions for Site 8.	113
126	Relationship of Potential Crack Growth in Structure to Gage Crack Growth Varies with Aircraft Usage.	114
127	Usage Variations Examined	114
128	Variation of Structure/Gage Flaw Growth Relationship for Small Flaw Growing from Hole .	115

LIST OF ILLUSTRATIONS (Concluded)

<u>Figure No.</u>		<u>Page</u>
129	Predicted Gage Crack Growth for Several Stress Levels - Baseline Spectrum	116
130	Crack Growth from Hole for Several Stress Levels - Baseline Spectrum.	116
131	Crack Growth from Hole Prediction Interpolated from Gage Crack Growth.	117
132	Spectrum Variations Examined.	117
133	Predicted Crack Growth in Gage for Several Spectrum Variations	118
134	Predicted Crack Growth from Hole for Several Spectrum Variations	119
135	Comparison of Predictions for Crack Growth from Hole for Several Spectra	120

LIST OF TABLES

<u>Table No.</u>		<u>Page</u>
1	Summary of Finite Element Analysis Results. . .	12
2	Adhesive Properties Used for Property Variations Study	31
3	Temperatures Recorded During First Bonding Test.	39
4	Temperatures Recorded During Second Bonding Test.	40
5	Temperatures Recorded During Third Bonding Test.	43
6	Test Program Summary.	54
7	Tensile Test Results.	59
8	Comparison of Average Measured Tensile Properties with Design Properties From MIL-HDBK-5C. .	60
9	Stresses Used for Center Cracked Panel Tests. .	60
10	Summary of Load Transfer Test Results	67
11	Summary of Gage Stiffnesses Determined from Strain Survey	68
12	Constant Amplitude and Spectrum Tests to Investigate Sheet Thickness Effects	76
13	Wing Skin Stresses Parallel to Gage	102

LIST OF SYMBOLS

a	Half crack length in gage or crack depth from hole
A_{eff}	Effective area of unbonded length of gage, based on gage stiffness
A_3	Effective area of structure carrying gage
b	Half gage width
E	Young's modulus
E_{gage}	Young's modulus of gage material
E_{plate}	Young's modulus of plate carrying gage
f_1	Finite width and length correction to stress intensity factor in terms of strain
f_2	Finite width and length correction to stress intensity factor in terms of stress
f_3	Stepped plate correction to stress intensity factor
G	Shear modulus of adhesive
h	Half length of unbonded portion of gage
K	Stress intensity factor for gage bonded to plate
K_v	Stress intensity factor for uniform displacement applied to gage
K_σ	Stress intensity factor for uniform stress applied to gage
L_1	Length of thinner step in unbonded length of gage
L_2	Length of thicker step in unbonded length of gage
t_{eff}	Effective thickness of unbonded length of gage, based on gage stiffness
t_1	Thickness of thinner step in unbonded length of gage
t_2	Thickness of thicker step in unbonded length of gage
v	Half of assumed uniform displacement in unbonded length of gage
v_0	Half of assumed uniform displacement in carrier plate beneath unbonded length of gage

LIST OF SYMBOLS (Continued)

v_{temp}	Half of assumed uniform displacement of gage due to thermal stresses set up in adhesive during bonding
x	Location of strain gages on crack growth gages in load transfer tests
β	Stress intensity correction factor for gage bonded to plate
β_v	Stress intensity correction factor for uniform displacement applied to gage
β_σ	Stress intensity correction factor for uniform stress applied to gage
ϵ_{gage}	Strain in gage
ϵ_{plate}	Strain in plate carrying gage
γ_e	Maximum elastic shear strain in assumed bi-linear stress/strain curve for adhesive
γ_p	Shear strain at failure in assumed bi-linear stress/strain curve for adhesive
σ_{app}	Gross stress applied to plate carrying gage
σ_g	Gross stress in thin step of gage
σ_s	Gross stress in structure carrying gage
τ_p	Limiting shear stress in assumed bi-linear stress/strain curve for adhesive

SECTION I

INTRODUCTION

1. PROGRAM SUMMARY - The objective of this program was to evaluate the ability of a crack growth gage to monitor potential crack growth damage in fatigue critical areas of F-4C/D aircraft structure. Crack growth gages were designed and manufactured for use on the F-4 lower wing skin. The crack growth behavior of the gage and relationship of gage crack growth to potential crack growth in the wing skin was determined through analysis and test. Eight gages were bonded on the Air Force F-4C/D full scale fatigue test aircraft at Wright-Patterson AFB. Assessments were made of (1) the capability to predict crack growth behavior of the gages mounted on the fatigue test article, (2) the ability of crack growth gage to monitor potential crack growth damage at specified control points, and (3) the impact of manufacturing, installation, and data collection procedures on the utility of the gage as a damage monitoring device.

The crack growth gage (Figure 1) was designed to produce approximately one inch of crack growth in 12,000 spectrum hours when attached to the lower wing skin at sites having 30 ksi stress levels at limit load. Gage size was limited to reduce the impact of strain gradients in fighter wing skin on gage crack growth behavior. Chemical milling was used to minimize development of residual stresses during fabrication of the stepped thickness gage.

An element test program was performed to (1) determine the load transfer characteristics and crack growth behavior of the gage and (2) determine the relationship of gage crack growth to potential crack growth in fatigue critical areas of aircraft structure. The crack growth behavior of the gage under stress histories similar to those at installation sites on the full scale test article was determined. While static and constant amplitude fatigue tests verified analytical predictions, spectrum fatigue tests showed much more crack growth retardation in the gages than predicted. A subsequent test program showed that the increased retardation was dependent upon the thickness of the gage element containing the crack. A modification of the crack growth analysis was developed to correlate with thickness effects on retardation. The modified analysis was then used to correlate with element test results and to predict behavior of the gages on the test aircraft.

Four gages were bonded to the F-4C/D full scale fatigue test aircraft using FM-73 adhesive and a heating blanket and vacuum bag technique developed in the Primary Adhesively Bonded Structures Technology (PABST) program. The bonding was not successful because the 250°F cure temperature required for the FM-73 adhesive broke down the silicone-based adhesive used for bonding load pads to the test aircraft. Silicone contaminated the epoxy resin FM-73 adhesive and caused adhesive failure when loads were applied to

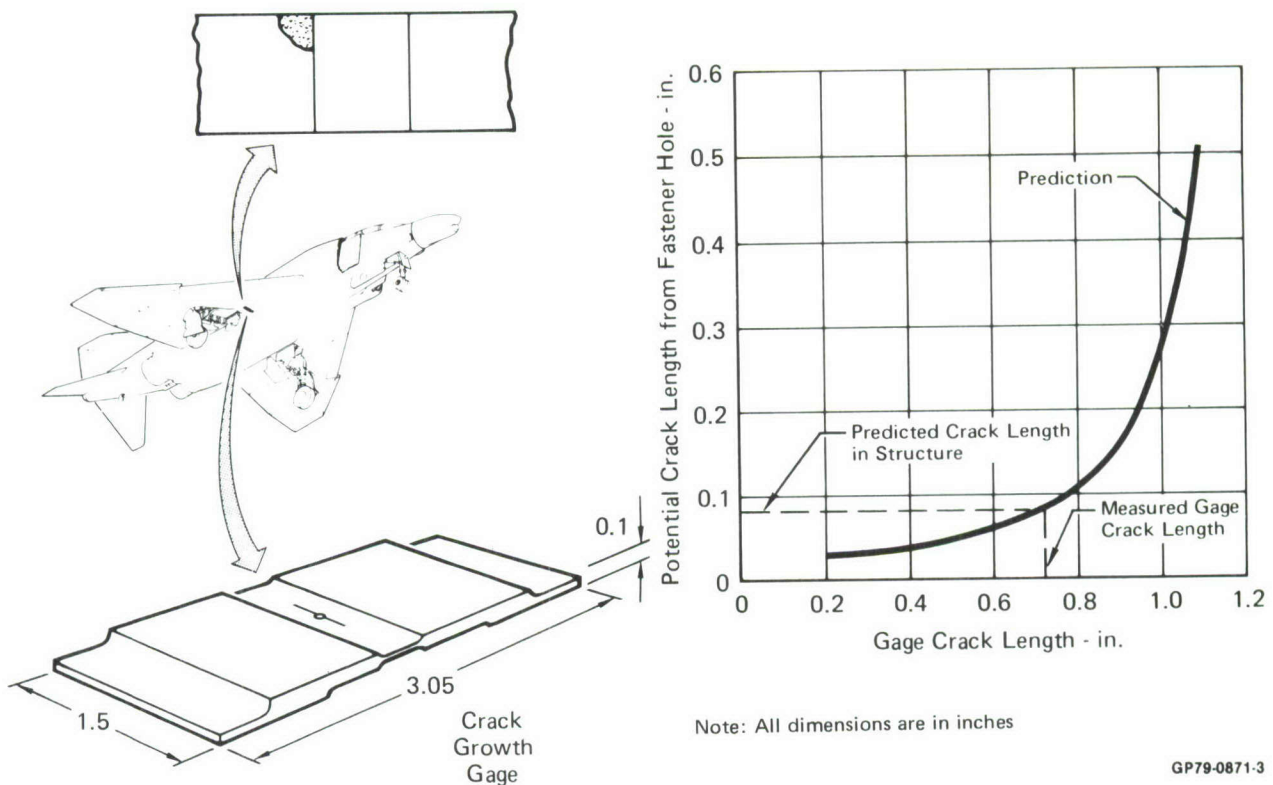


Figure 1. Use of Crack Growth Gage to Monitor Potential Crack Growth in Structure

the fatigue test article. The gages were removed and cleaned and eight gages were successfully bonded to the aircraft using a room temperature cure adhesive. Because of the durability limitations of the room temperature cure adhesive, four of the eight gages disbonded after 2000 spectrum hours of testing. Four gages produced crack growth through 4000 spectrum hours of testing. Data from gages on the full scale fatigue test generally agrees with the predicted behavior determined from element test results.

2. RESULTS AND CONCLUSIONS - Crack growth in gages bonded to an aircraft can be correlated with the stress history of the gage site on that aircraft.

Knowledge of the gage crack length alone is not sufficient to determine the potential crack growth in the structure. Crack growth retardation in thin sheets (less than 0.1 inches thick) is much greater than that in thicker fighter wing skins. Consequently, the relationship of gage crack length to potential flaw length in the structure is dependent on the usage (spectrum severity) of the aircraft.

Spectrum severity and potential crack growth in the structure can be determined by tracking both the number of aircraft flight hours and crack length in the gage. Test substantiation is required to verify the techniques used to determine potential growth of structural flaws from measured gage crack growth.

Gage manufacturing tolerances were predicted to have little impact on gage response.

Bonding of gages to the fatigue test article using FM-73 adhesive was not successful due to circumstances peculiar to that application. In element tests, FM-73 was found to predictably transfer strains to the gage until either adhesive or gage failure occurred. Applications of fatigue load cycles were not found to change load transfer to the gage prior to adhesive failure.

A comprehensive qualification program is required before accepting an adhesive and bonding procedure for gage attachment to fleet aircraft.

The small crack growth increments obtained in the gages during the full scale fatigue test required a crack length measurement technique which was more accurate than visual measurement. Faxfilm replicates of the gage surface were found to provide adequate crack length measurements.

Development of the gage concept is not complete. The analysis and test results obtained in this program provide a limited demonstration of the potential of a crack growth gage. Considerable further research is required to determine ability of a gage to track variations in service usage, demonstrate reproducibility of growth from gage to gage, develop simple procedures to reliably bond gages in a depot maintenance environment, demonstrate adequate gage service lives in fleet use, and determine procedures to collect and summarize individual aircraft gage data.

The potential usefulness of a gage for monitoring crack growth in aircraft structure has not been fully explored. The remainder of this report presents the analysis and test results of this program in considerable detail to aid future investigators in determining the full potential of the crack growth gage for service life tracking of fighter aircraft.

SECTION II

CRACK GROWTH GAGE DESIGN

The crack growth gage studied in this program was designed specifically for application to the lower wing skin of the F-4C/D aircraft. The design was based on the following criteria: (1) the gage must be small enough that it can be bonded to fighter wing skins without encompassing large strain differences, or degrading beneficial residual stresses near fastener patterns during bonding, (2) the gage must give measurable crack growth for each 1000 spectrum hours of test life, (3) the gage must be capable of being durably bonded to the aircraft, and (4) the gage must not buckle under the maximum compressive stress in the spectrum. The selected design satisfies all of the above criteria. Analyses performed to determine the impact of machining and bonding variables on gage stresses indicate that step thickness tolerances and bond cure temperatures have the greatest impact on gage behavior.

1. GAGE SIZE CONSIDERATIONS - Large strain gradients occur in lower wing skins of fighter aircraft. A bonded crack growth gage should be as small as possible so the gage is subjected to as uniform a strain as possible when mounted near fatigue critical locations. Also, the use of an elevated temperature cure adhesive in this program required caution in locating gages near fastener patterns having taper-loks or cold worked holes. High temperatures in those areas might relieve residual stresses and adversely impact structural fatigue life. The smaller the gage area, the lesser the thermal input required to cure the adhesive and the closer the gage can be mounted to critical fastener locations without disturbing residual stresses.

A design goal was that the gage experience measurable crack growth during each 1,000 flight-hour increment experienced in cyclic test. Crack growth increments of about 0.1 inch were selected as the minimum growth which might be visually measurable in the gage when bonded to the fatigue test article. Since the F-4 fatigue test was scheduled to obtain 12,000 flight hours following bonding of the gages, the total crack growth desired was 1.0 to 1.20 inches. This growth, coupled with an initial flaw size of 0.2 inch, required the gage width to be 1.5 inches. The remaining gage dimensions are consequences of this width selection. The overall gage size selected is about 60 percent of that suggested in Reference 1.

2. STRESS INTENSITY FACTOR - To insure measurable crack growth in each 1000 flight hour increment of cyclic test, a gage was developed which results in a nearly constant crack growth rate throughout its useful life. To obtain a constant crack growth rate, the stress intensity factor for the gage must be independent of crack length. Discussions with Dr. Peter Torvik, Air Force Institute of Technology, indicated that, based on his analyses in Reference 2, a stepped gage could be used to obtain a nearly constant stress intensity factor.

To verify the behavior of a cracked, stepped plate, NASTRAN finite element analyses were performed for the three crack growth gage configurations of Figure 2. Twenty node solid elements were used to model one quarter of the unbonded portion of the gage, as shown in Figure 3. Uniform displacements were prescribed at the interface of the gage and bonded joint. It was assumed that the displacement of the end of the gage is transmitted without rotation.

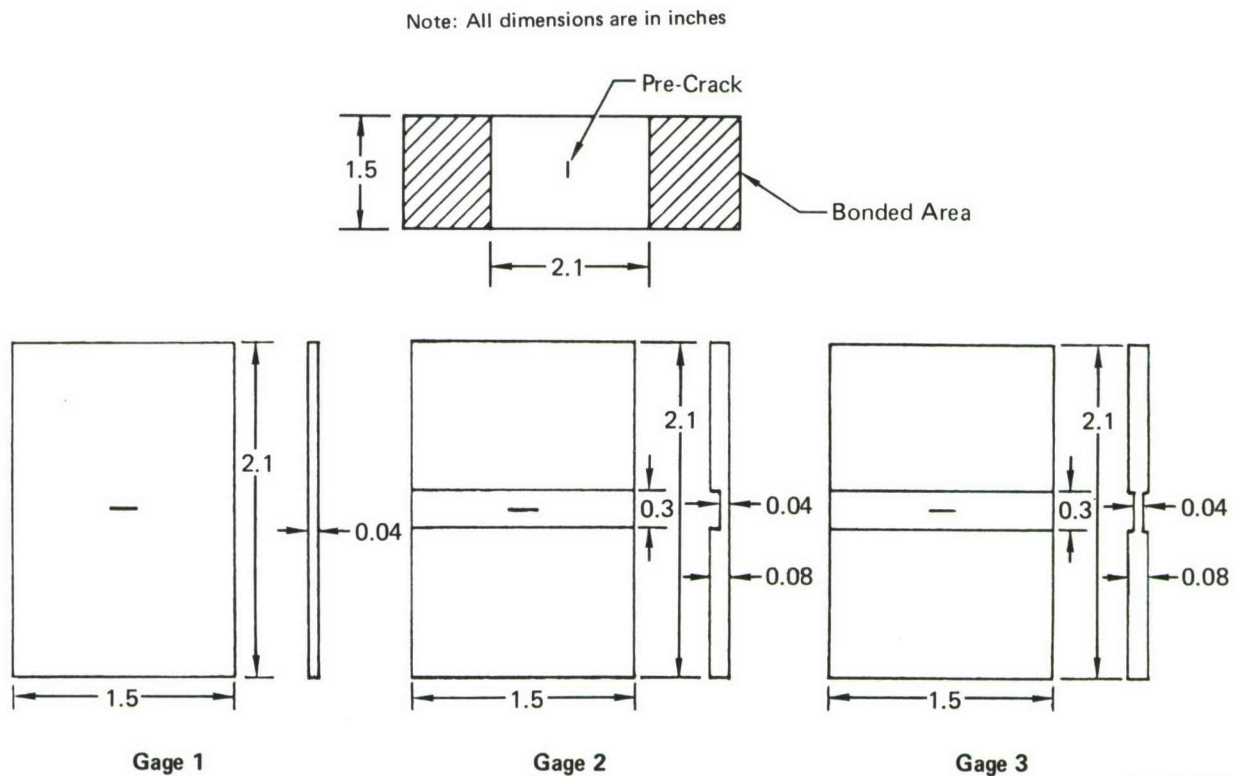


Figure 2. Preliminary Crack Growth Gage Configurations

GP79-0871-4

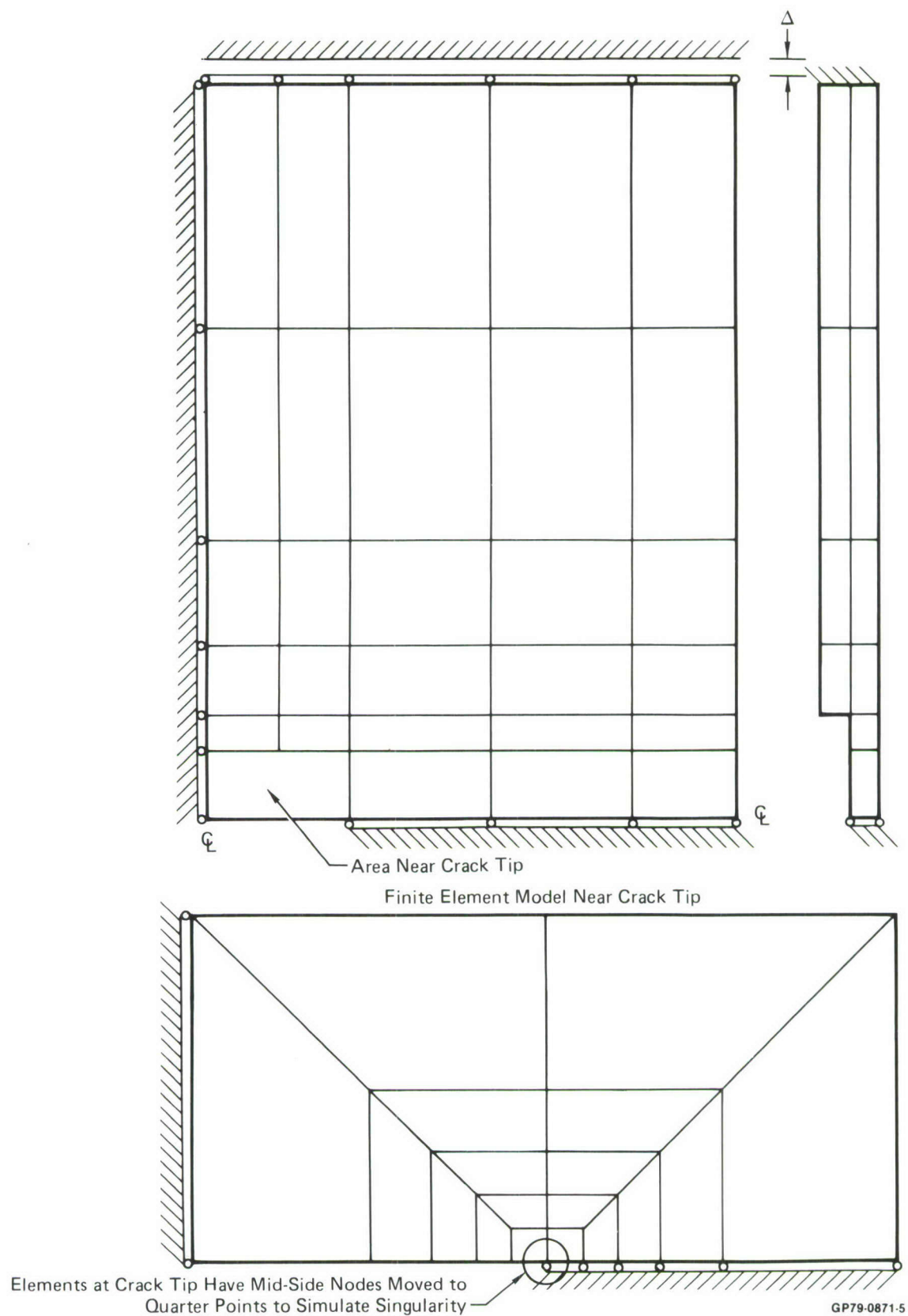


Figure 3. Solid Element Model Used to Determine Crack Displacements

Crack surface displacements along the modeled crack were used to determine stress intensity factors for each gage. If the crack surface displacements are assumed to be elliptical (as for a through crack in an infinite sheet) the stress intensity factor can be related to the crack surface displacement at any point along, the crack. The displacement V_x at location x on the crack half length a may be used to determine the stress intensity factor from

$$K = \frac{E v_x}{2} \sqrt{\frac{\pi a}{a^2 - x^2}} \quad (1)$$

Since crack surface displacements for the gage may not be elliptical, due to finite boundaries and step configurations, the stress intensity factor was considered to be the limiting value near the crack tip.

$$K = \lim_{x \rightarrow a} \frac{E v_x}{2} \sqrt{\frac{\pi a}{a^2 - x^2}} \quad (2)$$

Figure 4 shows the results of this analysis when applied to a center cracked, uniform thickness panel with uniform displacement applied. In determining the limiting stress intensity factor value, the displacements nearest the crack tip were ignored. These displacements may have been in error due to the transition from trapezoidal to square shaped elements adjacent to the crack tip, Figure 3. In cases involving a uniform thickness plate (Figure 4), the crack surface displacements should be nearly elliptical and the three near tip displacements were obviously in error. In cases involving stepped thickness plates (Figure 5), the crack surface displacements were changing significantly from an elliptic behavior near the tip. However in this case the effects of the step may cause the displacements to not be elliptical and it was more difficult to determine if the near tip displacements were in error. The three displacements closest to the crack tip were ignored in all of the analyses presented herein.

Regardless of the interpretation problems, good agreement with established stress intensity factors for uniform thickness plates were obtained as shown in Figures 6 and 7. Figure 6 shows comparison with Isida's results for uniform displacement applied to finite width, finite length plates of uniform thickness, Reference 3. Figure 7 shows very good agreement with Rice's solution for rigid displacement of a boundary near the crack plane, Reference 4. Agreement of these solutions with accepted values increased confidence in the NASTRAN analysis as applied to the stepped gage.

The NASTRAN analysis of Gage 2 did not agree with the behavior predicted from a closed form solution as shown in Figure 8. This closed form stress intensity factor for the stepped plate having the general dimensions shown in Figure 9, was synthesized from available solutions, to be

$$K = \beta_v \frac{E v}{h} \sqrt{\pi a} \quad (3)$$

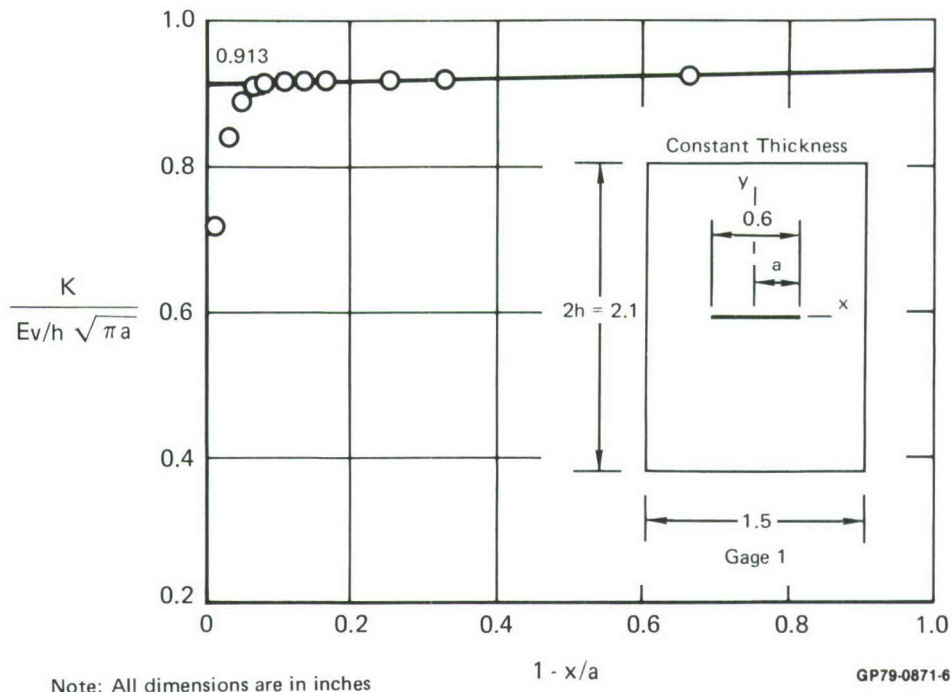


Figure 4. Typical Results from Finite Element Analysis of Uniform Thickness Plate

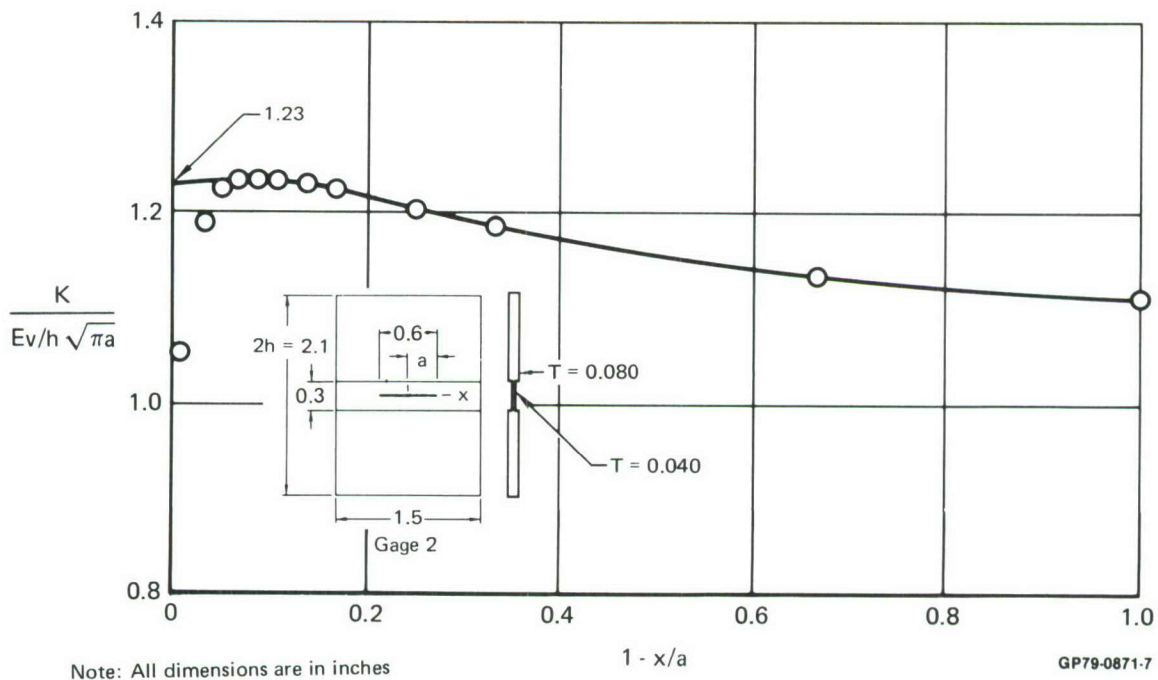


Figure 5. Typical Results from Finite Element Analysis of Stepped Thickness Plate

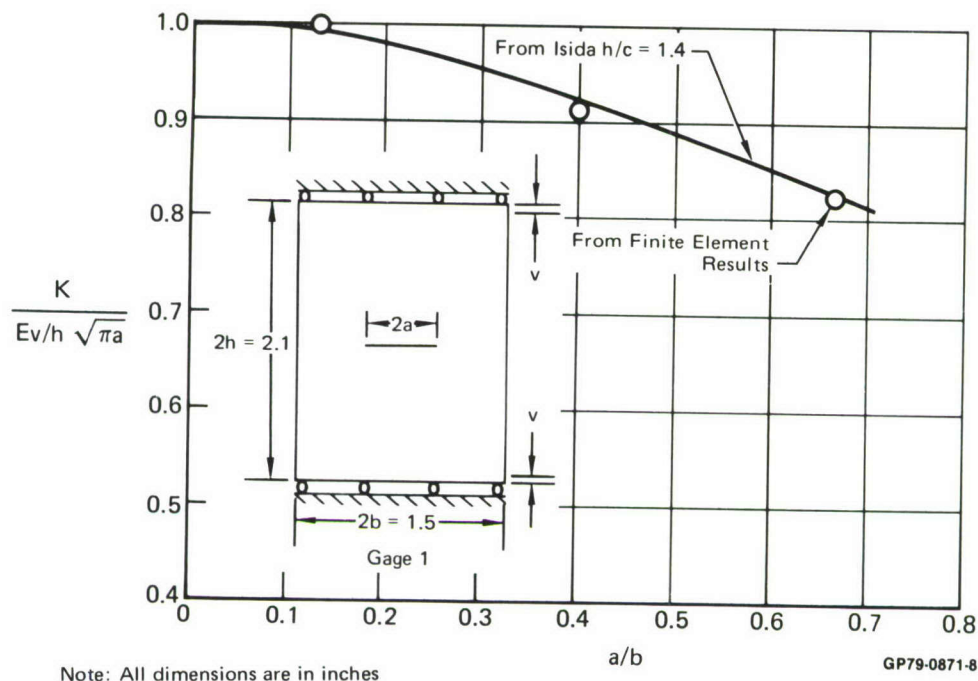


Figure 6. Comparison of Stress Intensity Factors Determined from Finite Element Analysis and Isida's Factors

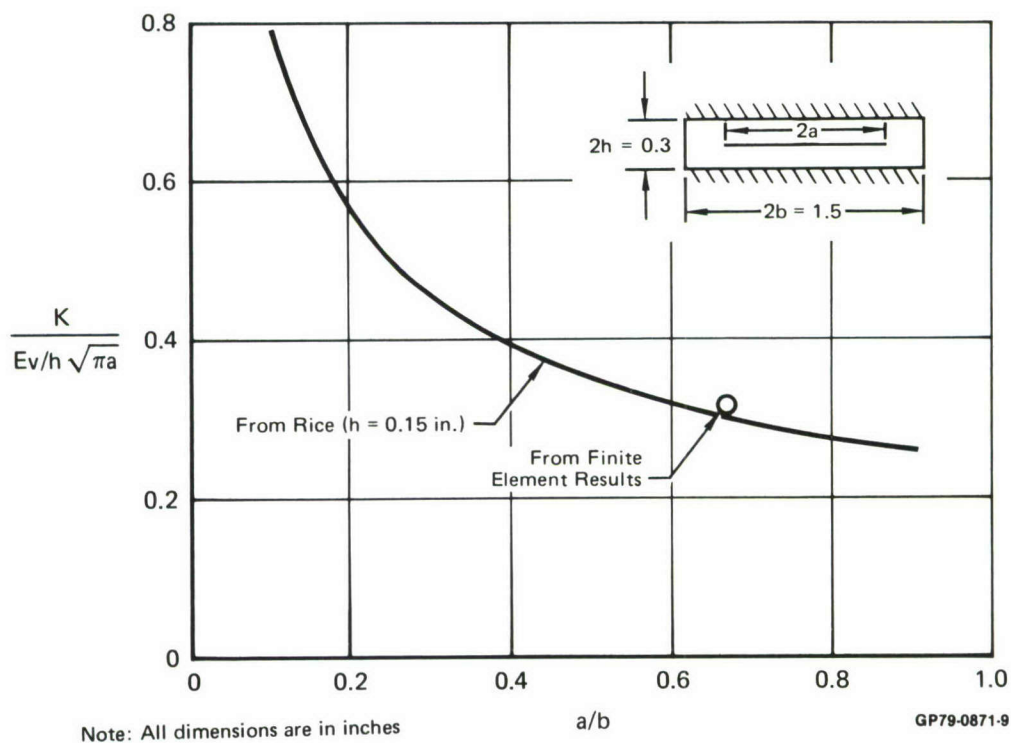


Figure 7. Comparison of Stress Intensity Factors Determined from Finite Element Analysis and Rice's Factors

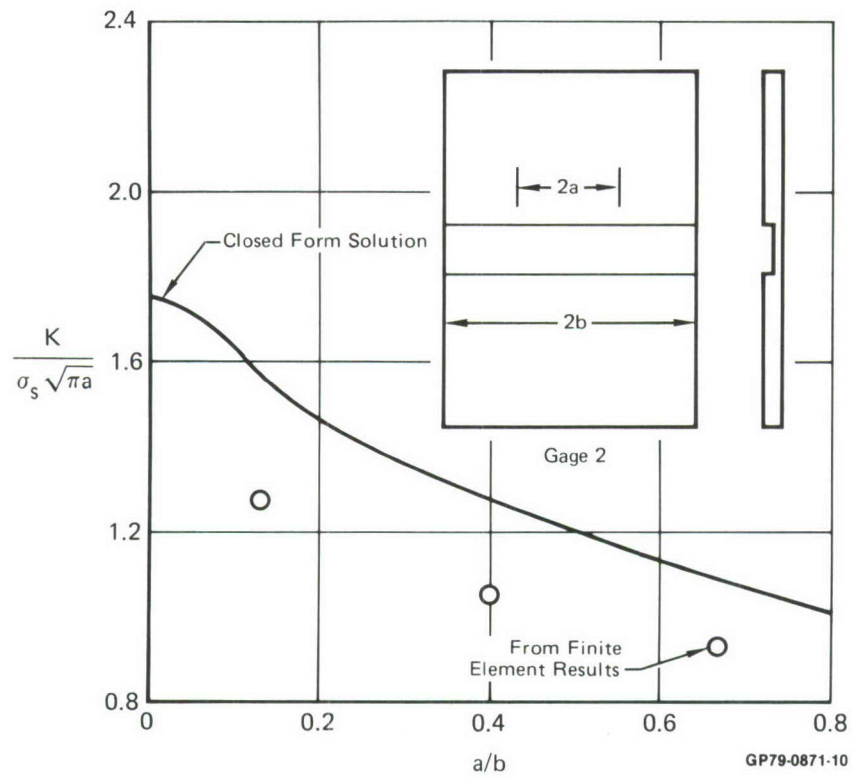


Figure 8. Comparison of Finite Element Analysis and Closed Form Solution for Gage 2

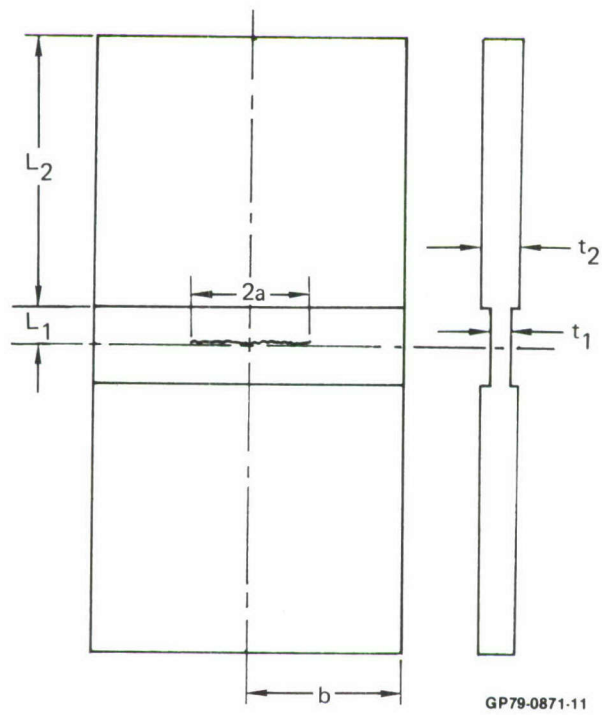


Figure 9. Generalized Gage Dimensions

where

$$\beta_v = \frac{f_1 f_2}{\frac{L_1}{h} + \frac{t_1 L_2}{t_2 h}}$$

f_1 is Isida's stress intensity factor correction for finite width and finite length plates subjected to uniform displacement (Reference 3), f_2 is Hilton and Sih's stress intensity factor correction for a stepped plate (Reference 5), and the factor,

$$\frac{1}{\frac{L_1}{h} + \frac{t_1 L_2}{t_2 h}}$$

is the increase in stiffness provided by the thicker step.

Further investigation of the NASTRAN analysis of Gage 2 showed that considerable bending was predicted to occur in the gage, (Figure 10). Bending apparently causes the significant reduction in stress intensity factor noted in Figure 8. When the symmetric step gage, Gage 3, was analyzed the results were much closer to the closed form solution (Figure 11). Table 1 summarizes all of the stress intensity factor results obtained from NASTRAN finite element analyses and compares those results with accepted solutions or predicted behaviors.

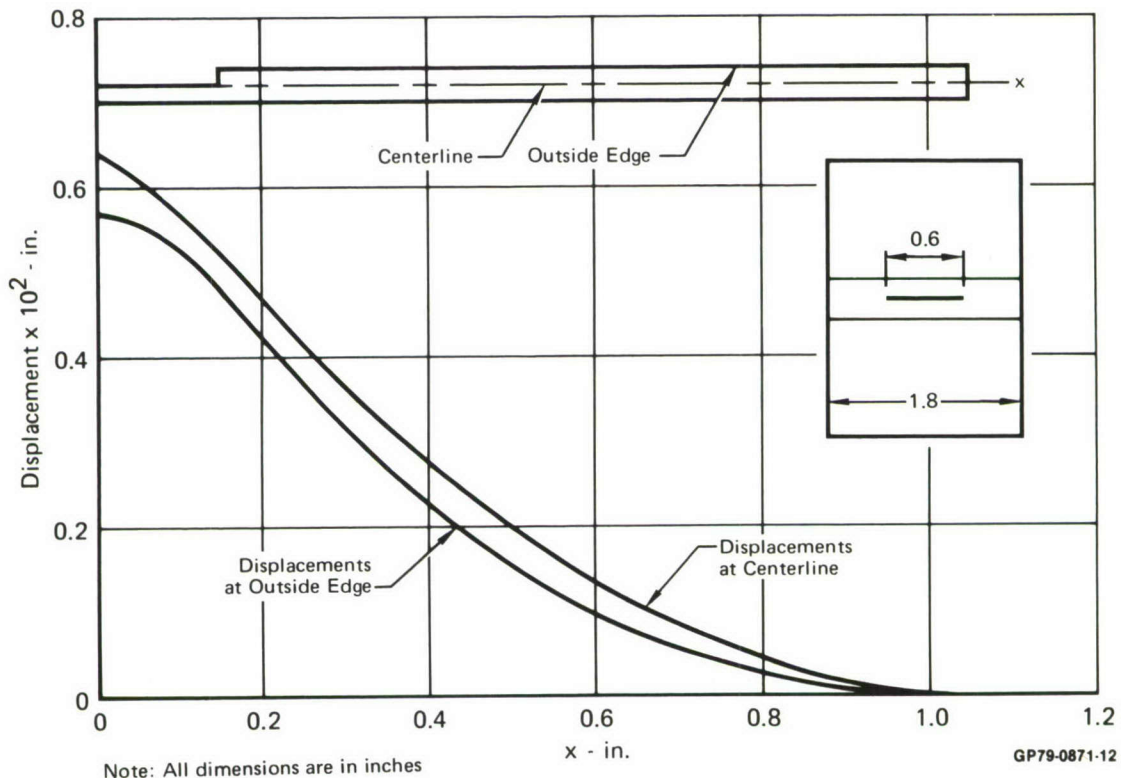


Figure 10. Finite Element Analysis Predicts Considerable Bending for Gage 2

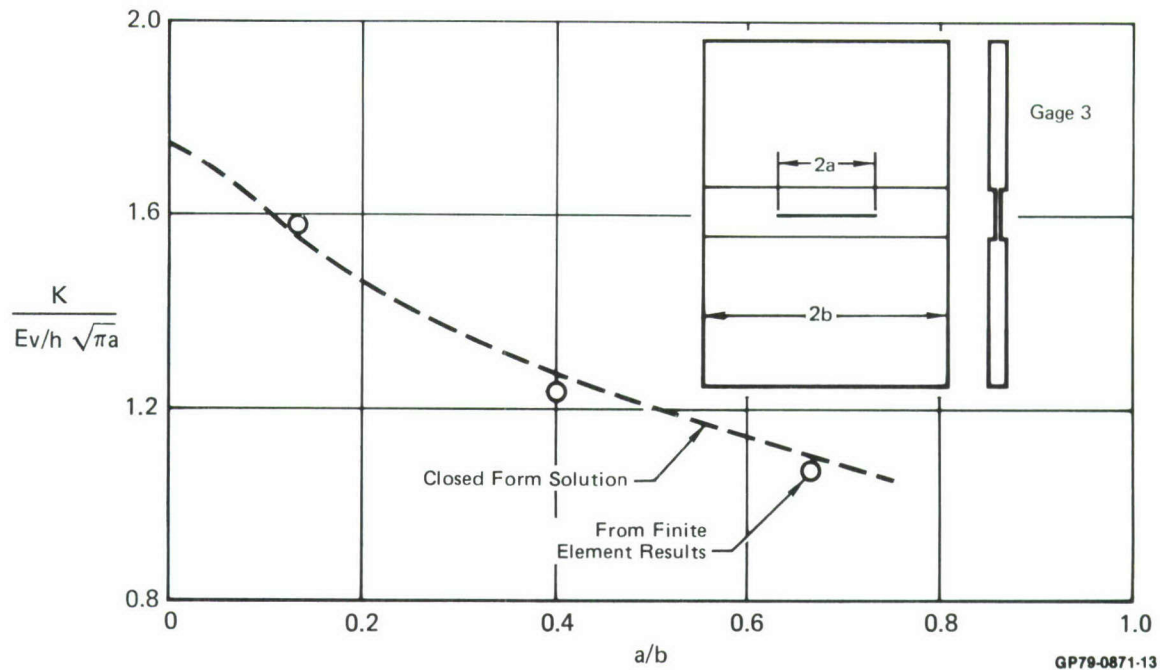


Figure 11. For Symmetric Gage, Finite Element Analysis Agrees with Closed Form Solution

TABLE 1. SUMMARY OF FINITE ELEMENT ANALYSIS RESULTS

Model No.	Description	a/b (1)	$\frac{K}{\frac{E_v}{h} \sqrt{\pi a}}$ from NASTRAN	$\frac{K}{\frac{E_v}{h} \sqrt{\pi a}}$ Available Solution
1	Flat Plate $h/b = 1.4$ (2)	0.1333	0.999	0.994 (3)
2	↓	0.4	0.913	0.927 (3)
3	↓	0.667	0.824	0.837 (3)
4	Flat Plate $h/b = 0.2$	0.667	0.337	0.327 (4)
5	Unsymmetric Stepped Plate	0.1333	1.267	—
6	↓	0.4	1.05	—
7	↓	0.667	0.933	—
8	Symmetric Stepped Plate	0.1333	1.577	1.555 (5)
9	↓	0.4	1.23	1.285 (5)
10	↓	0.667	1.07	1.105 (5)
11	Selected Gage	0.1333	1.38	1.40 (5)
12	↓	0.4	1.005	1.03 (5)
13	↓	0.667	0.79	0.80 (5)

Notes:

(1) a/b is the crack length to plate width ratio

(2) h/b is the plate length to width ratio

(3) Isida - Reference 3

(4) Rice - Reference 4

(5) Synthesized from Isida, and Hilton and Sih's solutions, References 3 and 5.

GP79-0871-14

In terms of the nominal stress in the gage the stress intensity factor can be expressed as

$$K = \beta_{\sigma} \sigma_g \sqrt{\pi a} \quad (4)$$

where $\beta_{\sigma} = f_2 f_3$, f_3 is Isida's stress intensity factor correction for average stress applied to finite width, finite length plates.

3. GAGE OPTIMIZATION - Crack growth analyses were used to optimize the configuration of the crack growth gage. All crack growth analyses in this program were performed using the Contact Stress model, References 6-8. A version of this model has been developed which predicts crack growth life within 25 percent under a wide variety of stress histories using only stress exceedance curve input rather than cycle-by-cycle stress history input. By adjusting model parameters using spectrum test results in 7075-T6 aluminum, we have confidence that measured and predicted crack growth gage behavior will be close, provided the stress intensity factor is accurate.

Preliminary crack growth predictions for the gages of Figure 2 were made using an average normalized stress exceedance curve for the lower wing skin of the F-4, assuming 30 ksi limit stress level in the wing skin and no strain loss in the adhesive. Results of these analyses, Figure 12, show that none of the gages gives the desired linear behavior - Gage 2 gives about the desired life but the non-linear behavior caused by bending and the accelerating crack growth rate were considered undesirable characteristics.

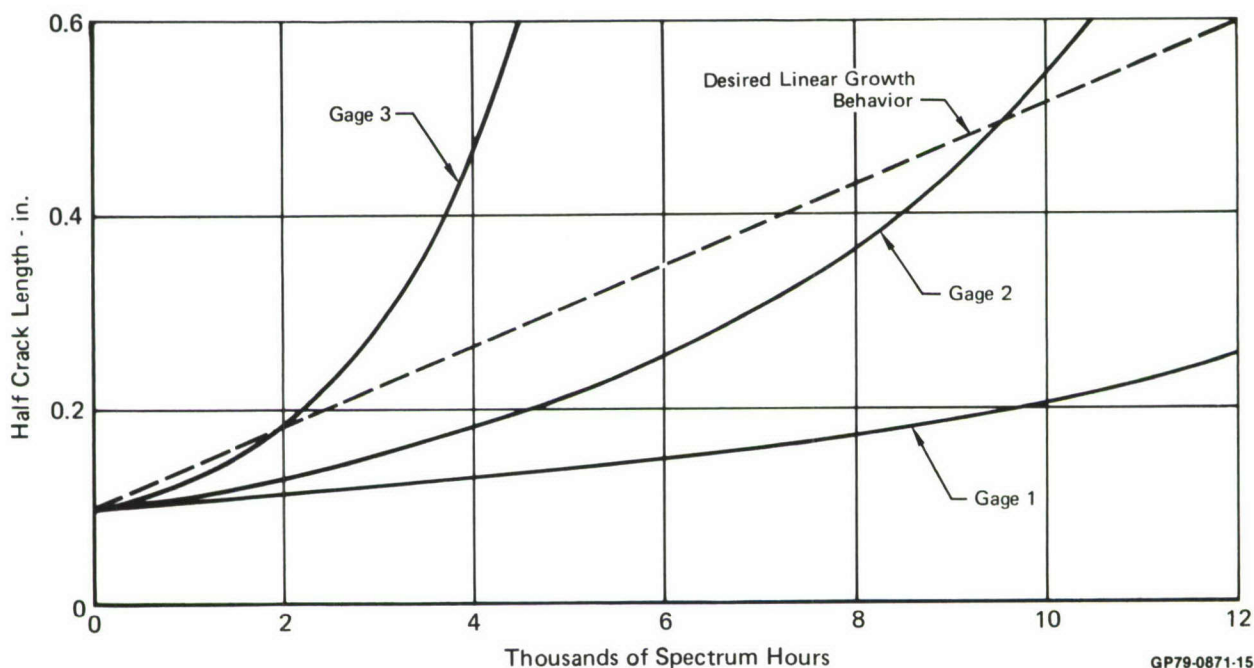


Figure 12. Comparison of Predicted Crack Growth for Candidate Gages with Desired Behavior

Parametric studies of crack growth gage geometries were performed using the stress intensity factor solutions of Equation (3). Variations in length to width ratio, step length to overall length ratio, and step thickness ratio were studied to determine configurations predicted to attain one inch of crack growth in 12,000 flight hours. Results of the crack growth analyses are shown in Figures 13-15. Gage configurations predicted to give the desired 12,000 hour service life are shown in Figure 16. Crack growth curves for each of these gage configurations are shown in Figure 17. Based on these analyses the gage with the shortest overall length, Gage A, gives the best crack growth response. While it has a slow initial rate, that rate is significantly higher than Gage B or Gage C and approaches the desired linear growth behavior. Gage A was selected for use in this program.

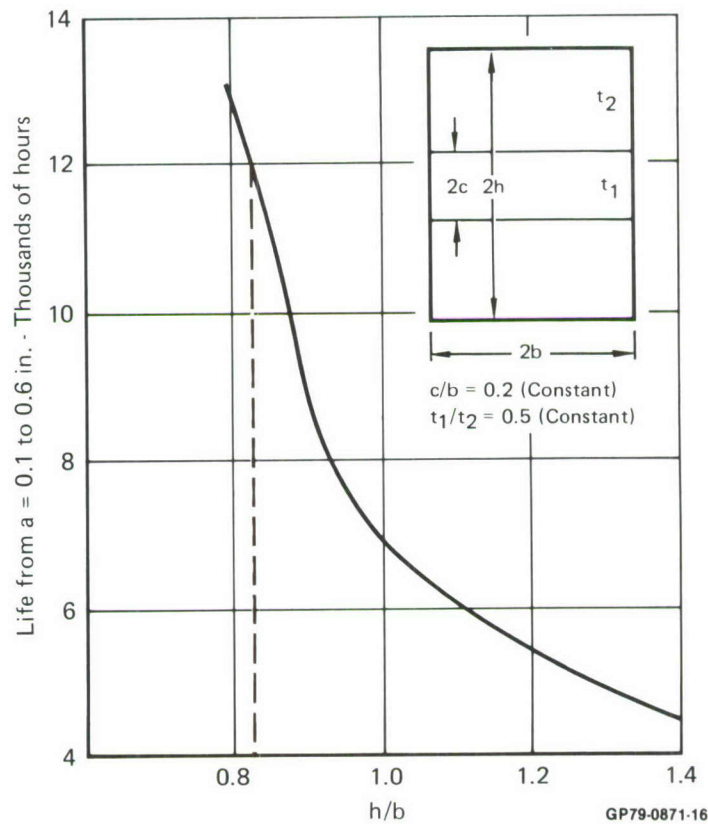


Figure 13. Effect of Changing Gage Length and Width on Life

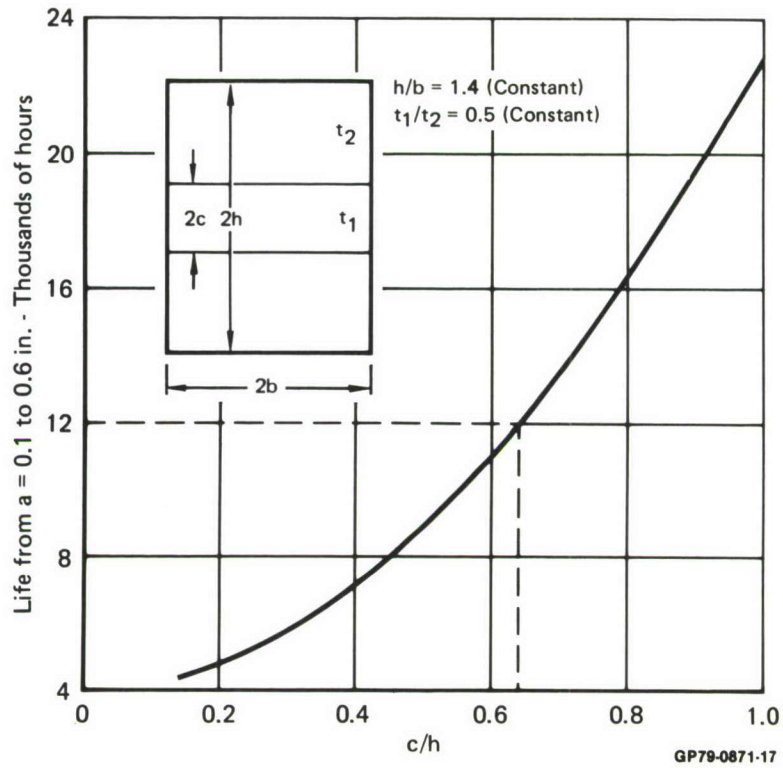


Figure 14. Effect of Changing Step Length on Life

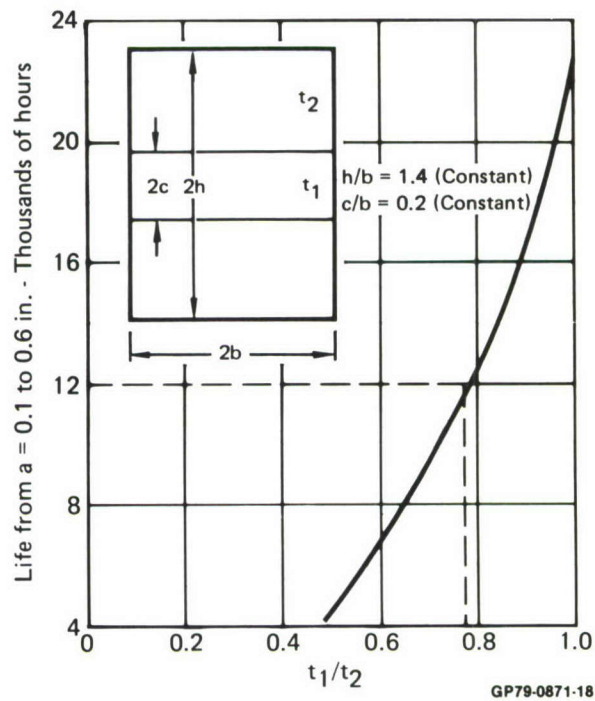


Figure 15. Effect of Changing Thickness Ratio on Life

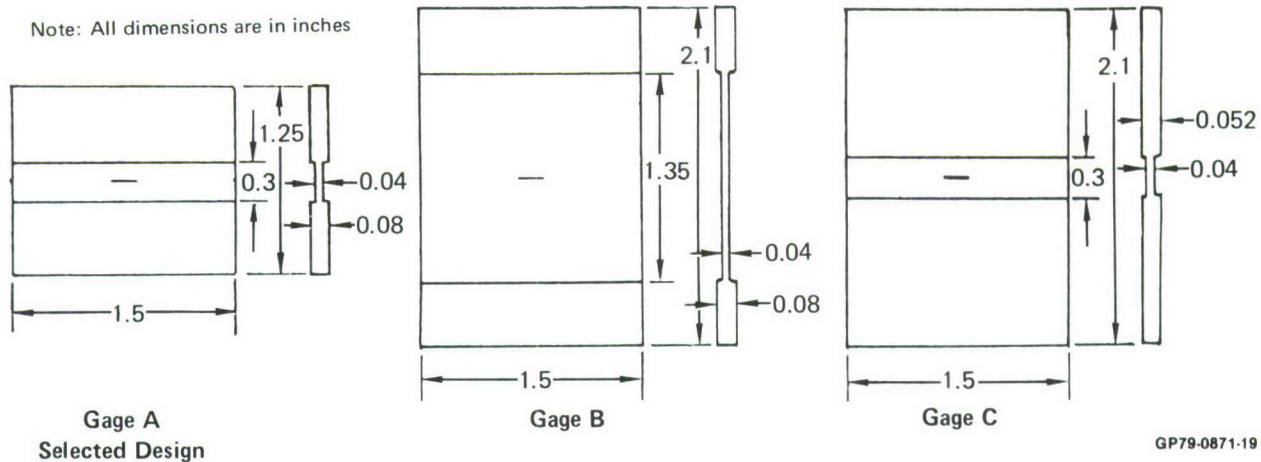


Figure 16. Three Gage Designs Predicted to Give 12,000 Hr Service Life

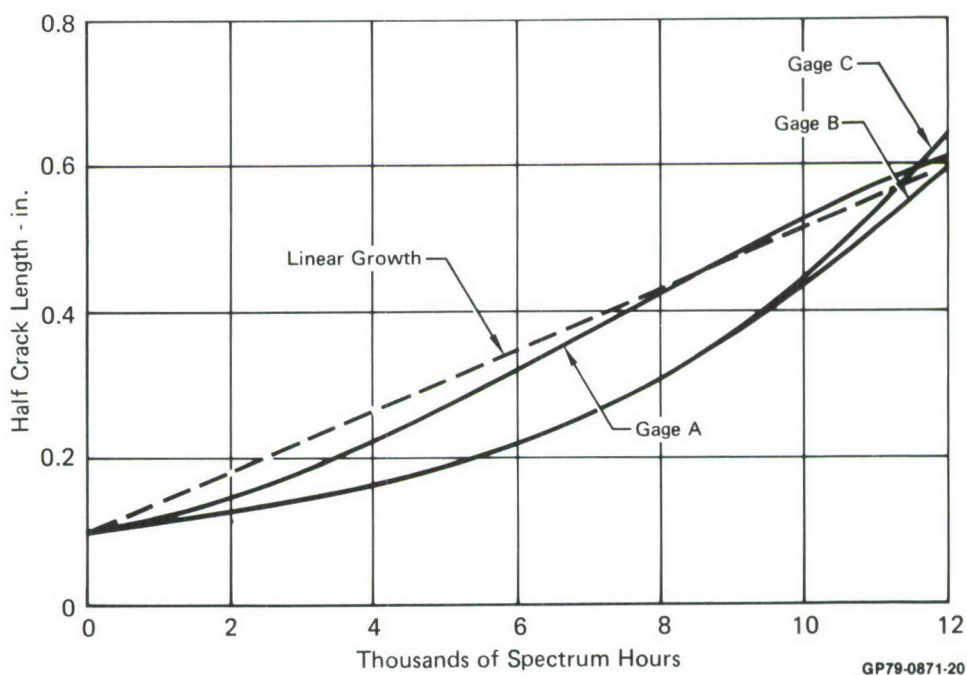


Figure 17. Crack Growth for Gage A Design is Closest to Linear Growth

NASTRAN finite element analyses were used to verify the stress intensity factor solution of Equation (3). Comparison of the results is shown in Figure 18, and shows very good agreement. These results were included in Table 1.

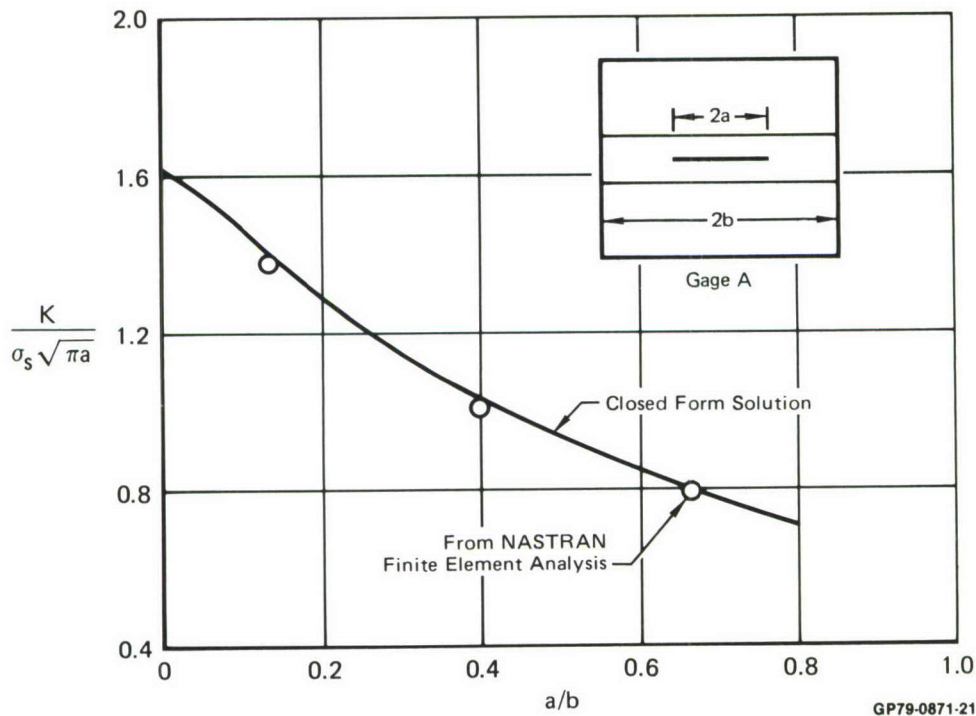


Figure 18. Finite Element Results Confirm Gage Stress Intensity Factor Computation

4. LOAD TRANSFER ANALYSIS - Gage geometry optimization was based on the assumption that the gage displacements were equal to the displacement of the wing skin. Actually the displacement of a crack growth gage bonded to a carrier plate (be it wing skin or test coupon) depends on the stiffness of the gage, the stiffness of the carrier plate, and the stiffness of the bondline. The stiffness of the gage depends on the gage crack length, the stiffness of the carrier depends on its thickness, and the stiffness of the bondline depends on the joint configuration and adhesive modulus.

The gage stiffness was determined from the stress intensity factors for the gage, Equations (3) and (4). The stress intensity determined by both equations is for uniform displacement of the unbonded length of the gage. Hence, the average stress for a given applied displacement can be found by equating stress intensity factors for stress and displacement.

$$K_{\alpha} = K_V = \sigma_g \beta_{\alpha} \sqrt{\pi a} = \frac{E_V}{h} \beta_V \sqrt{\pi a} \quad (5)$$

Then for any given crack length

$$\frac{\sigma_g}{\frac{E v}{h}} = \frac{\beta v}{\beta_\sigma} \quad (6)$$

Figure 19 presents the load (gross stress in the thin step)/displacement relationship as a function of crack length.

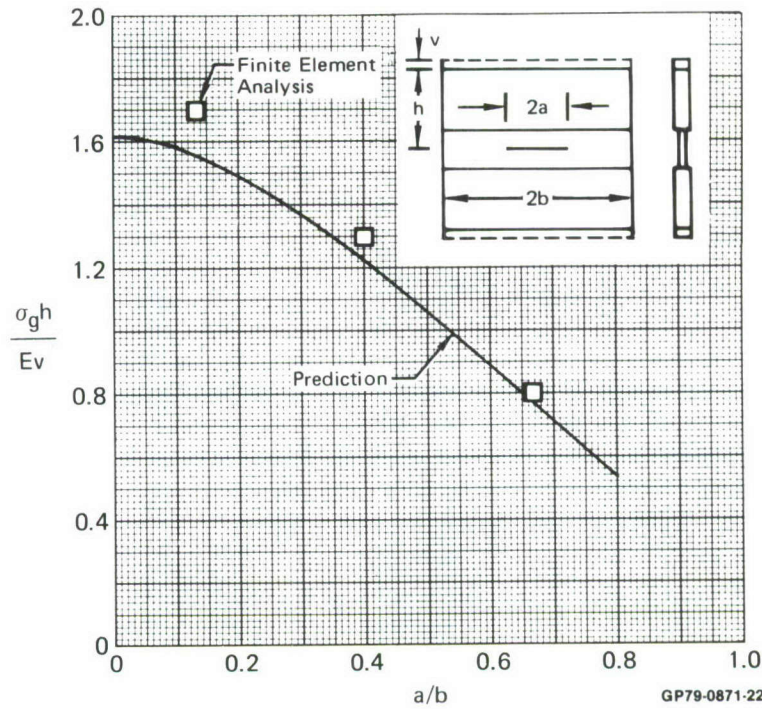


Figure 19. Gage Stiffness as a Function of Crack Length

Figure 19 shows a comparison of gage stiffnesses computed from NASTRAN finite element analyses and those derived from stress intensity factors, Equation (6). The correlation improves with increasing crack length. Gage stiffness with a crack is less than without a crack, consequently finite element stiffness predictions at short crack lengths are too large. The NASTRAN model may be too stiff at short crack lengths because of the change in element shape near the crack tip. The near tip displacements were previously noted (Section 2.) to be smaller than those estimated from closed form solutions. While the finite element predictions appear to be too large, they do provide support for Equation (6).

To determine the effect of carrier plate stiffness on gage displacement, the model shown in Figure 20 was used (test coupons had gages bonded to both sides). It was assumed that no strain was lost (or gained) in the bondline. The displacement/load characteristics of this system were determined to be

$$\frac{v_o}{P} = \frac{1}{2 \left(\frac{A_{eff} E}{h} \right) + \frac{A_3 E}{h}} \quad (7)$$

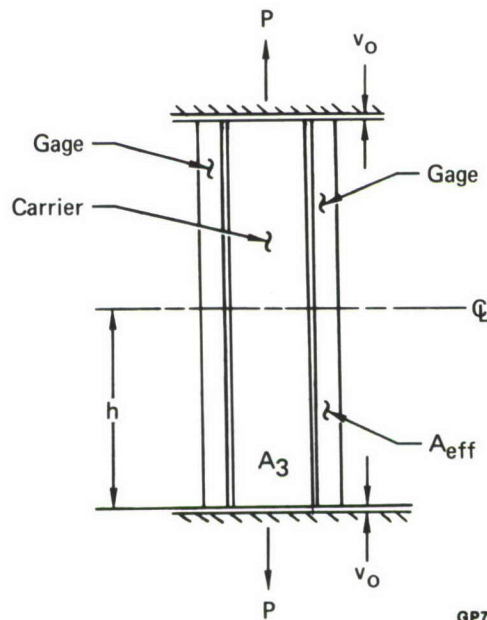
where $A_{eff} = t_{eff} w_g$, w_g is gage width, and the remaining parameters are defined in Figure 20. The effective thickness is defined as the constant thickness that would have the same axial stiffness as the stepped gage section. Without a crack, the effective thickness, $t_{eff}(o)$ is

$$t_{eff}(o) = \frac{L_1 + L_2}{\frac{L_1}{t_1} + \frac{L_2}{t_2}} \quad (8)$$

Where L_1 , L_2 , t_1 , and t_2 are defined by Figure 21. For a given crack length, the effective thickness is

$$t_{eff}(a) = \frac{\sigma_g(v, a)}{\sigma_g(v, o)} t_{eff}(o) \quad (9)$$

Where $\sigma_g(v, a)$ is the gross stress in the gage for displacement, v , and half crack length, a , from Equation (3); and $\sigma_g(v, o)$ is gage gross stress with the same displacement for a gage without a crack.



GP79-0871-23

Figure 20. Idealization Used for Specimen Compliance Analysis

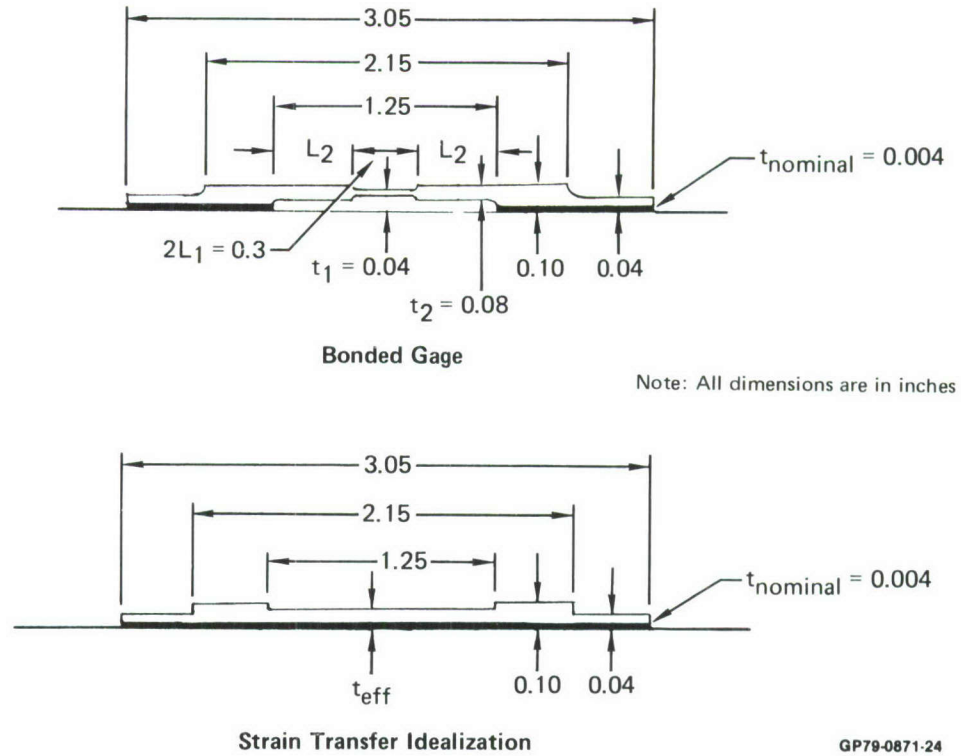


Figure 21. Strain Transfer Idealization of Bonded Gage

Defining the applied stress, σ_{app} , as P/A_3 , Equation (7) can be written

$$\frac{v_o E}{\sigma_{app} h} = \frac{1}{\frac{2A_{eff}}{A_3} + 1} \quad (10)$$

Equation (10) defines the displacement of the carrier plate for a given stress.

Stiffness of the bonded joint was determined using a doubler analysis developed by Hart-Smith, Reference 9. A computer routine based on Hart-Smith's closed form solution was used to determine the stress distribution of several joint configurations. The procedure performs both elastic and elastic-plastic stress analyses of the adhesive using an elastic perfectly plastic idealization of the adhesive shear stress-strain curve.

The adhesive selected for gage bonding in this program was FM-73. A measured shear stress-strain curve for FM-73 and the elastic-perfectly plastic idealization used for joint analyses are shown in Figure 22.

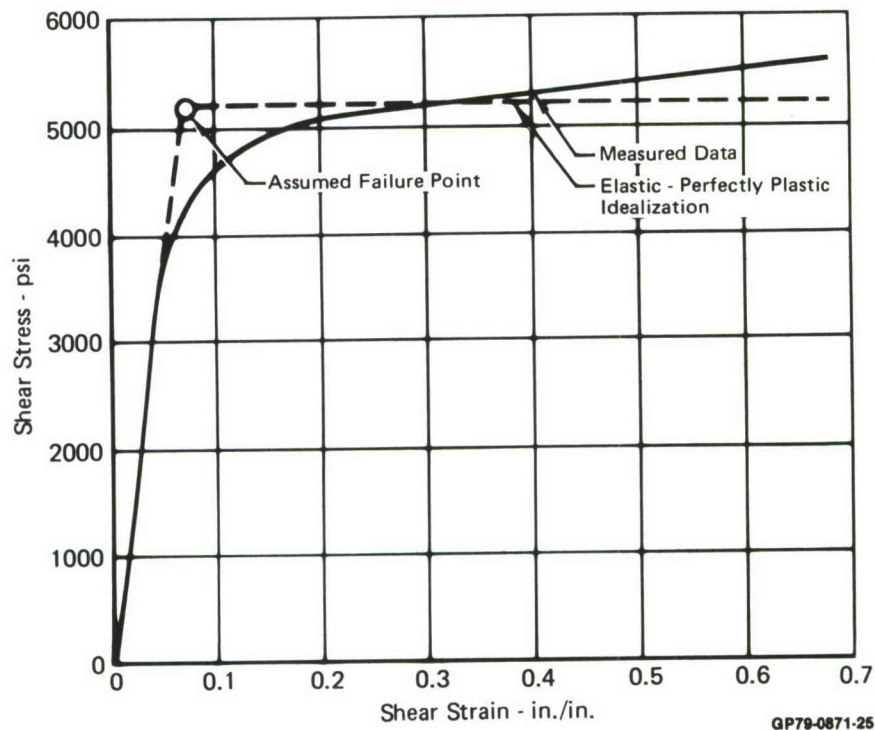


Figure 22. Measured and Idealized Shear Stress/Strain Curves

The strain transfer idealization for gages bonded to a test coupon is shown in Figure 21. The stepped free length of the gage was idealized as a constant thickness section (t_{eff} , Equation 9) continuously bonded to the supporting structure. Because adhesive stresses and strains are generally very small toward the middle of a doubler, modeling the section as bonded is not expected to significantly affect the results. For both test coupon and wing skin the carrier plate effective width was assumed to be 4 inches.

Results of the doubler analysis for a test coupon are shown in Figure 23 for a crack with a length 40 percent of the gage width. For a bond thickness of 0.004 inch (approximately the average thickness measured on the gage calibration specimens), about 0.024 in/in. shear strain is predicted at the edge of the actual gage bond length. This strain increases gage displacement beyond that in the carrier plate. This occurs because gage stiffness is greater in the bond area than in the free length, and the gage behaves as two bonded doublers with a weak link between them. Ends of doublers strain less than the carrier plate. Since the link is more easily strained than the doublers, it acquires more displacement than the carrier plate. Because the link stiffness decreases as gage crack length increases, the ratio of gage displacement to plate displacement increases as gage crack length increases. Typical results for gages bonded to a test coupon are shown in Figure 24.

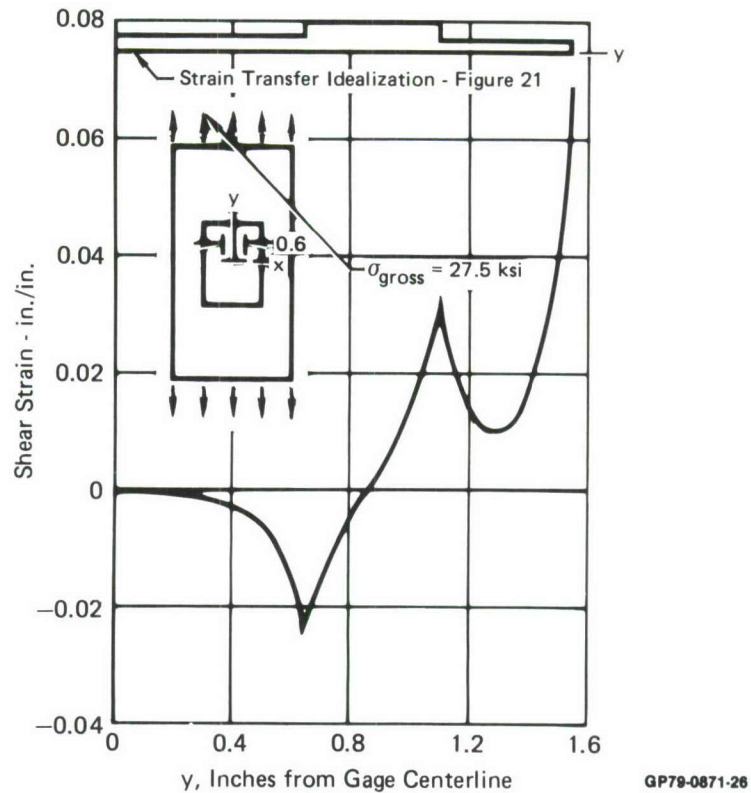


Figure 23. Typical Bond Shear Strain Distribution from Strain Transfer Analysis

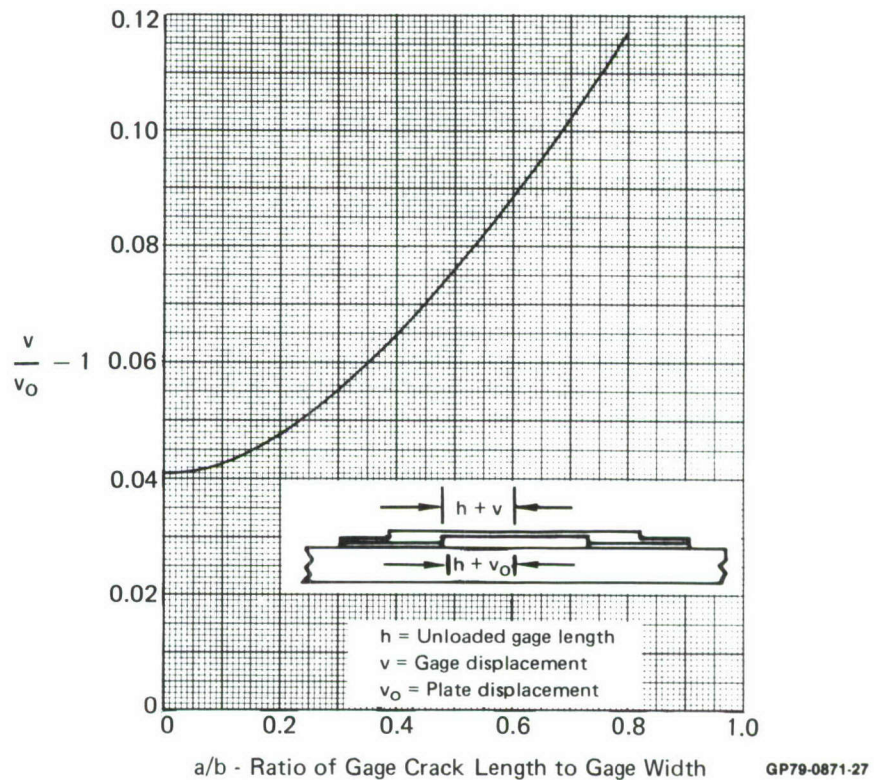


Figure 24. Strain Transmitted to Gage Increases with Gage Crack Length

Combining Equations (6), (10), and the bondline displacement relationship $\frac{v}{v_o}$ gives the following expression for gage stress in terms of stress σ applied to element test coupon.

$$\frac{\sigma_g}{\sigma_{app}} = \frac{\sigma_{gh}}{E_v} \times \frac{v}{v_o} \times \frac{E v_o}{\sigma_{app} h} \quad (11)$$

This relationship was used to derive stress intensity factors for the gage (Equation 4). The relationship of gage stress to carrier plate stress for the gage calibration specimen is plotted as a function of gage crack length in Figure 25.

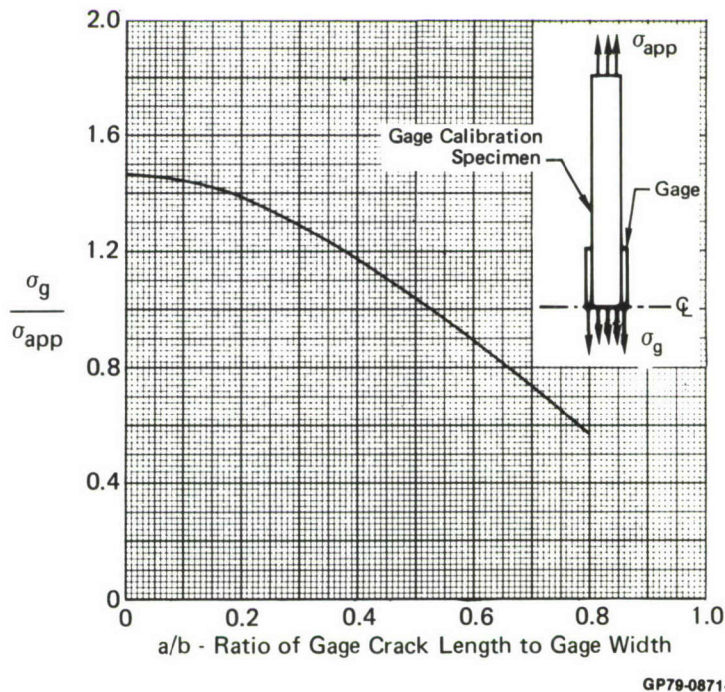


Figure 25. Nominal Relationship of Gage Stress to Stress in Gage Calibration Specimen

5. STRENGTH ANALYSIS - Analyses were performed for joint strength and gage buckling.

Early in gage design, chem-milling was selected as the preferred fabrication process because it was thought that mechanical machining might produce residual stresses on the surfaces of the gage which would adversely affect the gage crack growth behavior. One limitation of the chem-milling process was that a tapered joint of proper dimensions could not be obtained within the short lead time available for gage fabrication. Therefore, an analysis was performed to determine if an adequate stepped-lap joint could be obtained.

Joint strengths were computed using Hart-Smith's analysis routine (Reference 9) and the elastic-perfectly plastic shear stress-strain curve shown in Figure 22. The assumed plastic shear stress limit was selected so that the strain energy at ultimate strain for the idealized curve was equal to that for the measured stress-strain data. This results in an idealized adhesive which is somewhat stiffer than the actual adhesive, with a lower ultimate shear strength. The elastic analyses are based on the assumption that joint failure occurs when the maximum shear stress in the adhesive reaches the plastic limit. Basing the gage design on analyses using the high stiffness and low ultimate stress values should preclude any significant occurrence of plastic strains in the joint and result in a durable bond in room temperature, dry conditions. Parametric analyses for doublers having mid-section thicknesses twice that of the ends show that the optimum step length is about one half the bond length, Figure 26. Joint strength for this optimum step lap joint exceeds that for a tapered joint of the same overall dimensions. The optimum step length was used for the gage design.

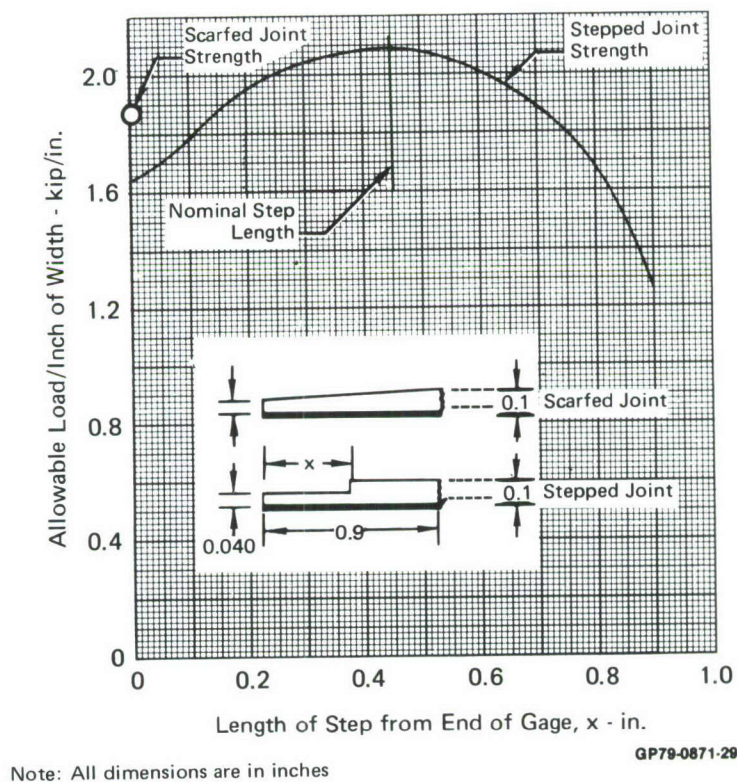
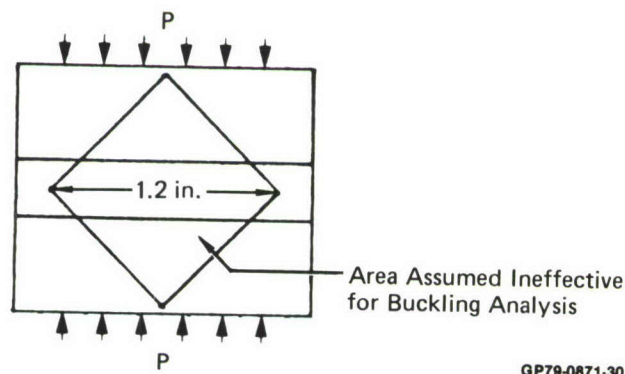


Figure 26. Impact of Step Length on Joint Strength

The gage load is 3000 lbs for a carrier plate stress of 35 ksi. The predicted joint strength using the conservative assumptions of adhesive stiffness and strength is 1.5 in. x 2.06 kip/in = 3090 lbs.

To determine the gage buckling load, an elastic beam column analysis was performed. In the analysis the gage was idealized as a fixed end column. The maximum useable crack length (1.20 inches) was assumed present in the gage. The load was assumed to shear around the flaw with the material inside a 45° line being ineffective. Therefore, as shown in Figure 27, a 1.20 inch diagonal square of material was considered ineffective. Even with this area considered ineffective, the buckling load of the gage is predicted to be 4800 lbs. This value is considerably greater than the maximum expected compression load, 1160 lbs., that occur with the gage applied to a F-4 lower wing. The maximum compression load corresponds to 12 ksi compressive stress in the structure.

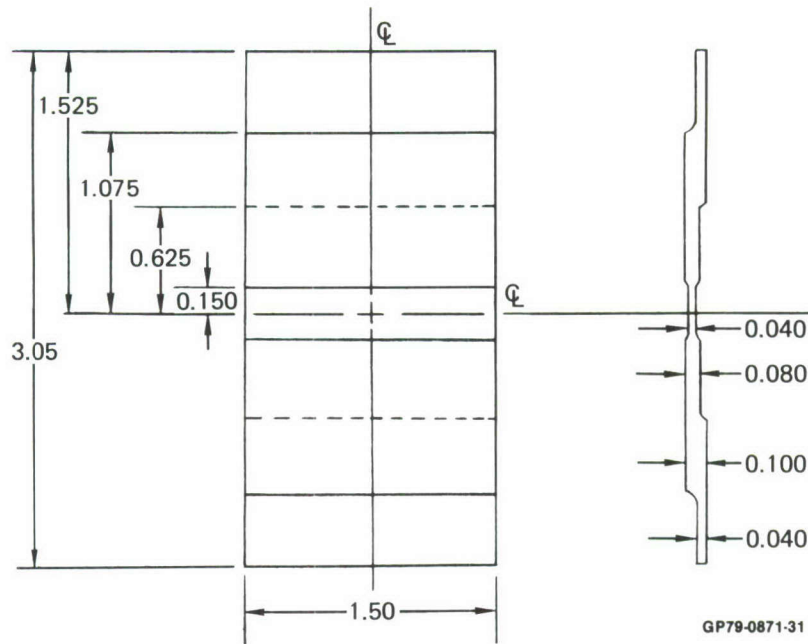


GP79-0871-30

Figure 27. Idealization Used for Buckling Analysis

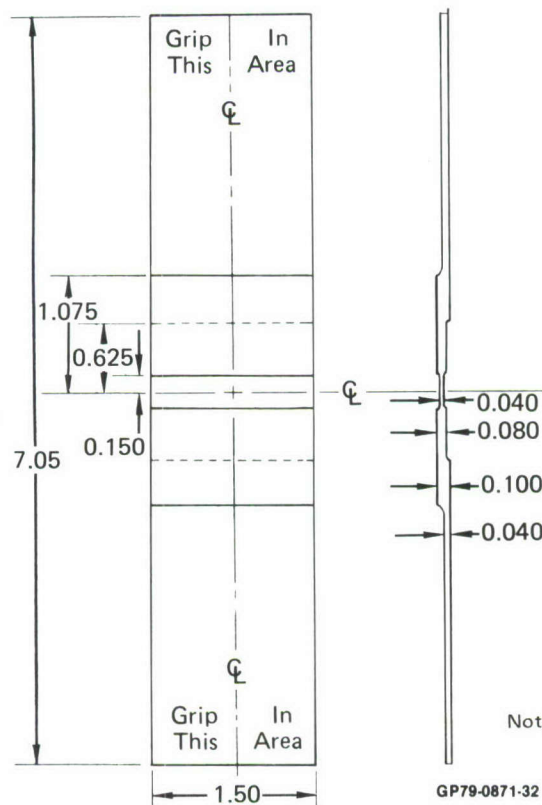
6. GAGE CONFIGURATION - The selected gage configuration is shown in Figure 28. The precracking configuration is shown in Figure 29. The initial flaw is an 0.050 inch diameter hole, saw cut equally on each side to 0.10 inch total flaw length. This flaw is then precracked under constant amplitude loading until the total flaw length is 0.20 inches. The grip areas are then removed.

7. EFFECTS OF MANUFACTURING TOLERANCES ON GAGE STRESS - In this evaluation manufacturing tolerances considered were length, width, and thickness variations of the stepped unbonded length of the gage. Adhesive joint tolerances included variations to joint step lengths and thicknesses, and adhesive modulus and strength. Installation variations included bondline thickness and gage orientation. Maximum variation from nominal gage stress is computed to be less than seven percent, and occurs with variations in step thickness.



Note: All dimensions are in inches

Figure 28. Selected Gage Configuration



Note: All dimensions are in inches

Figure 29. Precracking Configuration for Selected Gage

Gages were chem-milled from 0.125 inch thick 7075-T6 aluminum sheet. Figure 28 shows gage configuration and manufacturing tolerances. These tolerances were used to evaluate the impact of machining tolerances on gage stress. These tolerance evaluations were based on the same methodology used to compute the nominal gage stress, i.e., Equation (6) in Section 4. Gage stress was computed for maximum and minimum values of free length and width, and overall and step thicknesses.

The impact of gage free length and width tolerances on gage stress is summarized in Figure 30. The greatest effect occurs at the longest crack length and is calculated to be less than two percent. The impact of gage step length tolerance (Figure 31) is a little greater than length/width tolerances. Maximum variations from nominal stresses are computed to be less than three percent for crack lengths up to 70 percent of the gage width.

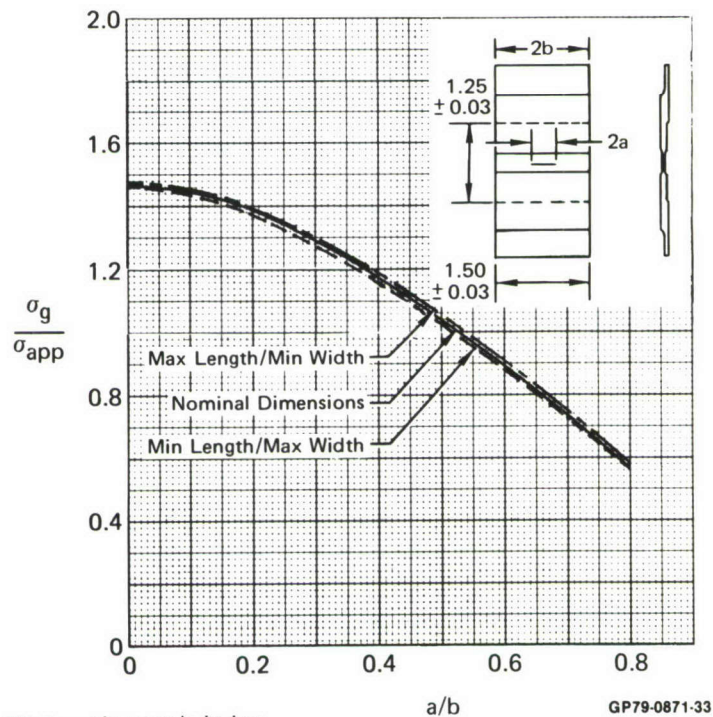


Figure 30. Impact of Free Length and Gage Width Tolerances on Gage Stress

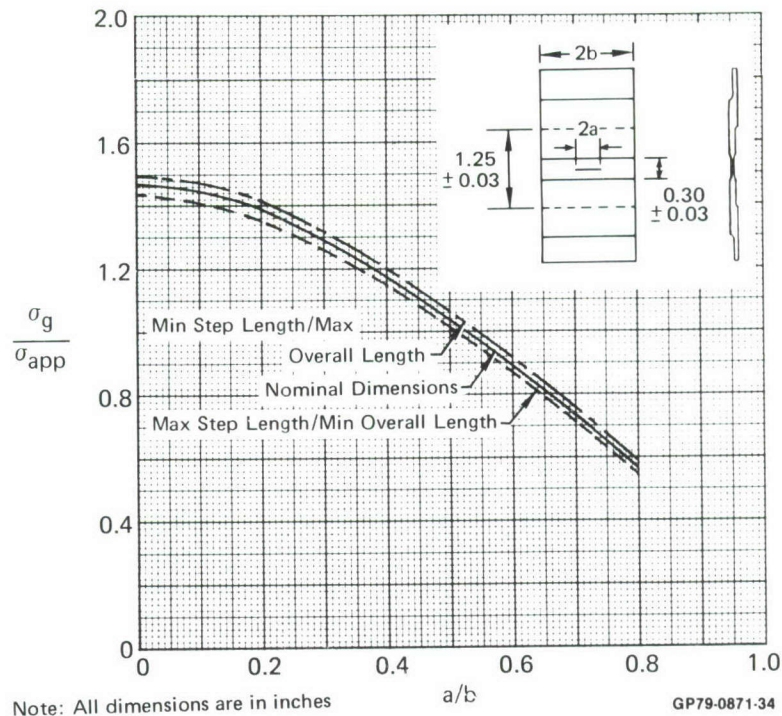
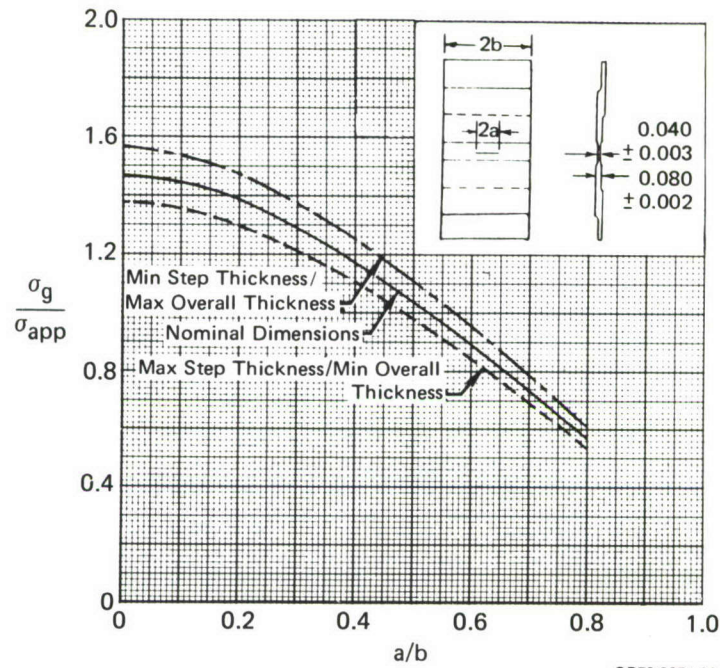


Figure 31. Impact of Step Length and Overall Length Tolerances on Gage Stress

Step thicknesses have the greatest impact on gage stress, (Figure 32). Maximum variations from nominal stress relationship are less than seven percent, and almost independent of crack length.

One of the most noticeable tolerance problems which occurred during chem-milling was step mismatch from back to front on the thin step shown in Figure 33. Step mismatches often occurred even though tolerances on step length were held on both front and back side of the gage. Step mismatches can cause a small increase in gage stress (Figure 34). Maximum mismatch within tolerances increases gage stress by less than one percent.

a. Effects of Adhesive Joint Variations on Gage Stress - Adhesive joint variations studied included step length and width tolerances and bondline modulus and strength variations. Adhesive joint variations were found to have little effect on gage behavior. Joint strength is not significantly affected by small variations from the nominal step length (Figure 26). Using maximum tolerances mismatches on joint step lengths or thicknesses results in less than 0.2 percent variation in gage stress.



Note: All dimensions are in inches

Figure 32. Impact of Step Thickness and Overall Thickness Tolerances on Gage Stress

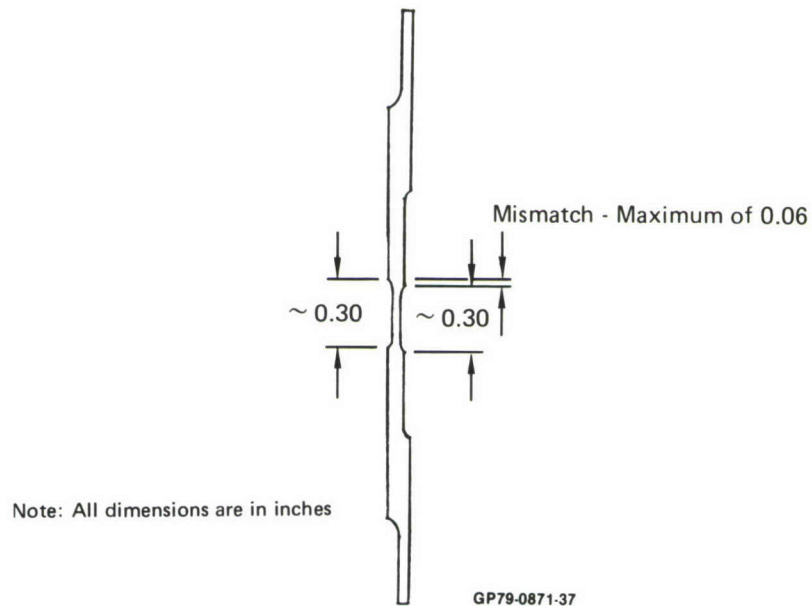


Figure 33. Step Mismatch from Front to Back

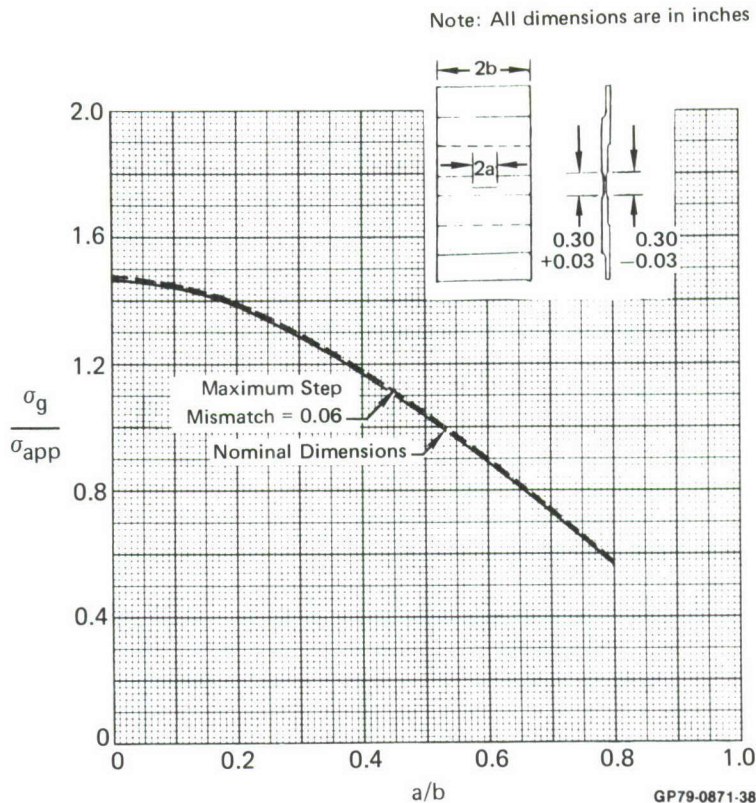


Figure 34. Impact of Step Mismatch on Gage Stress

To assess the impact of variations in adhesive modulus and strength, analyses were performed using modulus and strength data for FM-73 at temperatures of 160°F and -50°F in dry air. Preliminary design data was obtained from Reference 10 for room temperature, 160°F, and -50°F and was used to obtain properties for this analysis (Table 2). The impact of adhesive properties is less than one percent even under extreme conditions (Figure 35).

b. Effects of Gage Installation Variations on Gage Stress - Installation variations evaluated in this study include bondline thickness and gage alignment. Scrim cloth in the FM-73 adhesive film was used to control bondline thicknesses. Bondline thicknesses were measured after bonding and found to range from 0.002 inches to 0.0062 inches. The average thickness (0.004 inches) was used for prediction of nominal gage stress. The impact of adhesive thickness tolerance on the gage stress relationship (Figure 36) was less than three percent of the nominal gage stress.

TABLE 2. ADHESIVE PROPERTIES USED FOR PROPERTY VARIATIONS STUDY

Temperature	τ_p psi	G psi	γ_e	γ_p
70°F	5200	76,000	0.0686	0.68
-50°F	7300	91,200	0.0800	0.34
160°F	2630	60,800	0.0432	1.02

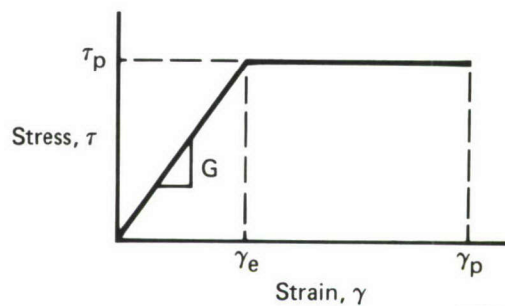
Notes:

τ_p is plastic limit shear stress

G is initial elastic shear modulus

γ_e is shear strain at plastic limit shear stress

γ_p is ultimate shear strain



GP79-0871-39

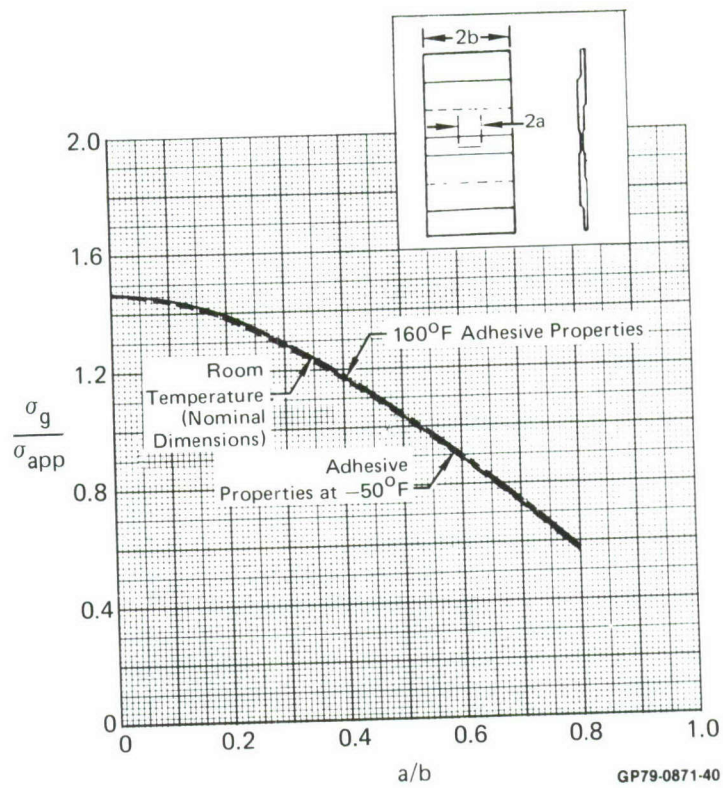


Figure 35. Impact of Adhesive Properties on Gage Stress to Element Stress Relationship

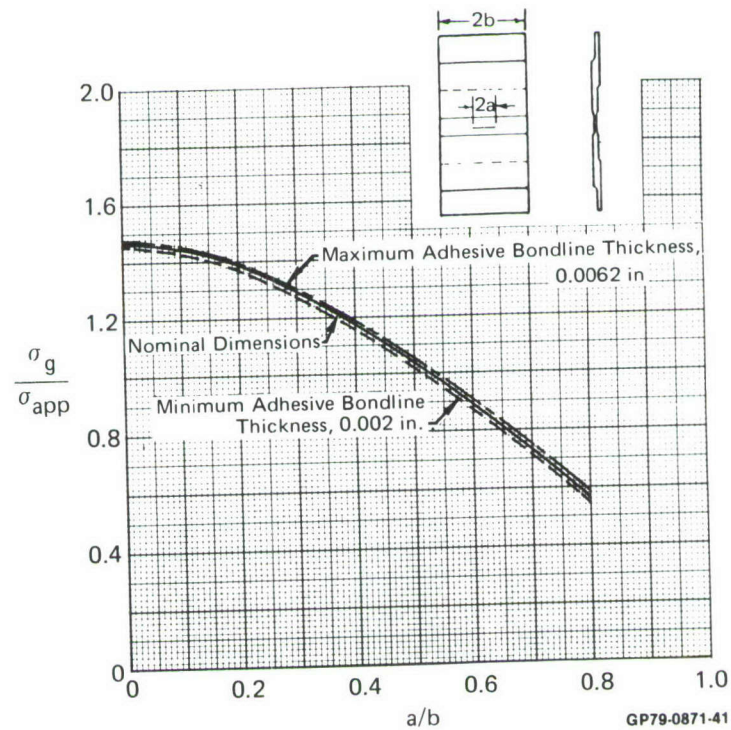


Figure 36. Impact of Adhesive Thickness Variations on Gage Stress

For small gage misalignments from the principal strain direction, the primary effect is reduction of gage axial stress. The reduction in axial stress is proportional to the square of the cosine of the angle of misalignment and is less than 0.8 percent at five degrees misalignment. Gage alignment with the principal strain direction of element coupons was not a problem. Maximum misalignment was less than five degrees. Crack growth in a gage having large misalignment with respect to the principal strain in the carrier plate is influenced by shear and bending in the gage as indicated in Figure 37.

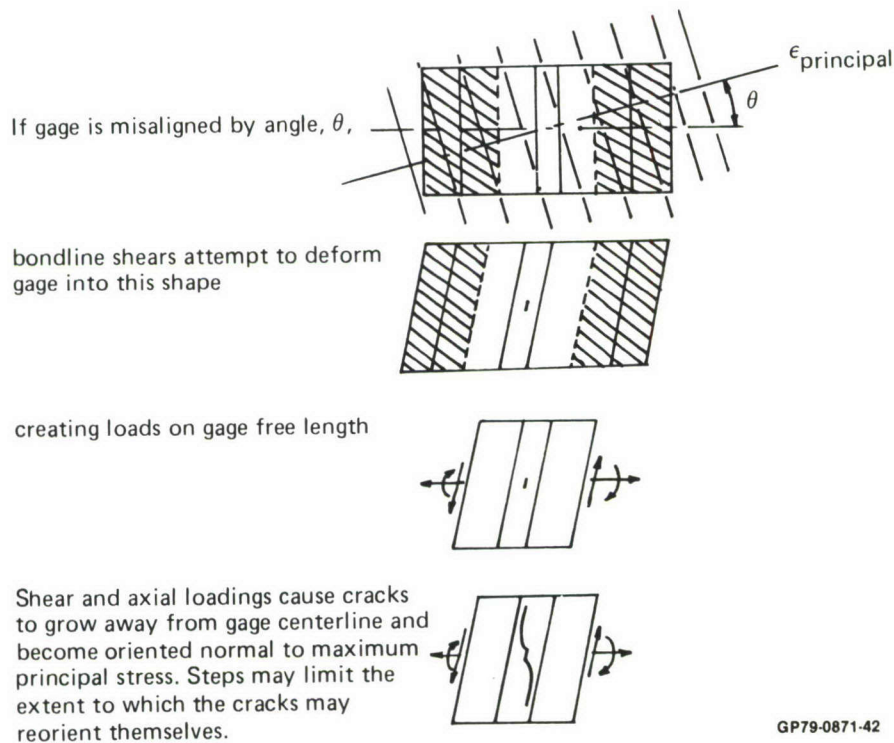


Figure 37. Effect of Gage Misalignment with Principal Strain Direction in Structure

SECTION III

GAGE ATTACHMENT

Adhesive bonding was used in this program to attach gages to test coupons and to the wing skins of the F-4 test article. FM-73 adhesive was selected based on strength, durability, service environment, and cure temperature considerations. A standard field repair surface treatment and bonding technique was used. While bonding to test coupons was successful, bonding to the F-4 fatigue test article was beset by problems. On the first attempt the adhesive was not cured at a high enough temperature. On the second attempt the adhesive was properly cured; however, the additional heating evidently broke down the silicone-based adhesive used for load pad attachment. Silicone, which is a release agent for FM-73 adhesive, was absorbed by that adhesive during the bonding, causing it to fail upon application of load to the test article. Gages were subsequently bonded to the test article using a room temperature cure adhesive, EA9309.1, and half of the gages remained bonded through 4000 spectrum hours of testing.

The silicone problem was peculiar to the fatigue test article. However, other difficulties encountered demonstrate that more research is required to produce gage bonds which can endure service environments and loading conditions.

1. ADHESIVE SELECTION - Adhesive bonding offers a good potential for transferring a reproducible and predictable amount of load from the component to the gage. The attachment will not degrade the structural integrity of the attached component, and is adaptable to many applications. An adhesive was selected according to three requirements. The first was that the strength and modulus of the adhesive must be capable of producing the desired load transfer characteristics. The second was that the adhesive should be capable of surviving exposure at the peak service temperature while maintaining adequate mechanical properties. The third requirement was that exposure to stress-humidity cycles should not degrade the bond to the extent that service failures are experienced.

The best combination of strength, temperature resistance, and environmental durability is given by state of the art epoxy film adhesives. These adhesives can be applied with vacuum bags and thermostatically controlled heat blankets for the in-the-field bonding.

American Cyanamid's FM-73 was selected for this program based on its capability to give better quality bonds than higher cure temperature adhesives when applied with a vacuum bag. FM-73 was used in the Primary Adhesively Bonded Structure Technology (PABST) program. Mechanical property data on this adhesive was obtained from that program. Results of adhesive joint analyses such as

those presented in Figure 38 indicate that elastic joint strengths obtained with FM-73 adhesive are nearly the same as those obtained with FM-300 or FM-400, both requiring higher cure temperatures.

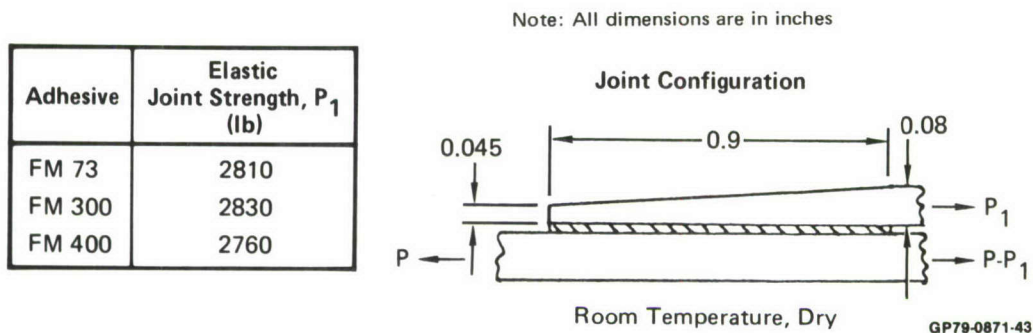


Figure 38. Major Adhesive Systems Give Same Elastic Joint Strengths

The maximum operating temperature of FM-73, as used by MCAIR, is 180°F. This is approximately the same as the peak service temperature of transport aircraft (hence, its use in the PABST program). Analysis of a typical mission profile for an F-4 indicated that maximum wing skin temperatures would be around 110°F experienced during ground static conditions. Wing skin temperatures during a maximum velocity dash could reach nearly 255°F. However, data from Reference 11 show that less than 0.5% of flight hour life time would involve conditions producing wing skin temperatures approaching this maximum. These infrequent high temperatures may require a reevaluation of available adhesive systems prior to installation on fleet aircraft. However, the ability of FM-73 to provide superior in-the-field bonds may outweigh its strength at temperature limitations and make it an acceptable adhesive system for bonding the gages to fleet aircraft.

2. SURFACE PREPARATION - The metal surface treatment utilized before attaching the gage is important for successful bonding. Surface treatment affects bond durability, however, it does not affect load transfer characteristics. A traditional surface preparation for aluminum is abrasion, followed by solvent wiping, Pasa Jell 105 treatment, and a decomped water rinse. This treatment is a standard for field repair.

For this program, with limited access to the bonding surface, the Pasa Jell 105 (PJ105) treatment was used. The PJ105 treatment gives performance equivalent to the phosphoric acid anodize (PAA) for non-environmental tests. If future tests indicate that the environmental performance of PAA is superior to PJ105, it could be substituted without affecting load transfer characteristics. For the current program, the interference of whiffletrees and load pads coupled with MCAIR experience with PJ105 made this treatment more desirable for surface preparation of the test wing.

The gages were treated with sulfuric acid and sodium dichromate primed with primer BR-127. This surface treatment is standard for F-4 and F-15 aircraft.

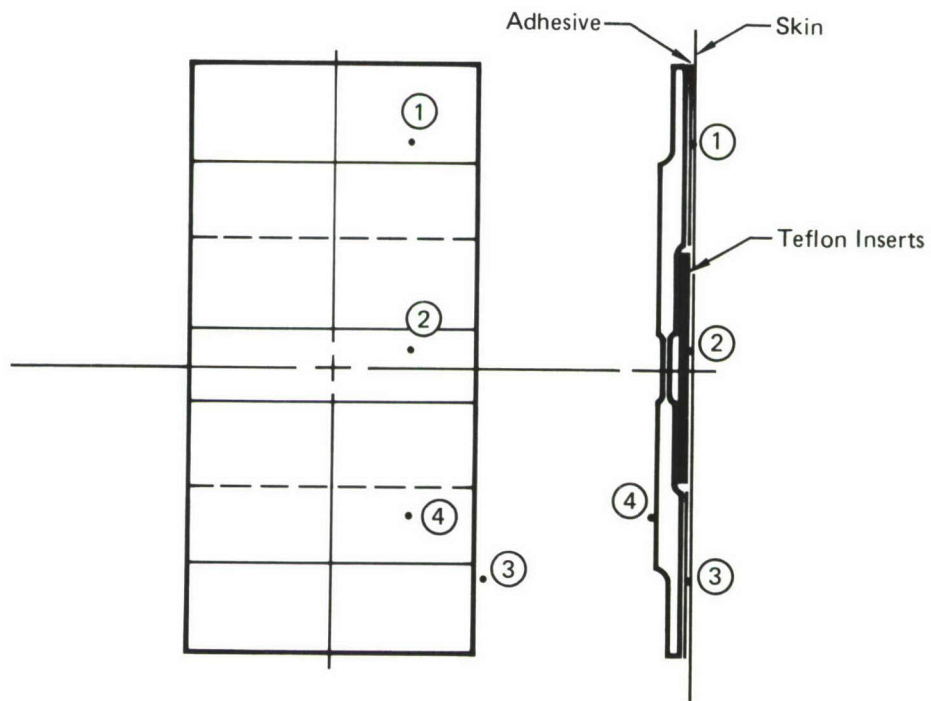
Bonding surface treatments were applied after pre-cracking the gages to prevent contamination of the bonding surfaces in the pre-cracking operation. Drilled holes and induced cracks were masked to prevent attack by surface treatment solutions which might affect crack growth. Corrosion inhibiting primer (BR-127) was applied to crack gage bonding surfaces immediately after surface preparation to simulate preparation for application in the field. Permissible delay before bonding is 14-21 days.

3. GAGE BONDING - Gages were bonded to the test coupons using vacuum bags for pressure and an autoclave for heating. Teflon pads were placed beneath the unbonded length of gage to preclude bonding in that area and to reduce gage bending under load. Test coupons were anodized to the same specifications as the wing skins to determine if special care was required to remove such anodize. One series of specimens had to be rebonded because the anodize was not sufficiently removed, however, generally bonds to test coupons provided the predicted load transfer throughout each test.

To develop a procedure for bonding crack growth gages to F-4 lower wing skins using FM-73 adhesive, gages were bonded to an F-4J fatigue test article at MCAIR. The first gage bonding test was performed to simulate conditions used earlier during unsuccessful bonding of gages to the F-4 fatigue test article at Wright-Patterson AFB. The second bonding test was performed to determine whether the proper adhesive temperatures could be maintained using wing skin temperatures as control. The third bonding test was performed to measure wing skin temperatures near the bond area during the cure cycle.

In the first bonding test a gage was bonded to the left hand lower wing skin near the junction of the main spar and torque rib at B.L. 44.5. Thermocouples were located as shown in Figure 39. The vacuum bag bonding technique shown in Figure 40 was applied using two 4 inch x 5 inch heating blankets over the gage.

Temperatures measured during the first bonding test are presented in Table 3. This test simulated the conditions used earlier to bond gages to the F-4 test article at Wright-Patterson AFB. The maximum temperature obtained in the adhesive was 170°F, insufficient to properly cure FM-73. First attempts to bond gages to the AFFDL fatigue test article were performed by maintaining 250°F at thermocouple location 4, for one hour. Adhesive temperatures apparently were about 150-160°F. This explains the improper cure obtained at that time.



GP79-0871-44

Figure 39. Crack Growth Gage - Thermocouple Locations for Bonding Tests

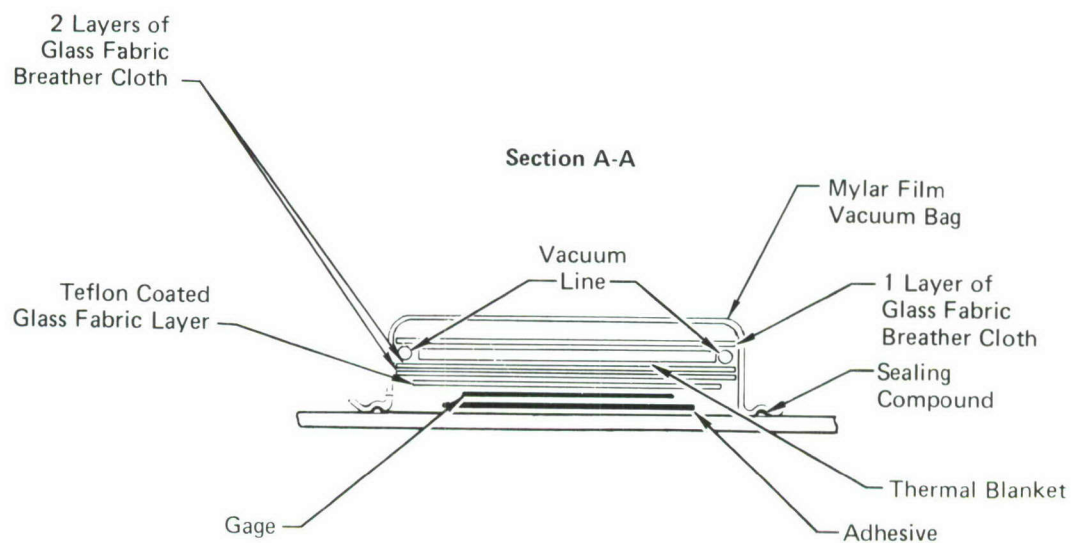
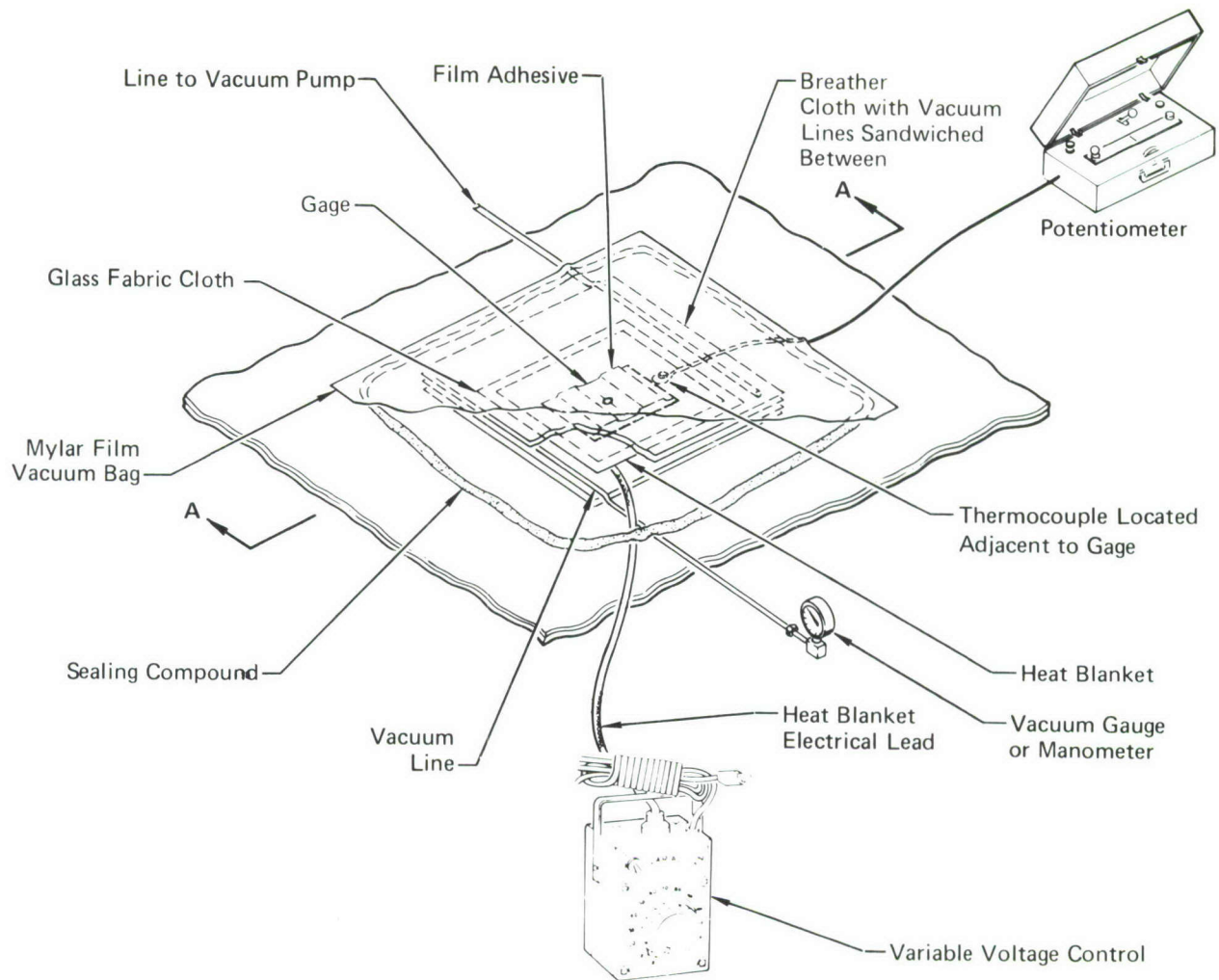


Figure 40. Gage Bonding Technique

GP79-0871-45

TABLE 3. TEMPERATURES RECORDED DURING FIRST BONDING TEST

Elapsed Time (min)	Thermocouple Locations ⁽³⁾ - °F			
	1	2	3	4
0	100	100	80	80
5	155	125	195	255 ⁽⁴⁾
10	160	—	200	265
15	165	130	200	265
25	170	130	220	290
35	170	132	225	292

Notes:

1. Gage bonded to F-4J fatigue test article left hand lower wing skin near main spar and torque rib at BL 44.5
2. Gage bonding performed using two 4-in. x 5-in. heating blankets in vacuum bag
- (3) Locations shown in Figure 39
- (4) Temperature used at Wright-Patterson AFB, 25 - 27 July 1978

GP79-0871-46

To determine if the adhesive could be heated to the 250°F required for proper cure, a second bonding test was performed with a single four inch by five inch blanket applied over the gage and two 1 foot square blankets also applied, offset so that the edges were two inches or more away from the spar and rib fastener patterns. All blankets were enclosed in a vacuum bag. Temperatures recorded during heating are presented in Table 4. The test indicated that 250°F could be obtained with this technique. The adhesive cured under this combination of heating cycles.

To check the use of wing skin temperatures as a control for adhesive temperatures, a third bonding test was performed by bonding a gage at a location 7.8 inches forward of the main spar fastener pattern at B.L. 100 on the lower right hand wing skin. Because temperatures measured at thermocouple location 3 on the wing skin were nearly the same as those measured in the adhesive, this location was used to control bonding measured in the adhesive. To determine the temperature gradient near the gage during bonding, thermocouples were taped to the wing skin at 2 inch intervals toward the main spar, as shown in Figure 41.

The cure cycle includes a half hour heating to the control temperature, one hour to 1.5 hours at temperature, followed by a half hour cool down. Temperatures measured at each thermocouple location are presented in Table 5. The control temperature used was 300°F at thermocouple location 1, Figure 41. The maximum temperatures obtained are plotted in Figure 42. Temperatures exceeded 200°F up to seven inches from the center of the gage. This cure cycle resulted in a properly cured adhesive.

TABLE 4. TEMPERATURES RECORDED DURING SECOND BONDING TEST

Elapsed Time (min)	Thermocouple Locations ⁽³⁾ - °F			
	1	2	3	4
0	123	115	129	—
5	137	125	230	250
7	175	—	—	290
9	205	—	—	—
10	220	185	275	320
15	240	200	290	350
20	250	210	295	355
25	255	—	—	—

Notes:

1. Gaged bonded to F-4J fatigue test article left hand lower wing skin near main spar and torque rib at BL 44.5
2. Gage bonding performed using one 4-inch x 5-inch heating blanket and two 1 foot square heating blankets offset away from fastener pattern - all within vacuum bag
- (3) Locations shown in Figure 39

GP79-0871-47

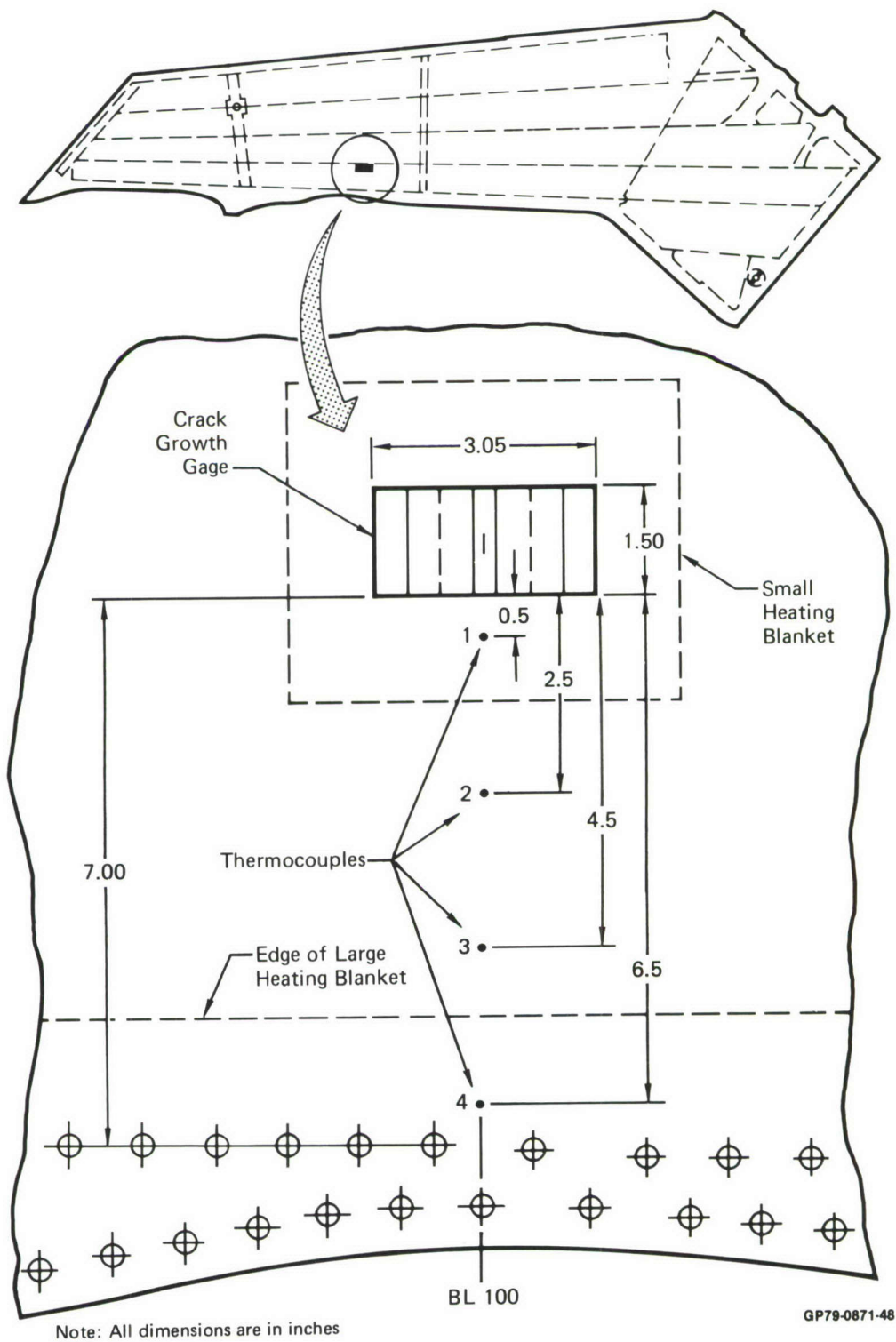


Figure 41. Thermocouple Locations for Third Bonding Test

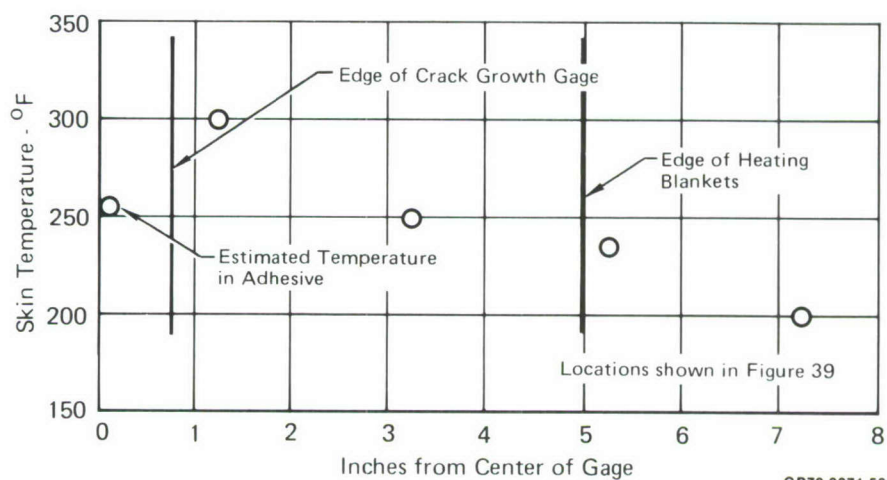
TABLE 5. TEMPERATURES RECORDED DURING THIRD BONDING TEST

Elapsed Time (min)	Thermocouple Locations ⁽³⁾ - °F			
	1	2	3	4
0	110	110	112	113
2	160 ⁽⁴⁾	—	—	—
3	165	—	—	—
8	185	155	142	130
13	198	—	—	—
15	210	—	—	—
18	220	175	165	143
20	240	—	—	—
23	260	205	190	157
25	280	—	—	—
28	300	230	210	173
30	305	—	—	—
33	310	—	—	—
48	305	250	228	192
68	300	250	232	195
78	310	—	—	—
88	300	255	235	200
103	300	250	235	200

Notes:

1. Gage bonded to F-4J fatigue test article right hand lower wing skin near main spar at BL 100
2. Gage bonding performed using one 4-inch x 5-inch heating blanket and two 1 foot square heating blankets - all within vacuum bag
- (3) Locations shown in Figure 41
- (4) Variac turned up too high, cut back at this time

GP79-0871-49



GP79-0871-50

Figure 42. Maximum Temperatures Recorded During Third Bonding Test

The procedure used in the third gage bonding test was used to bond crack growth gages to the F-4 fatigue test article at Wright-Patterson AFB. The elevated skin temperatures associated with this bonding procedure required precautions and controls to prevent residual stress relaxation near taper-loks and cold-worked holes.

Skin temperatures measured during the adhesive cure cycle can reach 300°F. According to MIL-HDBK-5C, pg. 3-260, holding 300°F for 1.5 hours in 7075-T651 aluminum then returning to 80°F results in about a one percent decrease in F_{ty} and F_{tu} . This is of little concern. However, during the cure when 300°F is held for an hour or more, the yield strength is less than 79 percent of the room temperature yield strength (pg. 3-262, MIL-HDBK-5C). There is concern that this reduction in yield strength at temperature could reduce the residual compressive stresses near taper-loks and cold-worked holes on which fatigue life improvement depends. The original compressive stress field would not be recovered when the skin was cooled to room temperature and fatigue lives could be reduced.

To prevent relaxation of compressive stresses near taper-loks and cold-worked holes, gage bonding was performed such that temperatures near such areas were held to a maximum of 200°F. This temperature results in less than a 10 percent reduction in yield strength at temperature.

To ensure temperatures near taper-loks and cold-worked holes are held to a maximum of 200°F, crack growth gage locations (center of gage) were selected to be at least 7.5 inches from the nearest fastener pattern.

SECTION IV

GAGE SITE SELECTION

Criteria for selection of locations for attaching crack growth gages to the F-4C/D full scale fatigue test article were based on gage size, predicted behavior, and bonding technique. The selected crack growth gage design covers an area about 3 in. by 1.5 in. This gage design was originally predicted to produce approximately one inch of crack growth in 12,000 spectrum hours of testing. The gages were bonded using a vacuum bag and heating blankets, requiring some care in gage location to preclude overheating areas having beneficial residual stresses, thereby relieving such stresses and reducing structural fatigue life.

1. CRITERIA - The primary gage sites were located on the lower wing skin. Based on the gage configuration, predicted behavior, and bonding procedure, several criteria for site selection are evident:

- o Sites should be near fracture critical areas.
- o Sites should experience about 30 ksi limit stress level.
- o Sites should avoid high stress gradients, fastener patterns, taper-loks, and load pads.

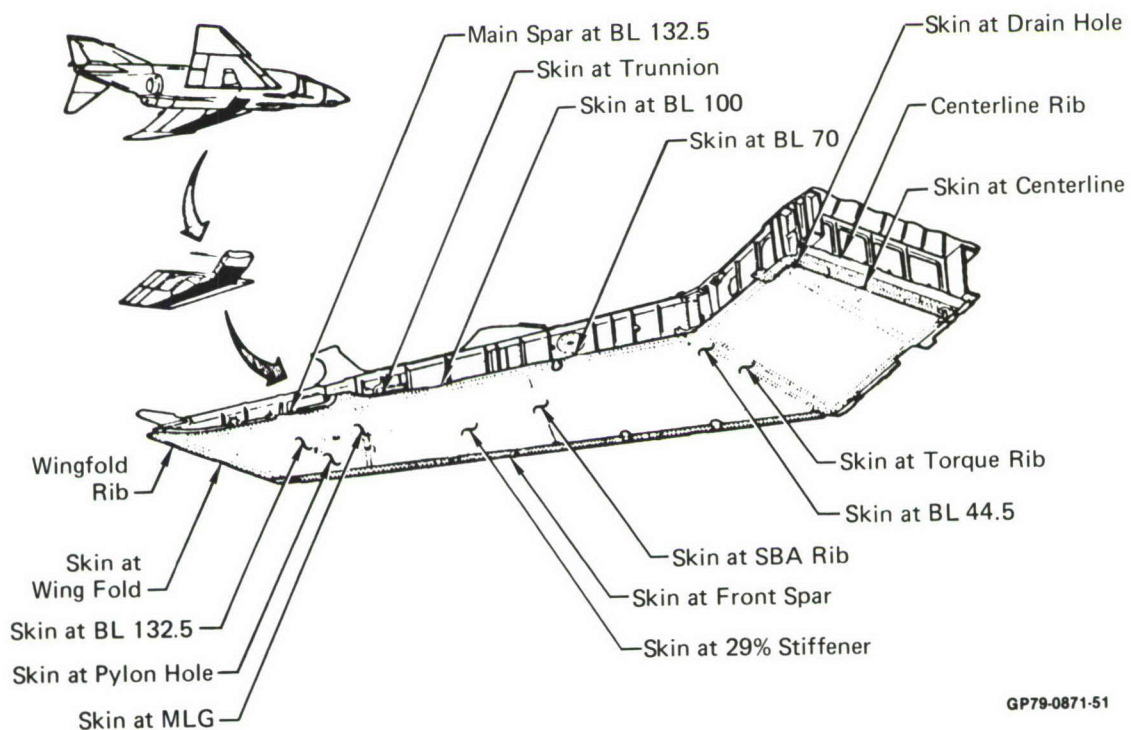
Sites should be near fracture critical areas so that the stress histories experienced by the gages will be similar to those experienced by the fracture critical areas.

The full scale fatigue test was scheduled to undergo 12,000 spectrum hours of testing following the 4,000 hour modifications. To obtain the maximum possible gage crack growth in that time, wing skin areas experiencing limit stress levels of 30 ksi were selected.

Areas near high stress gradients and concentrations were avoided for two reasons. First, the gage behavior would be sensitive to position and alignment in such areas. This could lead to aircraft to aircraft variability in gage response if the gage were applied to fleet aircraft. Second, areas immediately adjacent to the gage will receive some heating during the bonding cure cycle. Heating to 350°F can cause relaxation of plastic strains in high stress concentration areas and reduce beneficial residual stresses near taper-loks which are used in such areas on the F-4 lower wing skin. This would have a detrimental effect on airframe fatigue life. The 250°F cure cycle used for FM-73 should not cause substructure heating problems but bonding near areas having cold-worked holes or taper-lok fasteners should be avoided. Fastener patterns in general were avoided because of the local strain distributions they create.

An extensive strain survey of the lower skin was performed prior to fatigue testing the Air Force test aircraft. Results of that survey were useful for validation of stress history. Therefore the gages were applied in areas near those which were strain surveyed.

2. PRIMARY GAGE SITES - Fracture critical areas of the F-4 aircraft were identified in F-4 ASIP studies (Reference 12). Areas on the lower inner wing skin are shown in Figure 43. Three locations were selected as primary gage sites. These sites are on the right hand lower wing skin of the F-4C/D fatigue test article, identified in Figure 44. They are just forward of the main spar at BL.44.5, BL.100, and BL.132.5. All three of these locations were found in F-4 ASIP programs to produce fatigue cracks either in service or in test, Reference 12.



GP79-0871-51

Figure 43. Fracture Critical Areas of Lower Wing Skin Identified in F-4 ASIP program

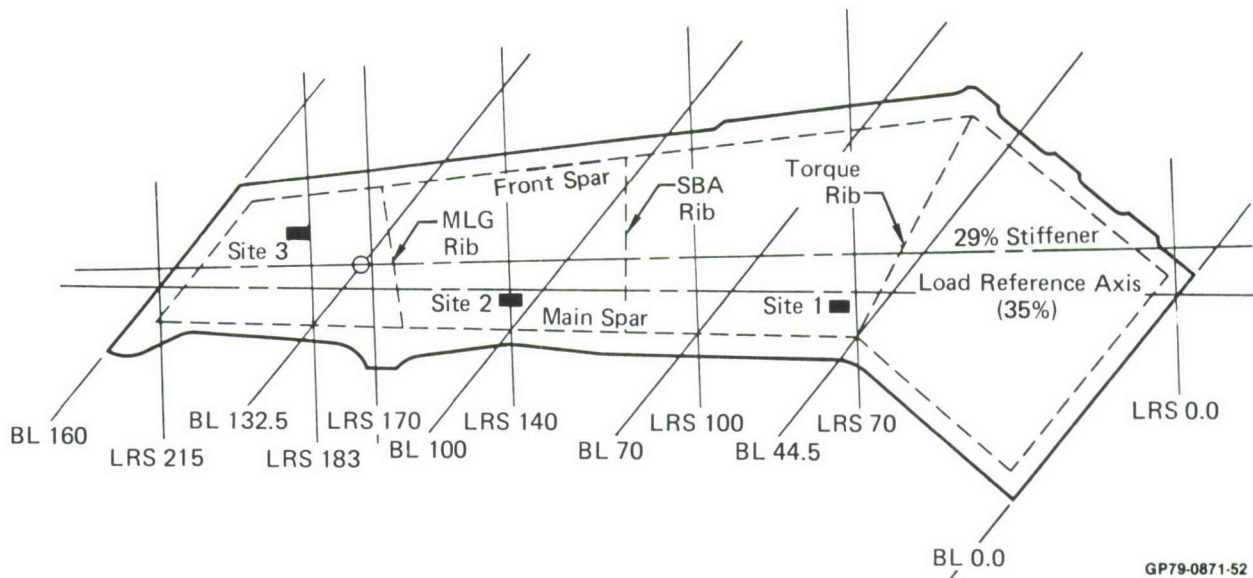
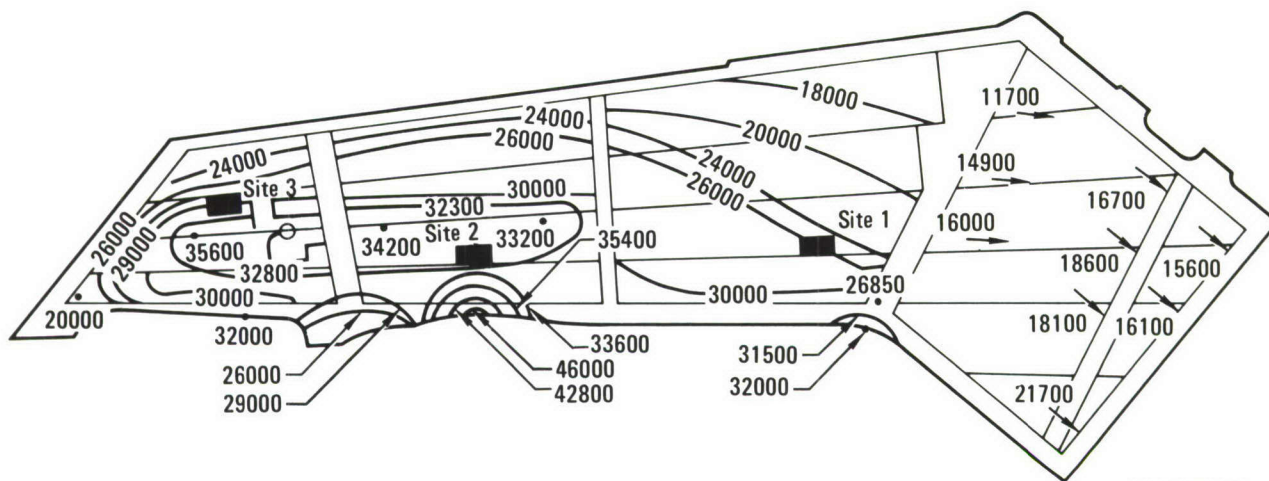


Figure 44. Primary Gage Sites

Each of these locations has a stress level at limit load of about 30 ksi (Figure 45). BL.100 has a slightly higher stress level, between 32.3 ksi and 33.6 ksi at limit load. Stress spectra, normalized by limit stress, are very similar in shape as shown in Figure 46. The locations are identified in Figures 47 and 48, and are close to strain gaged areas. The strain gage data permitted verification of the stress history used to predict crack growth gage behavior. The load pad location drawing shown in Figure 47 indicates that the gage locations are at least 3 or 4 inches away from the nearest load pad. Figure 48 indicates the proximity of the gages to taper-loks and fastener patterns in the skin. In selecting the gage locations shown, at least 7.5 inches of clearance between the gage and the nearest taper-lok was maintained.

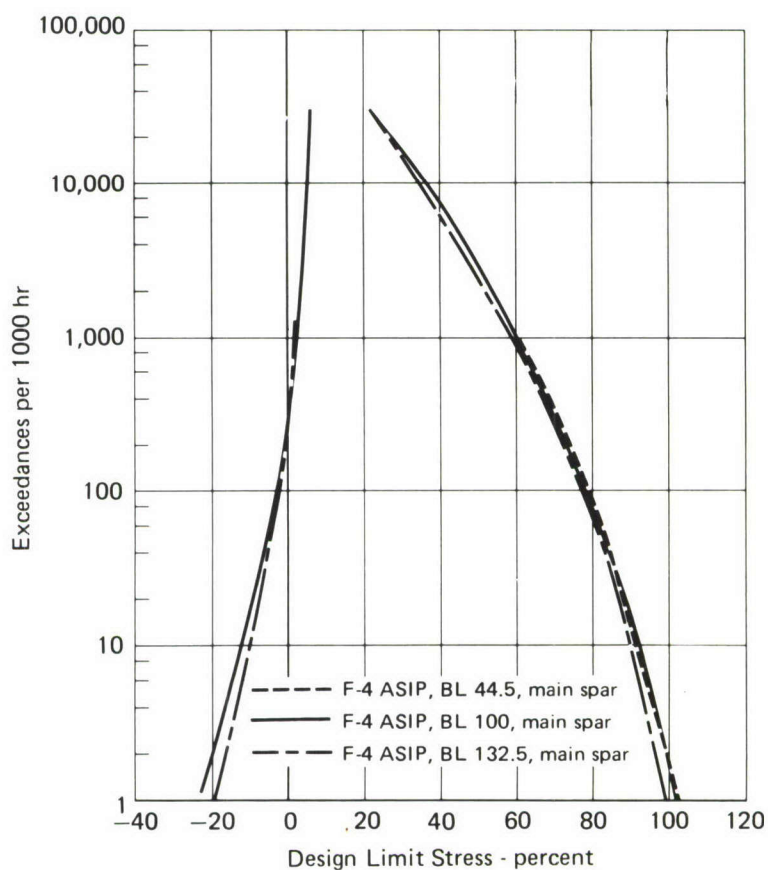
The fourth gage location duplicated the BL.100 location on the left wing skin. This location has produced some fatigue crack originations on other test articles after 4,000 spectrum hours.

3. ADDITIONAL GAGE SITES - After the four original gages disbonded, the areas and gages were cleaned and a total of eight gages were bonded to the lower wing skins using the room temperature cure, EA9309.1 adhesive. The room temperature cure allowed bonding of gages at B.L. 132.5 and B.L. 44.5 much closer to rib and spar fasteners than the original sites. The location of the eight crack growth gages are identified in Figure 49.



GP79-0871-150

Figure 45. Relationship of Primary Gage Sites to Stress Contours on Lower Wing Skin



GP79-0871-55

Figure 46. Lower Wing Skin Stress Spectra

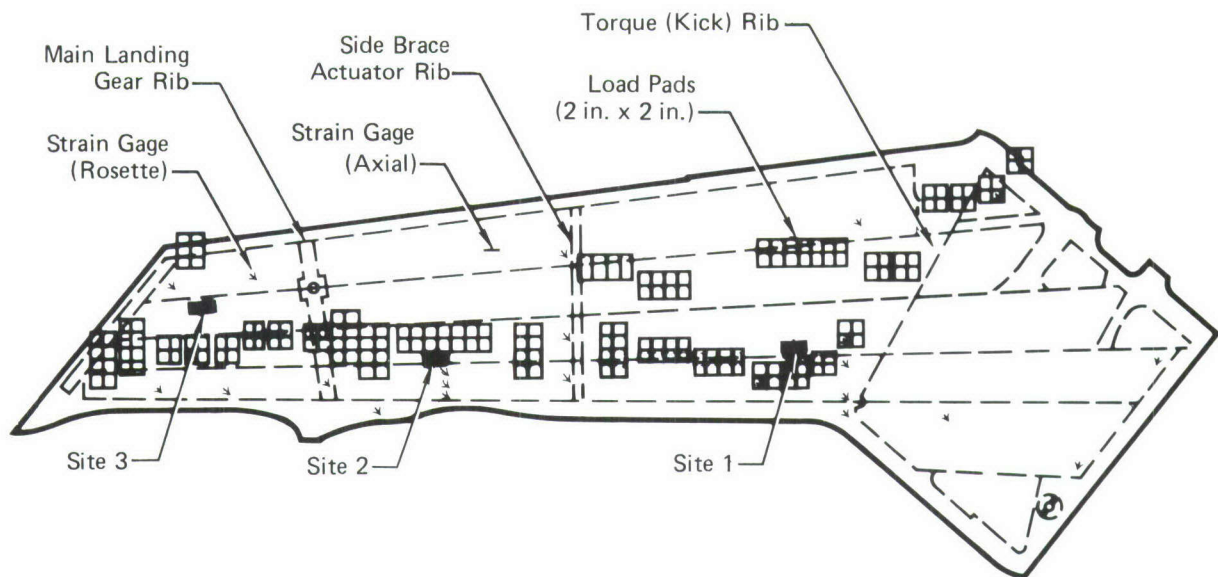


Figure 47. Relationship of Gage Sites to Load Pad Locations on Lower Wing Skin

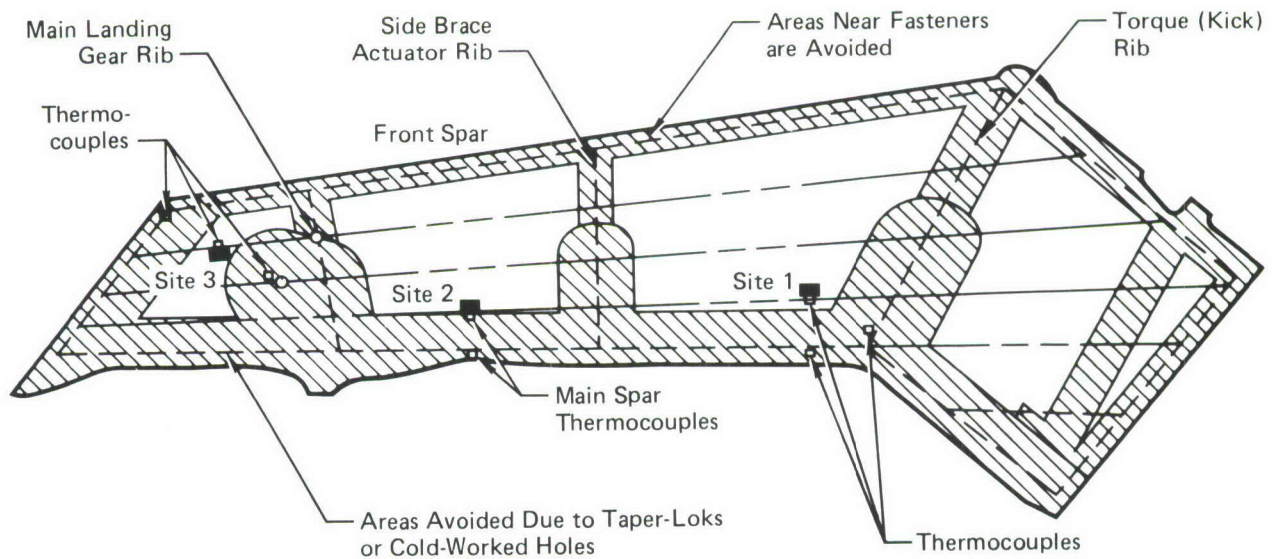


Figure 48. Gage Sites and Thermocouple Locations

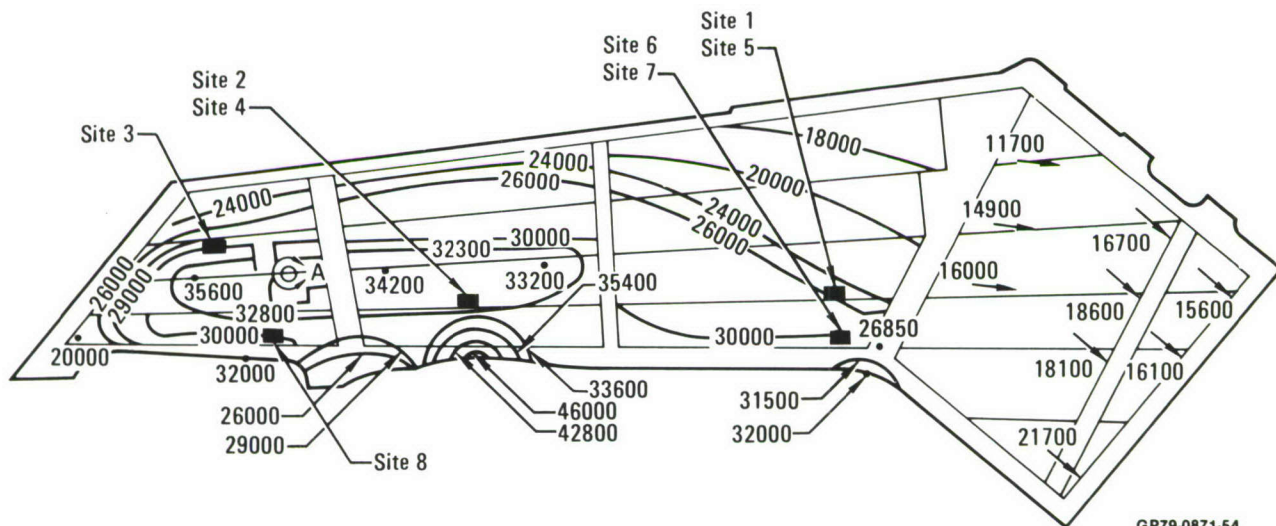


Figure 49. Location of Primary and Additional Gage Sites Relative to Stress Contours on Lower Wing Skin

4. OPTIONAL WING SITES - Six additional wing skin sites were identified as options to the primary sites. To determine locations of these sites it was assumed that the same gage geometry and bonding techniques would be used. Consequently the criteria for defining the optional sites were the same as those for the primary sites, Section 2. None of the optional gage sites were selected for gage attachment.

Six optional gage sites were selected on the right hand wing skin of the F-4C/D fatigue test article as shown in Figure 50. These sites correspond to the remainder of the fracture critical areas of the wing skin shown in Figure 43 (Section 2). All of these areas have experienced cracking during earlier fatigue tests, as noted in Reference 12. Any of the primary or optional gage sites could be duplicated on the left hand lower wing skin as additional optional sites.

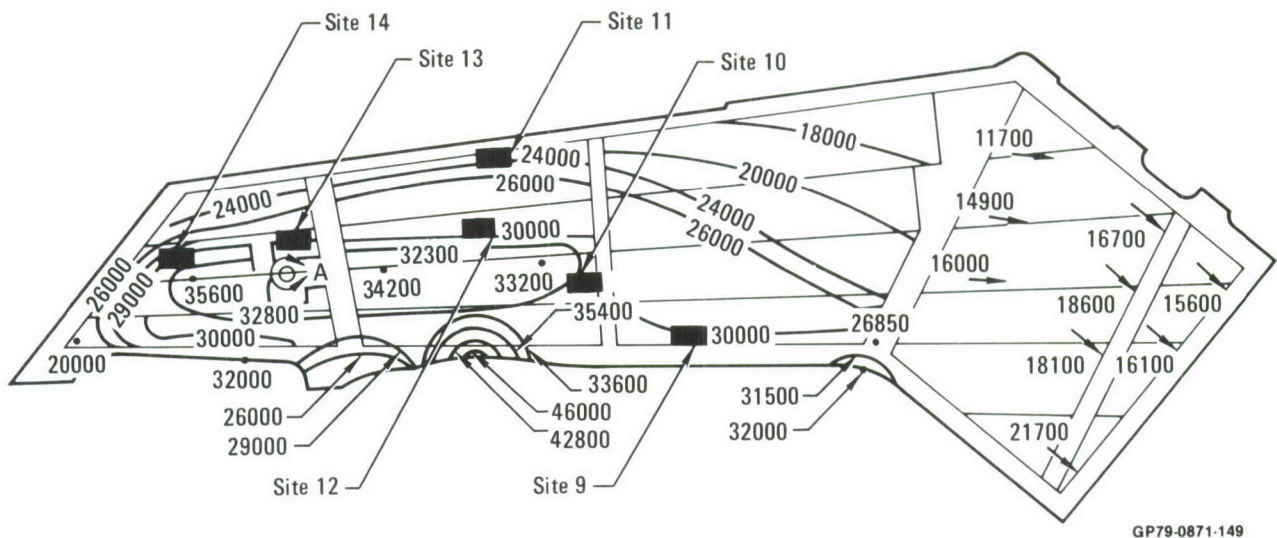
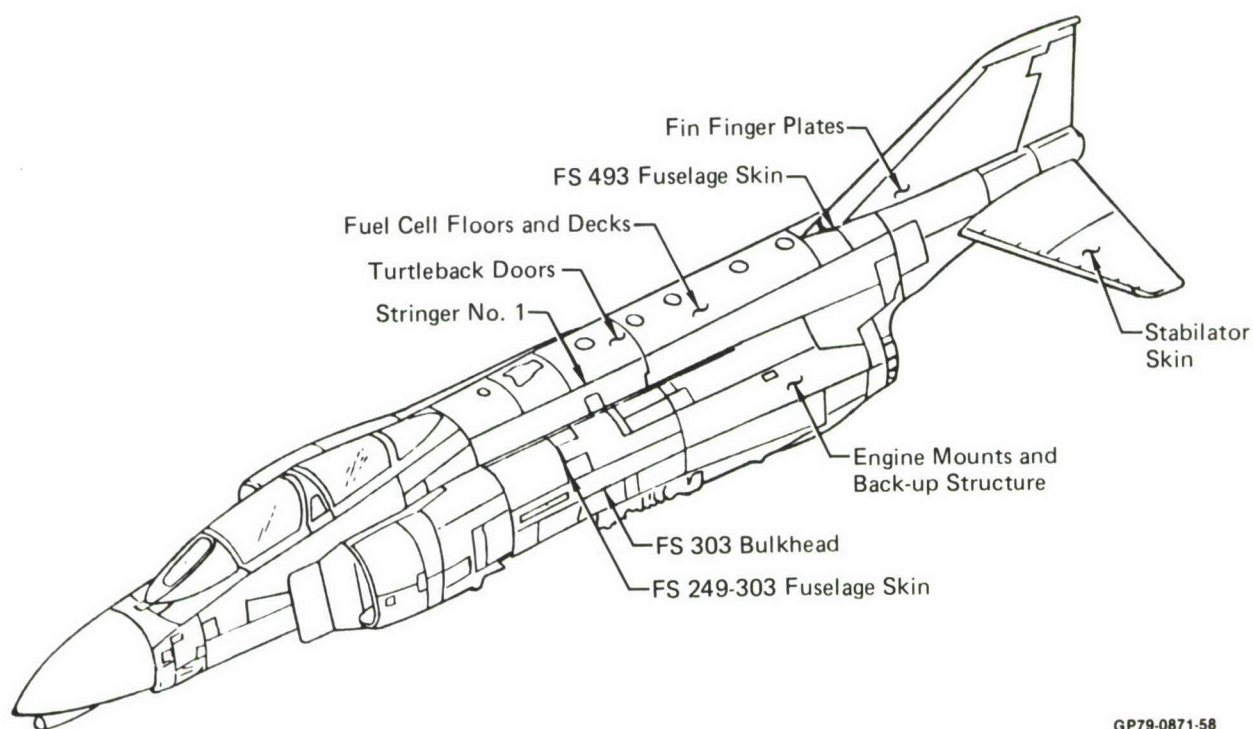


Figure 50. Optional Gage Site Areas Have Limit Stress Levels from 24 to 30 KSI

Optional wing sites need not be located on the lower wing skin. A potential gage location is the main spar web at BL.100. This site is accessible through the main gear well, and experiences a stress history similar to that of the skin at BL.100, one of the primary fracture critical locations of the F-4. However, since at least a 2 inch clearance is required to bond the gage to structure, the centerline of the gage would be near the wing neutral axis, reducing the limit stress level to about 11 ksi - too low to be of value with this gage configuration. For this reason, and because the stress gradient across the gage would add difficulty to crack growth prediction, this location and other non-mold line sites were not recommended for gage application.

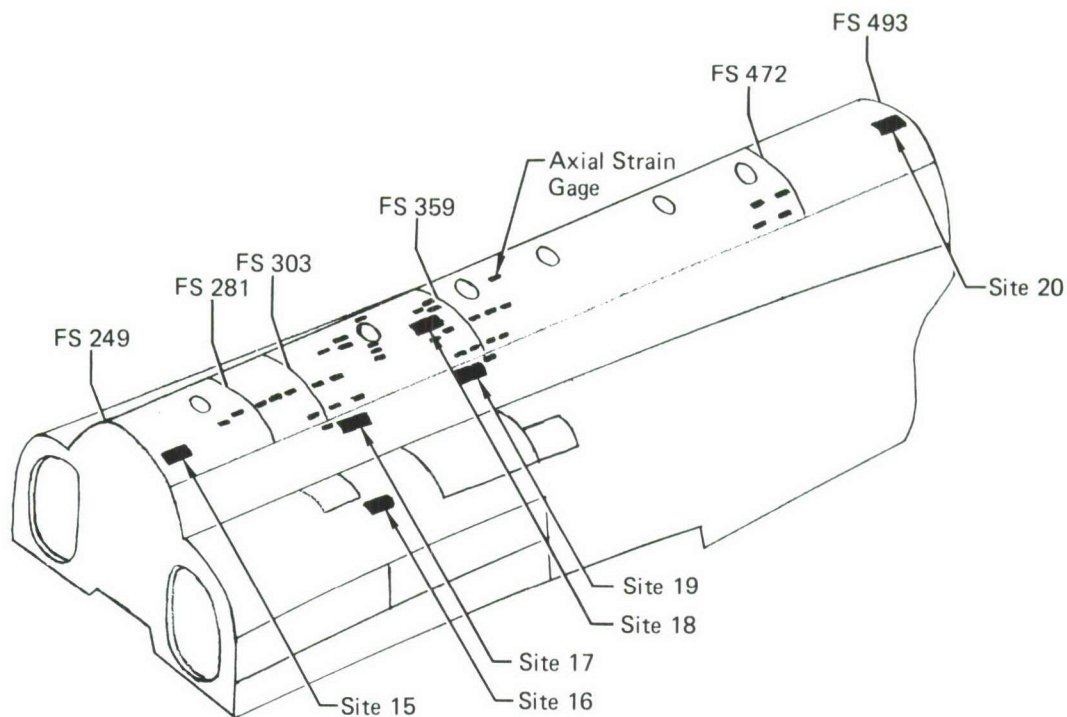
5. OPTIONAL NON-WING SITES - Six non-wing gage sites were identified using the criteria presented in Section 2. Since there are neither stabilators nor rudder on the fatigue test article, non-wing sites were restricted to fuselage locations. Stress levels in the fuselage skins are generally somewhat lower than in wing skins (less than 15 ksi in fuselage skins as compared to 30 ksi in wing skins). Using the current gage configuration, which is designed for 30 ksi limit stress level, the crack growth during 12,000 spectrum hours will be considerably reduced at limit stress levels less than 20 ksi. By adjusting the step sizes and lengths, it is possible to redesign the gage to provide better crack growth behavior at 10-15 ksi limit stress levels.

Fracture critical areas of the F-4 fuselage are shown in Figure 51. Six sites for crack growth gage application were selected for these areas and are shown in Figure 52. Only one of these areas has a history of cracking in service. Cracks have developed on seven aircraft in less than 500 service hours near gage site 16. The remaining sites have developed cracks during various fatigue test programs. Cracks have developed at Site 15 only in the F-4E(S) fatigue test program. Analysis shows the area to be fatigue critical for the F-4C/D aircraft also.



GP79-0871-58

Figure 51. Fatigue Critical Fuselage Areas Identified in F-4 ASIP program



GP79-0871-59

Figure 52. Optional Fuselage Gage Sites Selected from Fracture Critical Areas

Gages are not easily bonded at several fracture critical areas of the fuselage. Fuel cell wall, floors, etc. and FS303 bulkhead areas are not accessible for gage application or monitoring.

SECTION V

COMPARISON OF ELEMENT TEST AND ANALYSIS RESULTS

The majority of tests were intended to determine the crack growth behavior of the gage. The test program is summarized in Table 6 and consists of tests for material characterization, load transfer to the gage, gage calibration under constant amplitude and spectrum loadings, and gage validation under spectrum loading. The test specimens are shown in Figures 53-57.

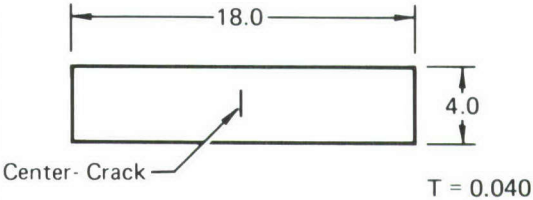
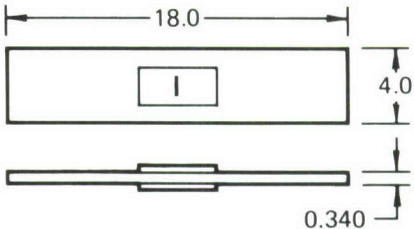
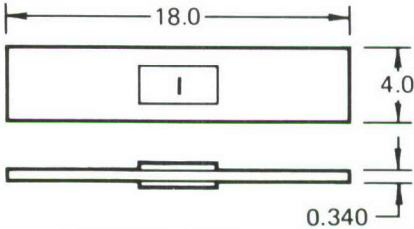
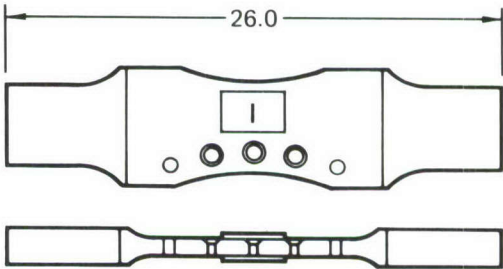
Crack growth analyses of the gage under both constant amplitude and spectrum loading were performed using the Contact Stress model, References 6-8, except as noted. The stress intensity factor solution was presented in detail in Section II. The baseline crack growth rate data is presented in the following section. Test results for center cracked panels of several thicknesses were used to modify the Contact Stress model to account for the greater crack growth retardation caused by thin sheets.

1. MECHANICAL PROPERTY AND BASELINE CRACK GROWTH DATA - In the element test program, three forms of 7075-T6 aluminum were used. These include 0.125 inch sheet used for gage fabrication, 0.5 inch thick plate (T651) used for specimen fabrication, and F-4 wing skin plate (T651) used for BL.44.5 specimen fabrication. Measured mechanical properties are presented in Table 7. Test specimens used are shown in Figures 53 and 54. Average values show good agreement with MIL-HDBK-5C values (Table 8).

To determine the crack growth rate behavior of the gage material, the center cracked panel specimens shown in Figure 55 were tested under quasi-constant amplitude loadings. Tests were performed in duplicate at stress ratios of 0.02 and 0.5 to determine the baseline crack growth rate data ($R = 0.02$), scatter, and effect of stress ratio (R) on growth rate. The sheet material was chem-milled to 0.04 inch thickness to simulate as closely as possible the material in the cracked ligament of the crack growth gage. Stress levels used for these tests, as a function of crack length are shown in Table 9.

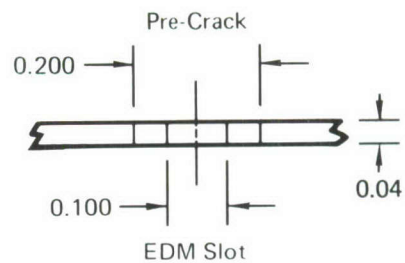
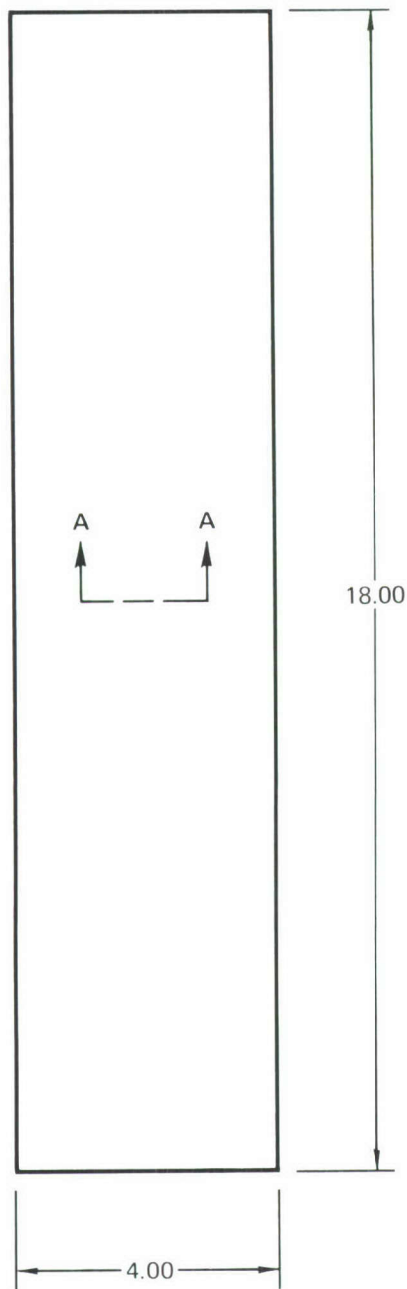
Crack growth rate data for both tests of the gage material at $R = 0.02$ are shown in Figure 58. The data indicates very little scatter. Also shown is the curve fit used for all subsequent crack growth analyses. Crack growth rate data for $R = 0.5$ is presented in Figure 59 for both tests. Scatter in these results is so small that it is difficult to see the points from the second test. The crack growth rates for the 0.5 stress ratio were predicted using a plane stress assumption in the Contact Stress model. The predicted rate is close to the data.

TABLE 6. TEST PROGRAM SUMMARY

Test Series	Number of Specimens	Test Purpose	Test Specimen
1	4	Measure da/dN of the lot of material used in gage manufacture	
2	5	Measure load transfer characteristics of gage in order to interpret crack growth behavior. Gages on one specimen were precracked.	
3	4 11	Gage calibration, constant amplitude loading Gage calibration, spectrum loading	
4	4	Validation of ability of gage to track spectrum loading	
Total	28		

Note: All dimensions in inches.

GP79-0871-53



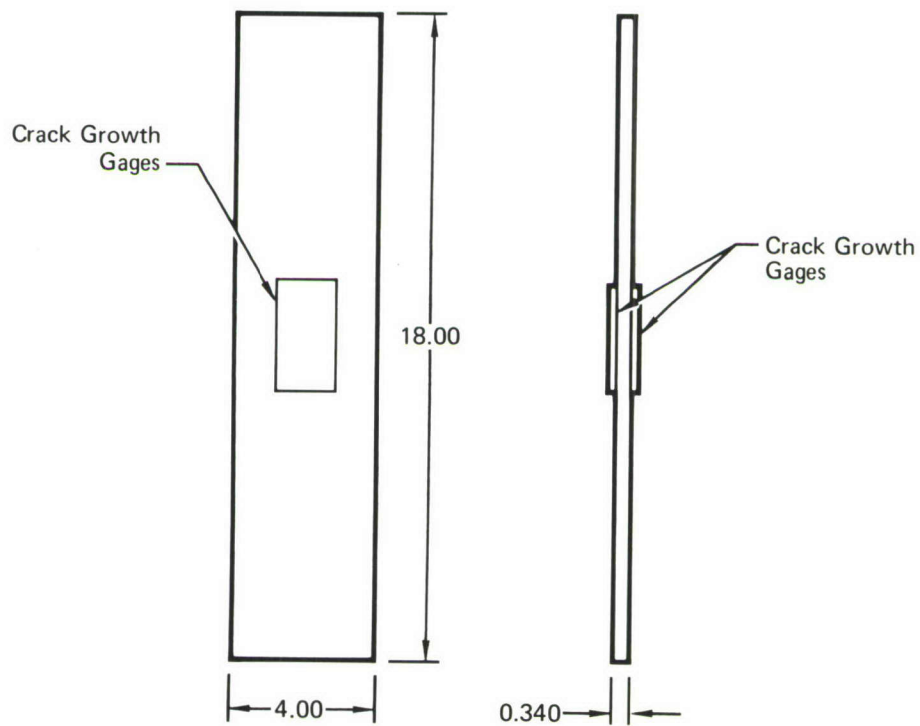
Details of
EDM Starter Slot
and Fatigue Pre-Crack

Section A-A

Note: All dimensions are in inches

Figure 55. Center Crack Panel Specimen

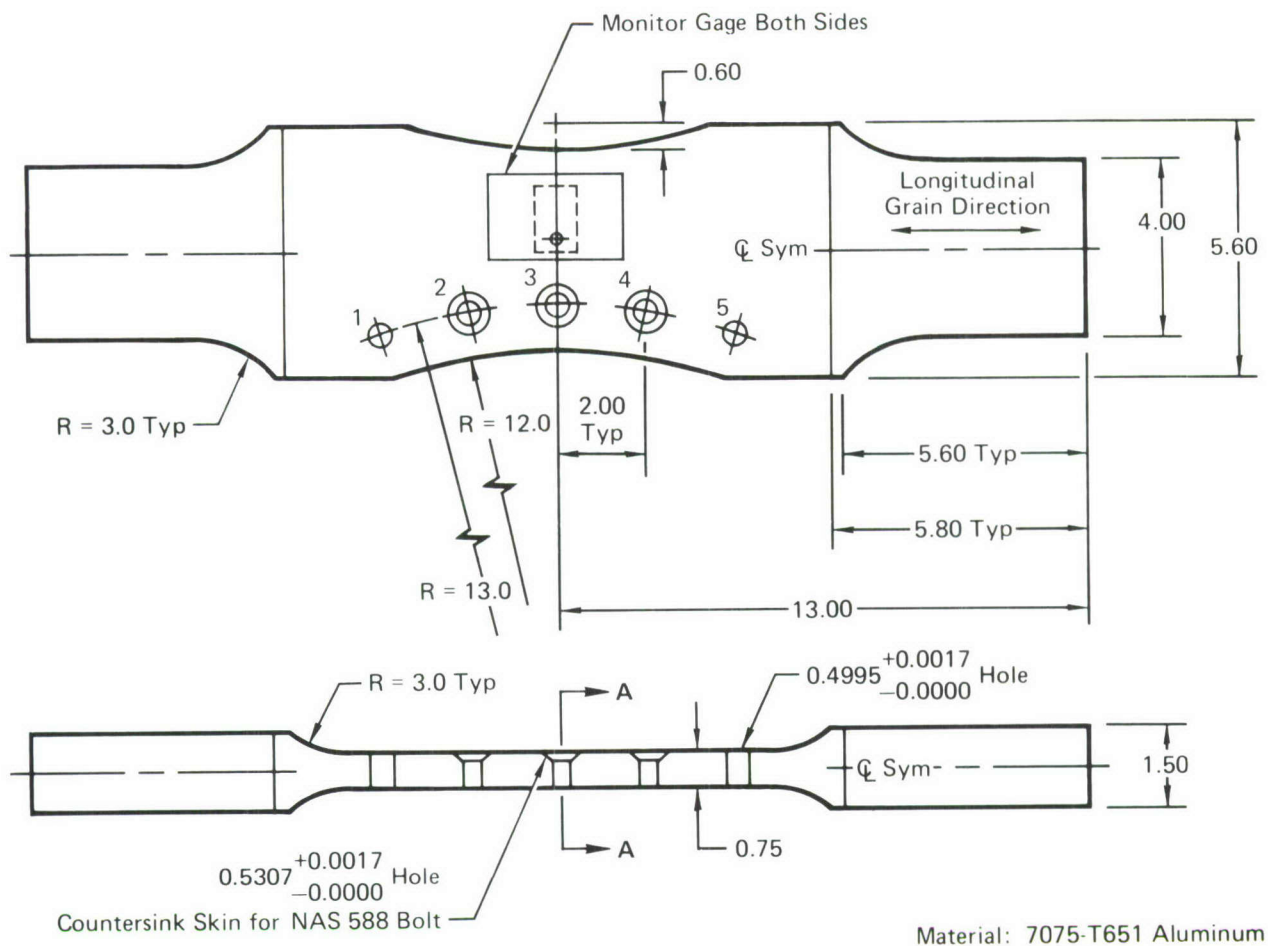
GP79-0871-62



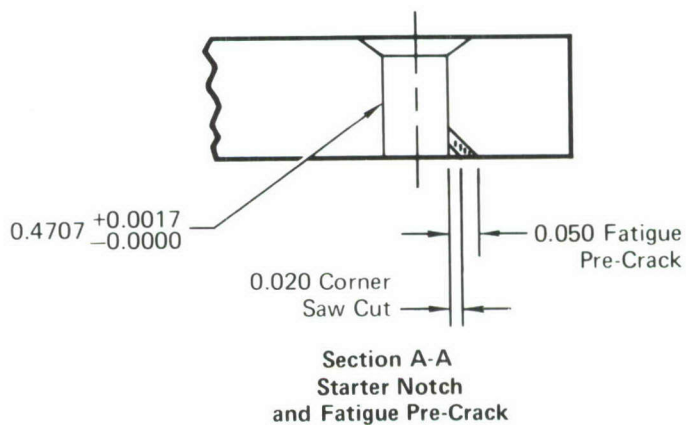
Note: All dimensions are in inches

GP79-0871-63

Figure 56. Crack Growth Gage Calibration Specimen



After Fatigue-Pre-Cracking
Pilot Hole was Reamed to
0.5307^{+0.0017}_{-0.0000} Leaving 0.020
Pre-Crack for Subsequent
Testing. Holes 1, 2, 4 and 5
were Drilled After Pre-Cracking.



Note: All dimensions are in inches

Figure 57. F-4 BL 44.5 Lower Wing Skin Element Fatigue Specimen

GP79-0871-64

TABLE 7. TENSILE TEST RESULTS

Specimen Type	Material	Specimen Number	Yield Strength (ksi)	Ultimate Strength (ksi)	Percent Elongation	Percent Reduction of Area	Modulus of Elasticity (psi x 10 ⁶)
Flat Tensile Specimen Figure 53	0.125 Inch Thick 7075-T6 Sheet Used for Gage Fabrication	1	73.0	79.0	7	NA	9.8
		2	75.5	80.0	6	NA	11.0
		3	75.5	81.5	8	NA	10.0
		Average	74.7	80.0	7	NA	10.3
Round Tensile Specimen Figure 54	0.5 Inch Thick 7075-T651 Plate Used for Specimen Fabrication	1	77.0	84.0	15	34.8	10.6
		2	77.5	85.0	14	32.4	9.8
		3	77.5	84.5	14	32.4	9.8
		Average	77.5	84.5	14	33.2	10.1
	7075-T651 F-4 Wing Skin Plate	1	73.5	83.5	9	17.5	10.1
		2	73.5	84.5	10	15.6	10.3
		Average	73.5	84.0	10	16.6	10.2


GP79-0871-65


TABLE 8. COMPARISON OF AVERAGE MEASURED TENSILE PROPERTIES WITH DESIGN PROPERTIES FROM MIL-HDBK-5C

Material	Mechanical Property, Units	Average Measured Value	MIL-HDBK-5C "B" Value
0.125 Inch Thick 7075-T6 Sheet Used for Gage Fabrication	F_{tu} , ksi	80.0	80
	F_{ty} , ksi	74.7	72
	E, ksi	10,300	10,300
	e, %	7	8
0.5 Inch Thick 7075-T651 Plate Used for Specimen Fabrication	F_{tu} , ksi	84.5	79
	F_{ty} , ksi	77.5	72
	E, ksi	10,100	10,300
	e, %	14	7
7075-T651 F-4 Wing Skin Plate	F_{tu} , ksi	84.0	77
	F_{ty} , ksi	73.5	68
	E, ksi	10,200	10,300
	e, %	10	5

GP79-0871-66

TABLE 9. STRESSES USED FOR CENTER CRACKED PANEL TESTS

Stress Level Number	Crack Length 2a (in.)	Maximum Stress Levels (ksi) 
1	0.2-1.1	9.2
2	1.1-1.5	11.5
3	1.5-2.0	14.7
4	2.0-2.5	16.3
5	2.5-Failure	18.2

 R = 0.02

GP79-0871-67

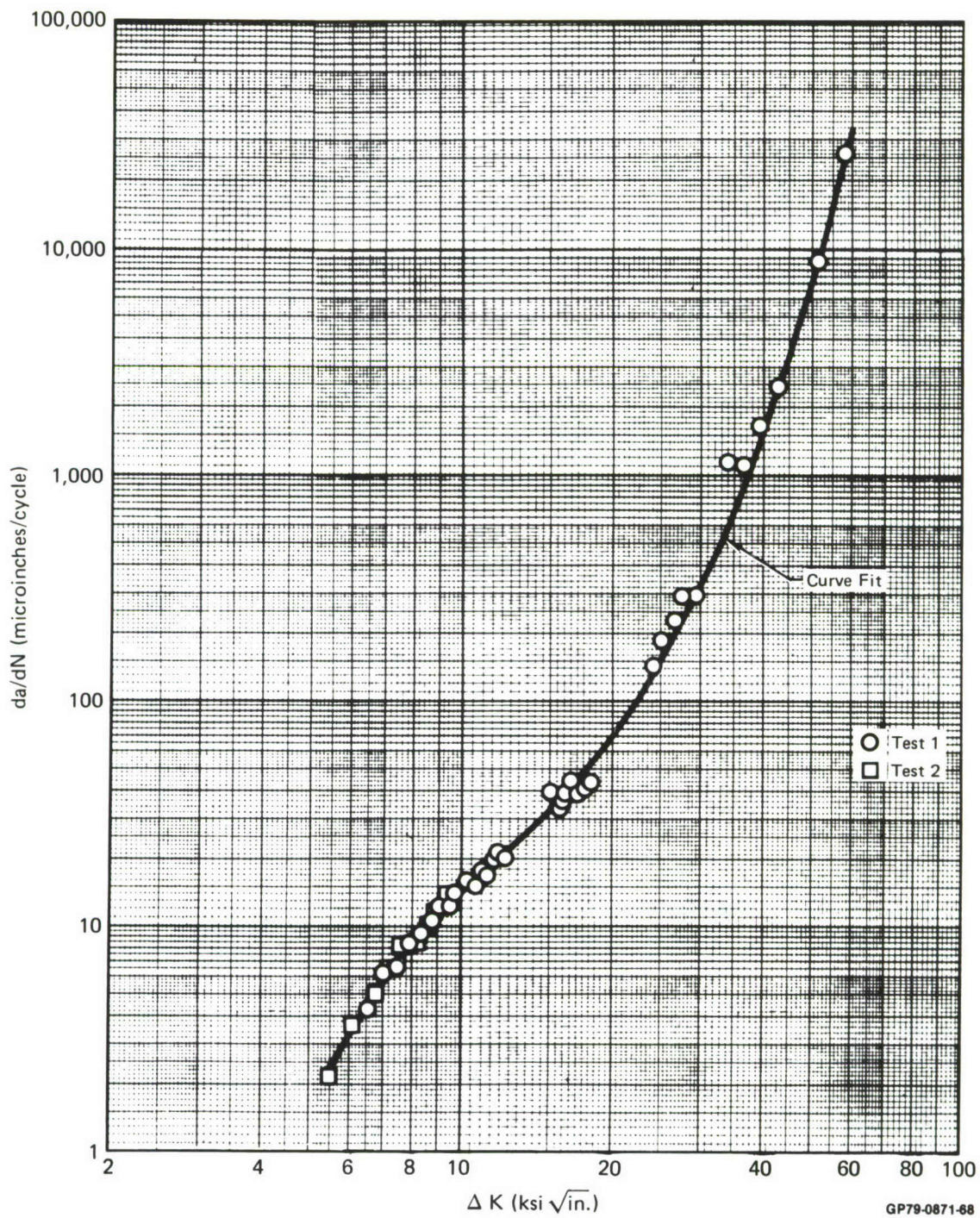


Figure 58. Crack Growth Rate for 7075-T6 Crack Growth Gage Sheet
 $R = 0.02$

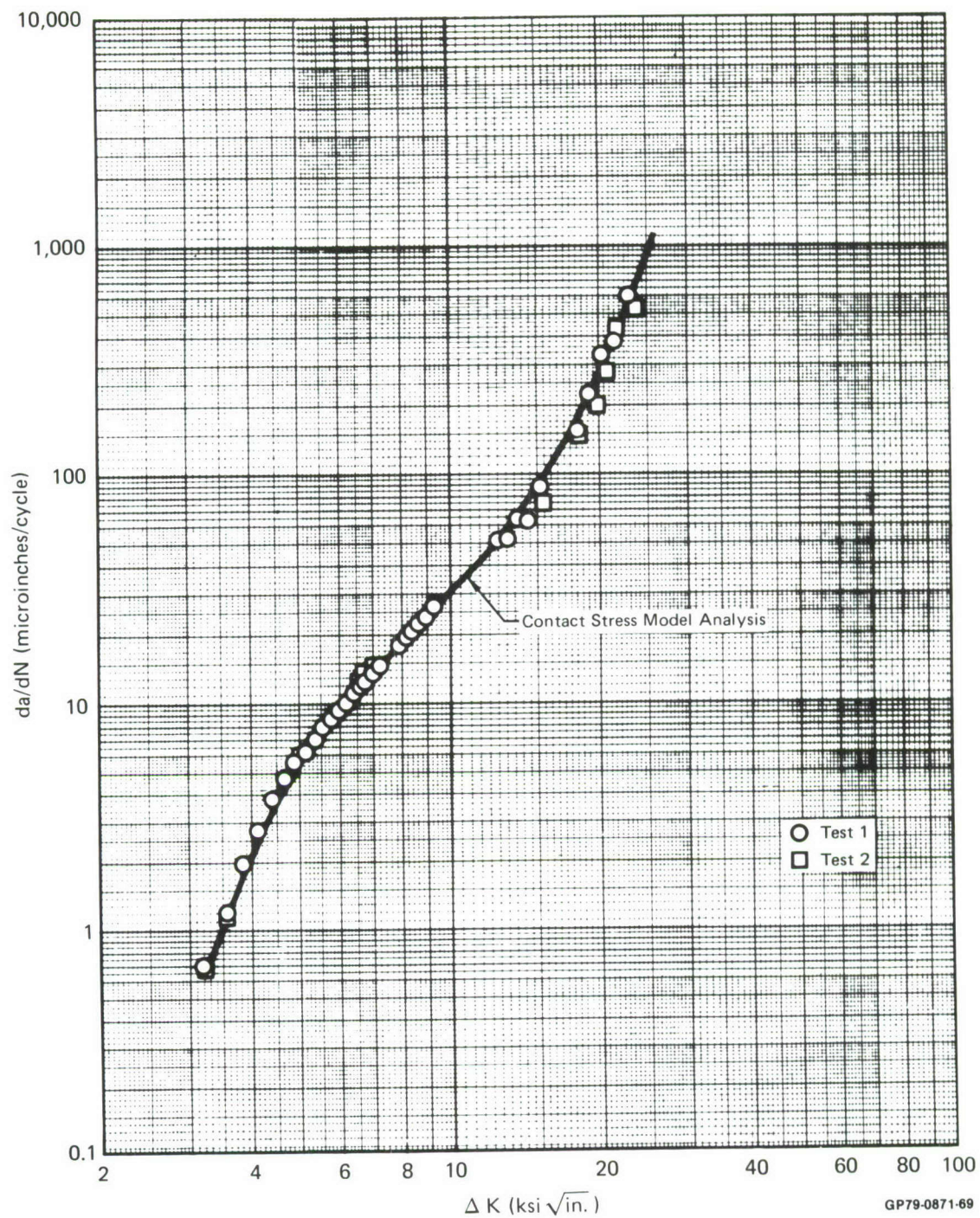


Figure 59. Crack Growth Rate for 7075-T6 Crack Growth Gage Sheet
R = 0.5

Constant amplitude crack growth tests were performed on center cracked panel specimens to determine the crack growth rate, and effect of stress ratio on the growth rate of the F-4 wing skin plate material. These specimens were taken from the center of the plate and milled to 0.25 inch thickness. The remaining dimensions are the same as those shown in Figure 55. Nominal stress levels are the same as those shown in Table 9.

Crack growth rate data for the $R = 0.02$ test of the wing skin plate material is shown in Figure 60 and for the $R = 0.5$ test in Figure 61. Generally, crack growth rates for the plate material are somewhat lower than those for the thin sheet (Figures 58 and 59) yet reflect a lower critical stress intensity factor (K_{IC}) in keeping with a thicker material. Also shown in Figure 60 is the curve fit to the $R = 0.02$ data used for analysis of crack growth in this material. The Contact Stress model prediction of crack growth rates for $R = 0.5$ are shown in Figure 61. The predicted growth rates are close to the data.

2. LOAD TRANSFER TESTS - Load transfer test results were useful in verifying the gage stress analysis, a total of five tests were performed. Element coupons were strain gaged as shown in Figure 62, strain gage 4 being omitted in one test involving a precracked gage. Strain results most useful in this analysis are summarized in Table 10.

The gage stiffness for an uncracked gage was determined from test results by considering the ratio of the average strain in the gage to the average strain in the carrier plate at locations 2 and 6 on both sides of the specimen (Figure 62). Table 11 summarizes test and analysis. Agreement is good, although strains in the carrier plate are a little higher than predicted because they are measured some distance from the crack growth gage. Predictions were based on planes, taken through the thickness and across the specimen width, remaining plane during deformation. This did not occur in the test specimen since the gage behaves as a local doubler, creating lower than average strains beside the gage, and higher than average in line with the gage.

Strains in gages 3 and 5 (Figure 62) correlate well with predicted strains at those locations as shown in Figure 63. Strains were predicted using a theoretical solution for the stress distribution near a series of collinear cracks, Reference 6. This solution for the stress, σ_x , at point x in the plane of a crack of length, $2a$, in a plate $2b$ wide is given as

$$\sigma_x = \sigma_0 \left[\sin \frac{\pi x}{2b} \right] \left[\cos^2 \frac{\pi a}{2b} - \cos^2 \frac{\pi x}{2b} \right]^{-1/2} \quad (12)$$

where σ_0 is interpreted as the average gross stress in the gage. Using values of average gage stress (σ_0) obtained from Figure 26, strains at the strain gage locations were predicted as a function of gage crack length. Computed strains using NASTRAN results show good agreement with the test results (Figure 63).

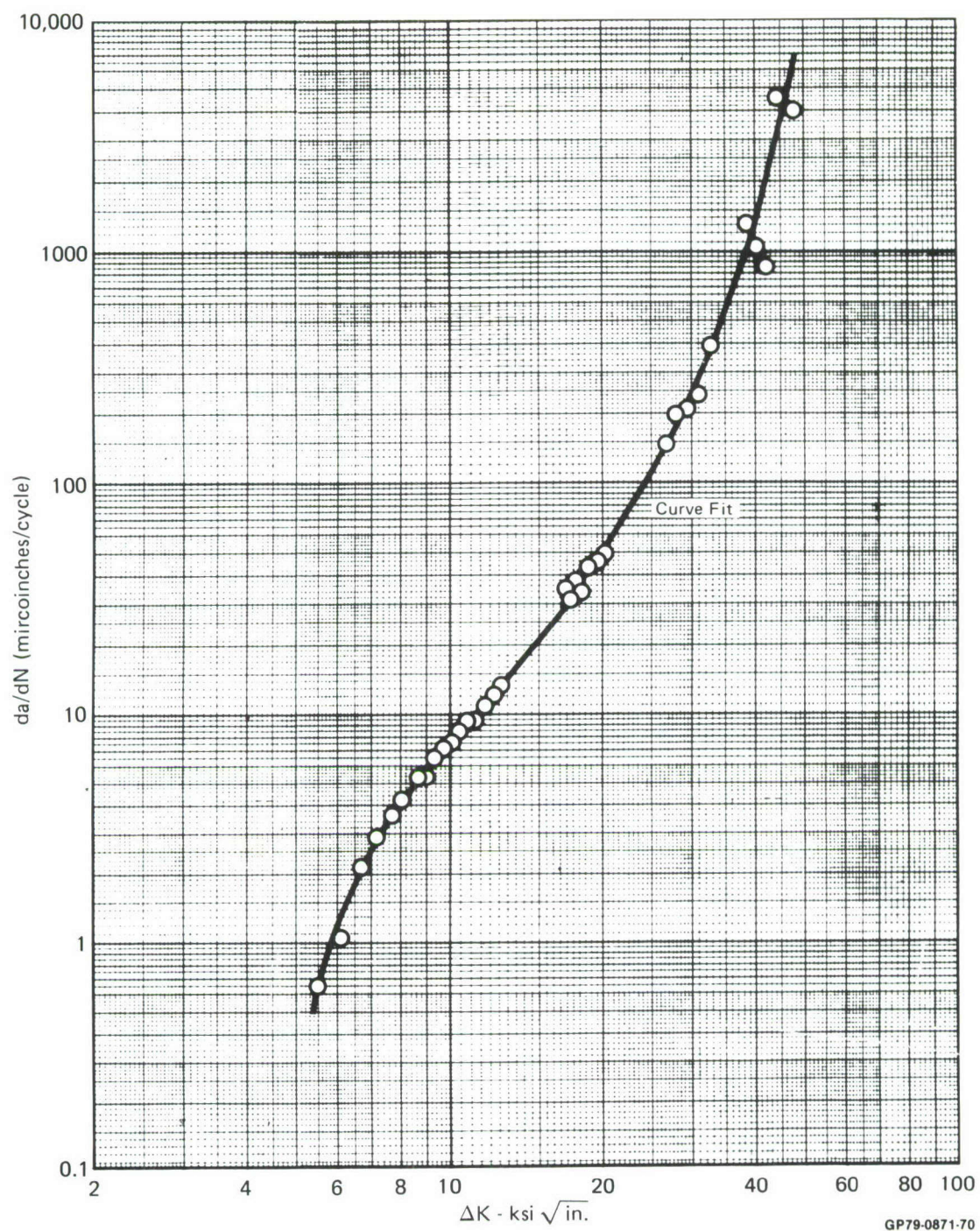


Figure 60. Crack Growth Rate for 7075-T651 F-4 Wing Skin Plate
 $R = 0.02$

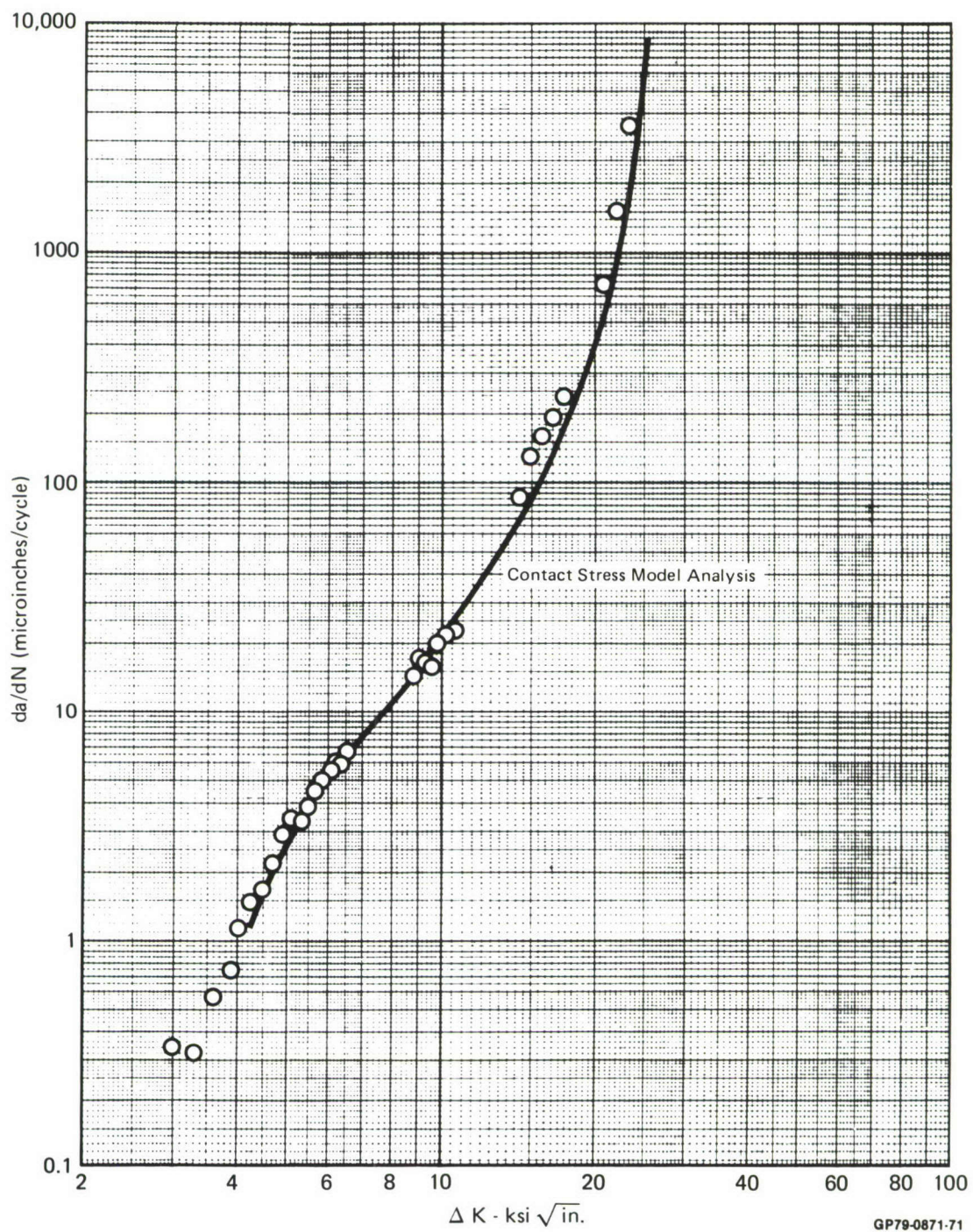


Figure 61. Crack Growth Rate for 7075-T651 F-4 Wing Skin Plate
R = 0.5

Note: All dimensions are in inches

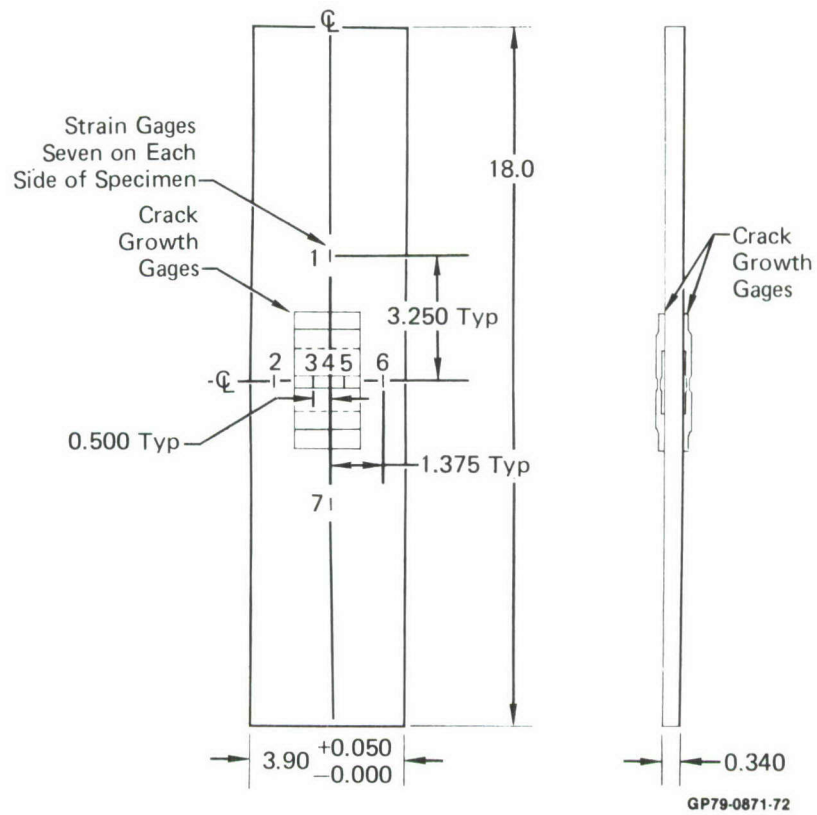


Figure 62. Load Transfer Test Instrumentation

TABLE 10. SUMMARY OF LOAD TRANSFER TEST RESULTS

Specimen Number	Cycles Applied	Stress (ksi)	Average of Strains on Both Sides of Specimen		
			1,7	2,6	3,4,5
1	0	30	3,096 ⁽¹⁾	2,763	4,199
	20,000		3,096	2,763	4,175
2	0		3,112	2,736	4,143
	20,000		3,110	2,772	4,027
3	0		3,122	2,773	4,184
	20,000		3,119	2,773	4,197
	40,000		3,133	2,774	4,247
	60,000		3,136	2,771	4,209
	80,000		3,147	2,737	4,182
	100,000		3,302	2,780	4,170
4	0		3,098	2,775	4,211
	20,000		3,089	2,734	4,224
	40,000		3,096	2,765	4,219
	60,000		3,110	2,858	4,213
	80,000		3,106	2,842	3,928 ⁽³⁾
	100,000		3,071	2,898	2,457
5	0.2 ⁽²⁾	30	3,100	2,760	4,193
	0.4		3,116	2,761	4,398
	0.6		3,092	2,795	4,771

Notes:

- (1) All strains are $\mu\text{in./in}$
- (2) Average total crack length of both gages on element coupon
- (3) One gage began debonding between 60,000 and 80,000 cycles

GP79-0871-73

TABLE 11. SUMMARY OF GAGE STIFFNESSES DETERMINED FROM STRAIN SURVEY

Specimen Number	Cycles Applied	Strain in Plate $\mu\text{in./in.}$	Strain in Gage $\mu\text{in./in.}$	$\frac{E_{\text{gage}}}{E_{\text{plate}}}$	$\frac{\epsilon_{\text{gage}}}{\epsilon_{\text{plate}}}$
1	0	2763 ⁽¹⁾	4199 ⁽²⁾	1.02	1.55 ⁽³⁾
	20,000	2763	4175		1.54
2	0	2736	4143		1.54
	20,000	2772	4023		1.48
3	0	2773	4184		1.54
	20,000	2773	4197		1.54
4	0	2775	4211		1.55
	20,000	2734	4224	1.02	1.58

Notes:

(1) Theoretical plate strain is $\epsilon_{\text{plate}} = 2576 \mu\text{in.}$

(2) Theoretical gage strain is $\epsilon_{\text{gage}} = 4270 \mu\text{in.}$

(3) Theoretical gage stiffness is $\epsilon_{\text{gage}}/\epsilon_{\text{plate}} = 1.613$

4* Gross applied plate stress = 30 ksi

GP79-0871-74

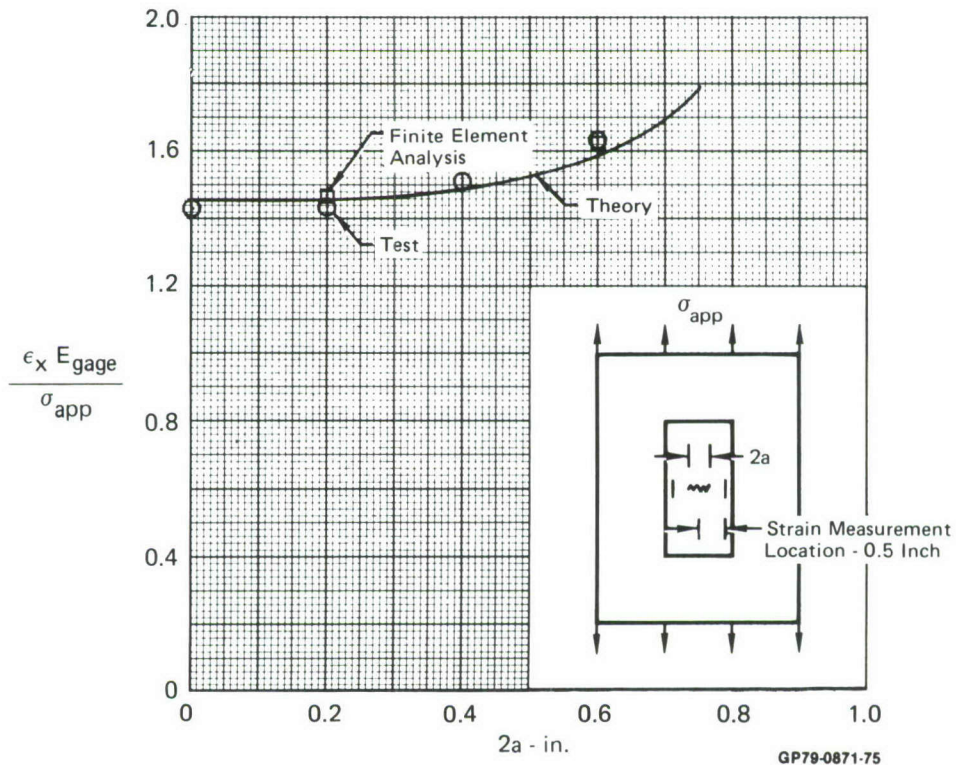


Figure 63. Comparison of Measured and Predicted Strains in Crack Growth Gages

These measured strains were also used to verify the predicted average gage stress. The average stress in terms of measured strains (ϵ_x) in the gage is

$$\frac{\sigma_g}{\sigma_{app}} = \frac{E \epsilon_x}{\sigma_{app}} \frac{\left[\cos^2 \frac{\pi a}{2b} - \cos^2 \frac{\pi x}{2b} \right]^{1/2}}{\sin \frac{\pi x}{2b}} \quad (13)$$

Comparison of average gage stress computed from test results and from NASTRAN finite element analyses are shown in Figure 64. These results compare favorably with the relationship determined by Equation 11, except for the NASTRAN results at short crack lengths wherein the finite element model is apparently too stiff.

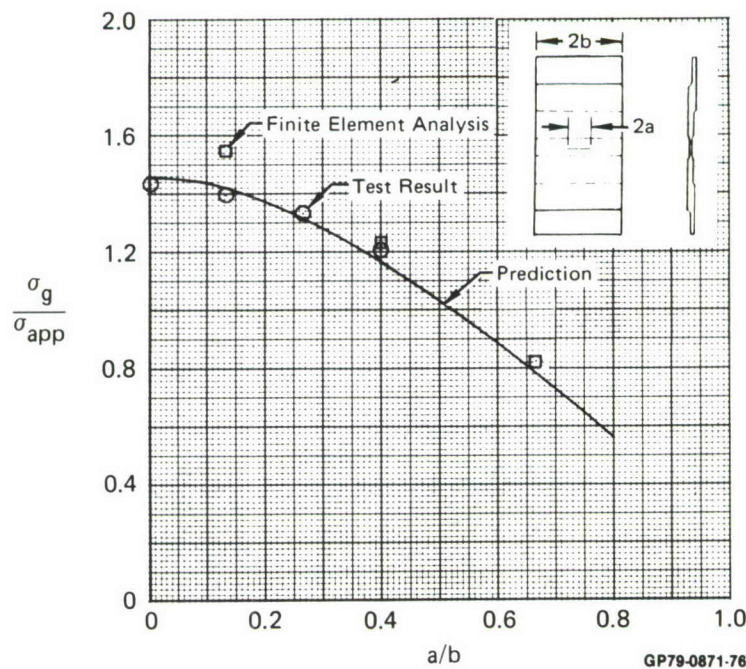


Figure 64. Comparison of Measured and Predicted Average Gage Stress

3. GAGE CALIBRATION (CONSTANT AMPLITUDE TESTS) - To validate stress intensity factors for gage calibration specimens, predicted and measured crack growth rates were compared for $R = 0.02$ constant amplitude loadings. Results are shown in Figures 65 and 66; predicted crack growth tends to be a little high at crack lengths of about 0.6 inch. Crack growth appears to accelerate as the crack approaches the edge of the gage. (The gage is 1.5 inches wide.) The extent of this acceleration is not predicted. Figures 67 and 68 present these same analysis and test data in a different format. In general the analysis and test results are in good agreement.

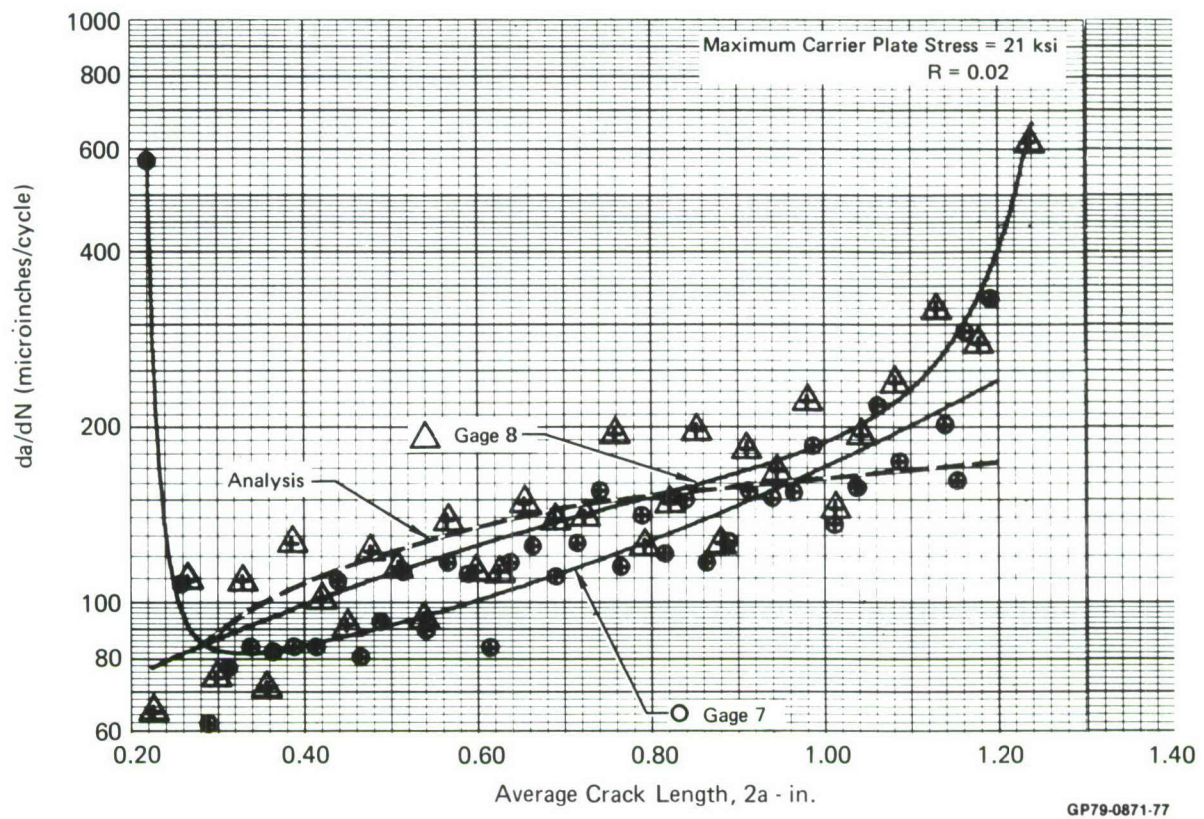


Figure 65. Predicted and Measured Crack Growth Rates for Gage Calibration Specimen - Test 1

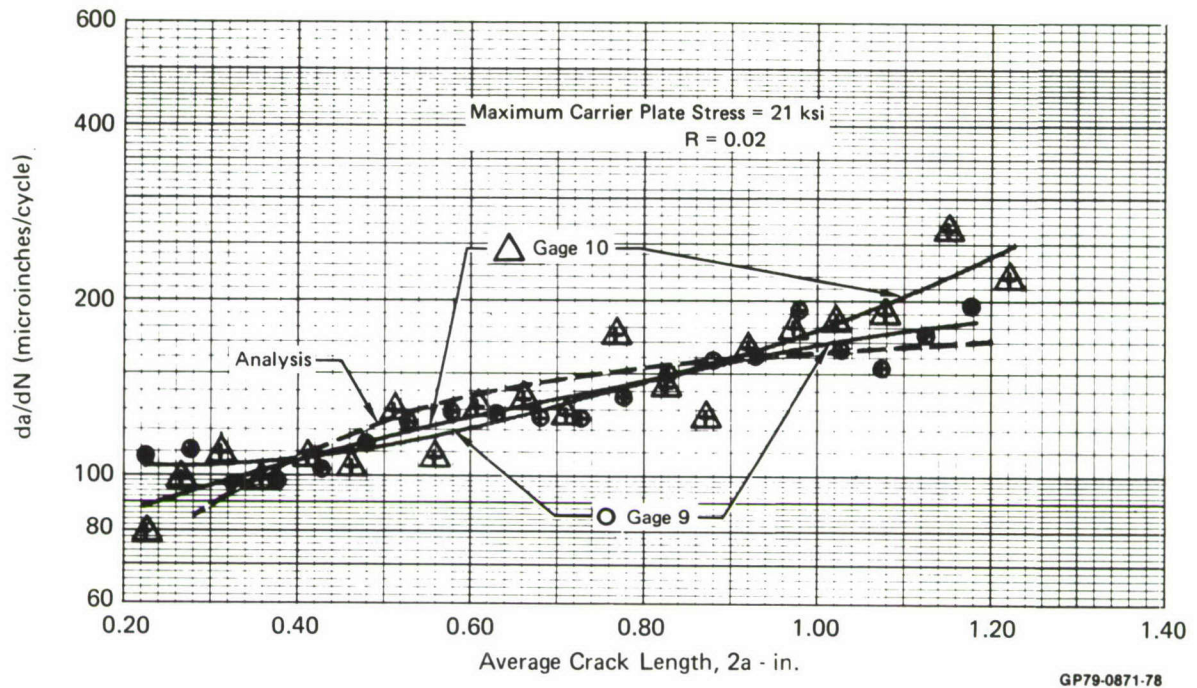


Figure 66. Predicted and Measured Crack Growth Rates for Gage Calibration Specimen - Test 2

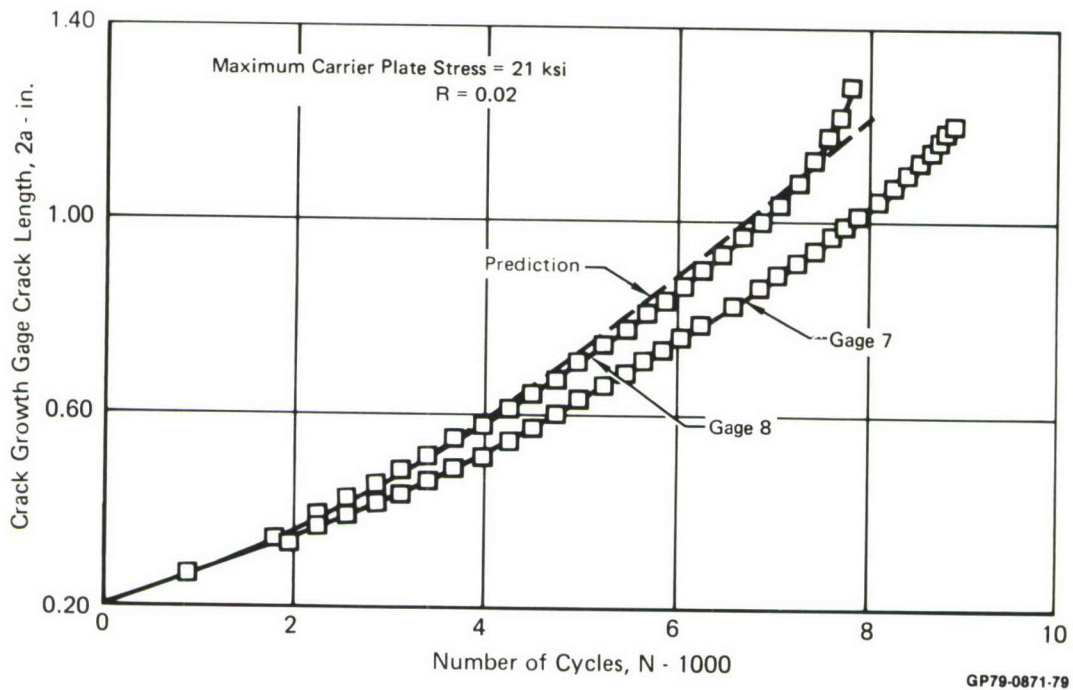


Figure 67. Predicted and Measured Crack Growth Rates for Constant Amplitude Gage Calibration - Test 1

Measured crack growth under $R = 0.5$ constant amplitude loading is compared with analysis results in Figure 69. This analysis was performed assuming plane stress plastic zone conditions exist at the gage crack tip. Test and analysis results for $R = 0.3$ constant amplitude loading are presented in Figure 70. The analysis predicts a growth rate about 5-10 percent slower than measured rates.

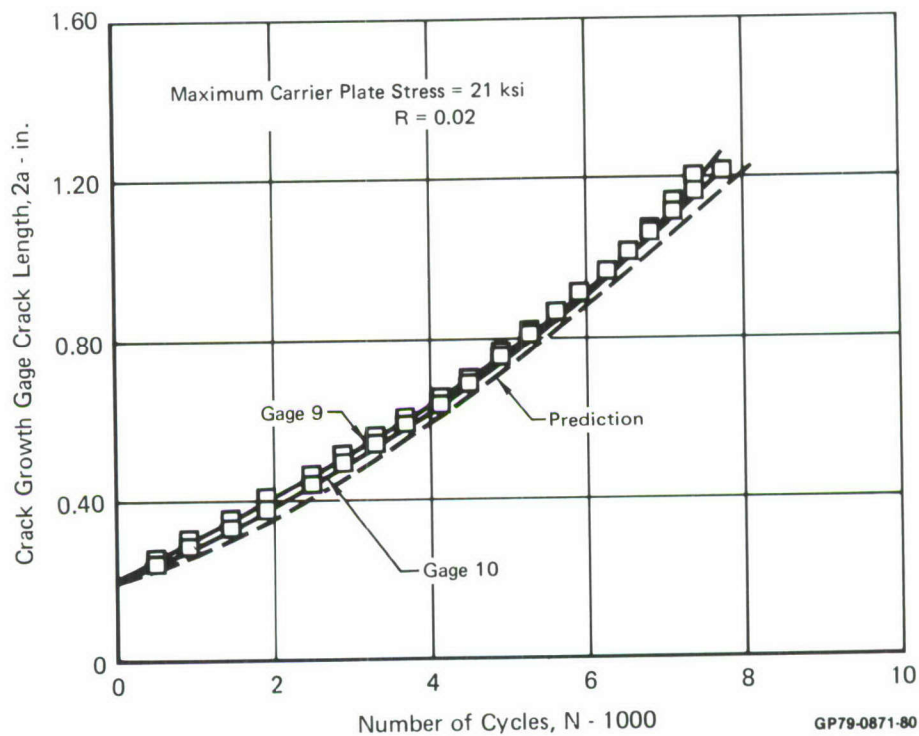


Figure 68. Predicted and Measured Crack Growth for Constant Amplitude Gage Calibration - Test 2

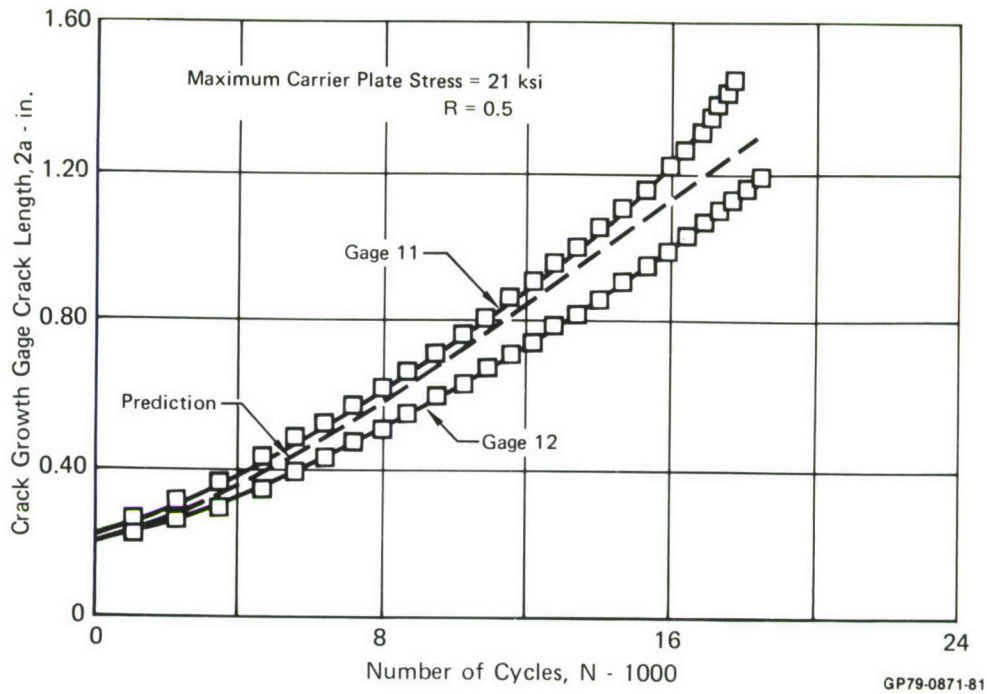


Figure 69. Predicted and Measured Crack Growth for Constant Amplitude Gage Calibration - Test 3

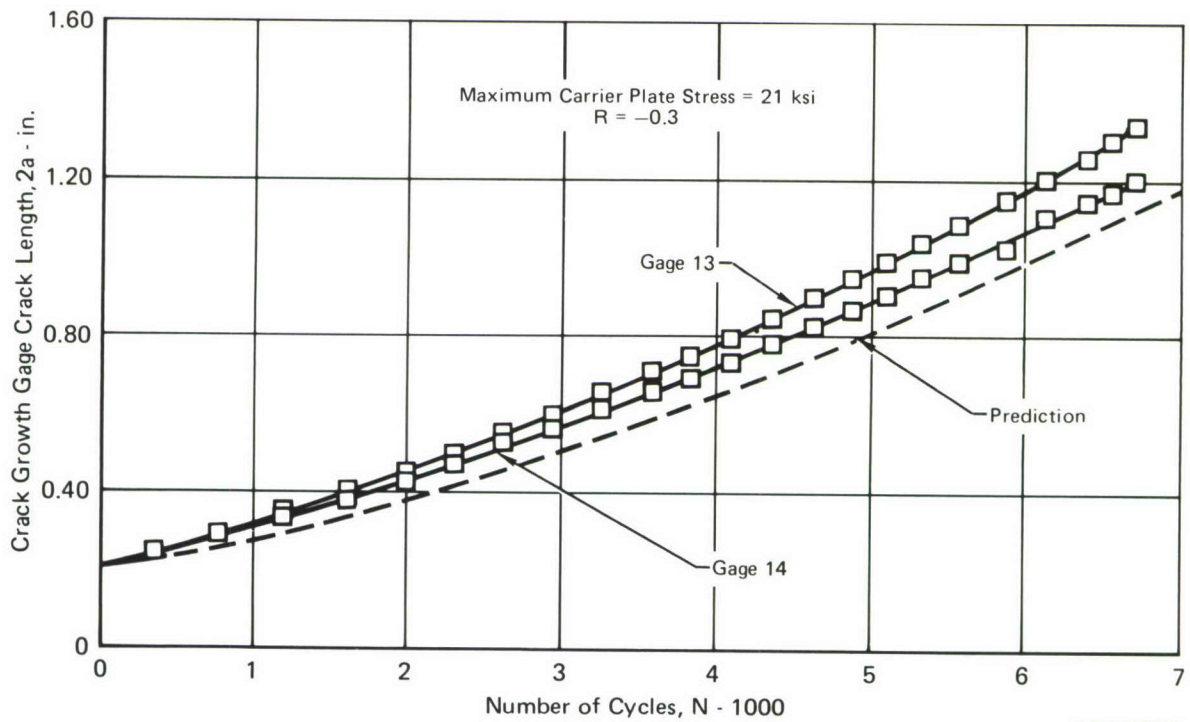


Figure 70. Predicted and Measured Crack Growth for Constant Amplitude Gage Calibration - Test 4

Generally, analyses using the Contact Stress model assuming plane stress plastic zone conditions give good agreement with the results of constant amplitude tests at all stress ratios.

4. EFFECT OF THICKNESS ON CRACK GROWTH RETARDATION - Gage calibration tests under spectrum loadings indicated that crack growth retardation was greater for the gages than that predicted by the Contact Stress model under assumed plane stress assumptions. As shown in Figures 71-72, the gage crack growth initially is faster than predicted then slows to a rate far less than predicted. To obtain correlation with the data, minimum effective stress levels used would have to exceed those analytically determined under plane stress conditions. In the Contact Stress model, retardation is predicted by determining a minimum effective stress level which reduces the stress ranges used for computation of spectrum crack growth. The relationship of the minimum effective stress level to the applied stress levels is indicated in Figure 73.

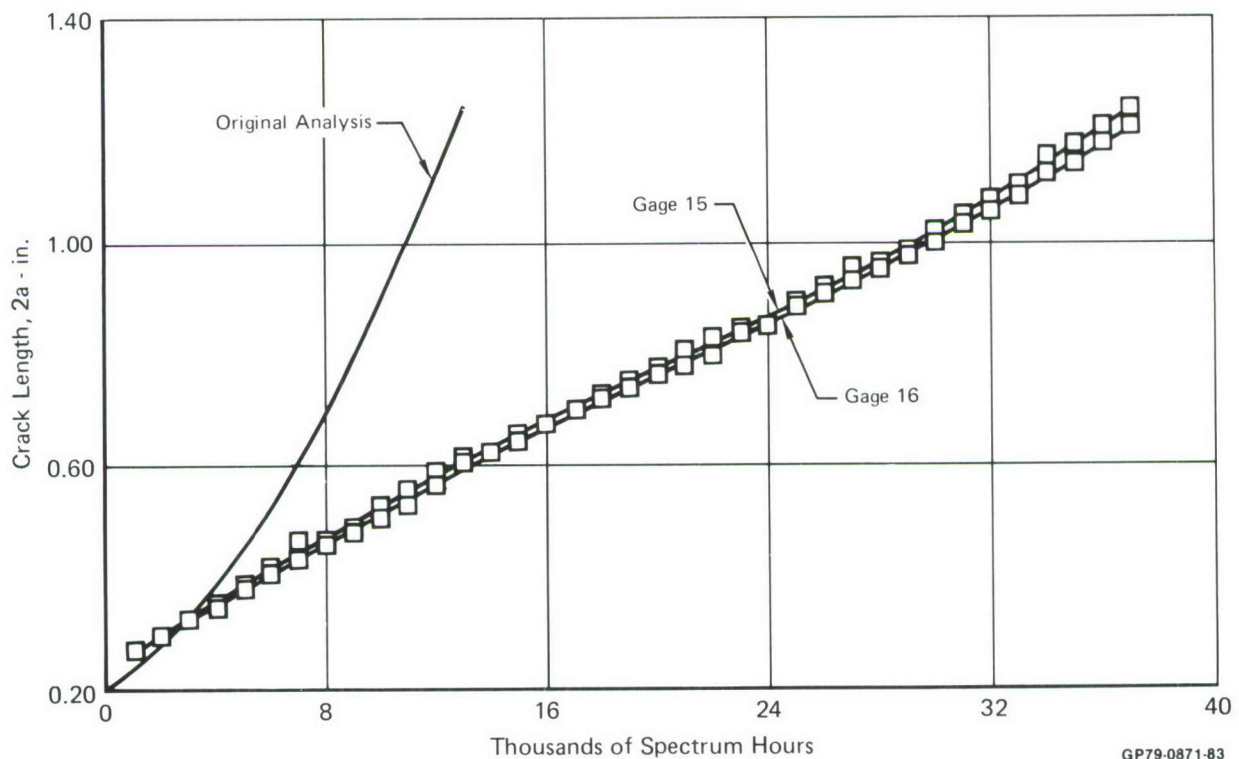


Figure 71. Comparison of Predicted and Measured Crack Growth in Gage Under BL 44.5 Lower Wing Spectrum

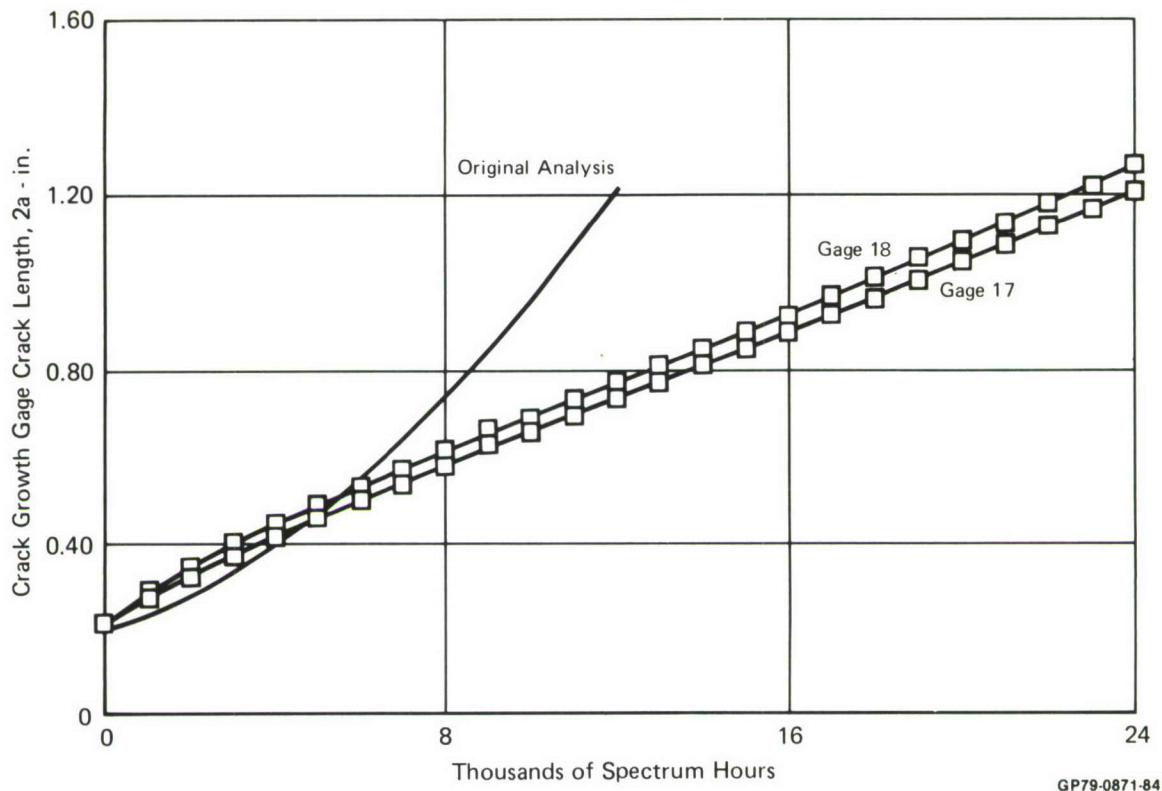


Figure 72. Comparison of Predicted and Measured Crack Growth in Gage Under BL 100 Lower Wing Spectrum

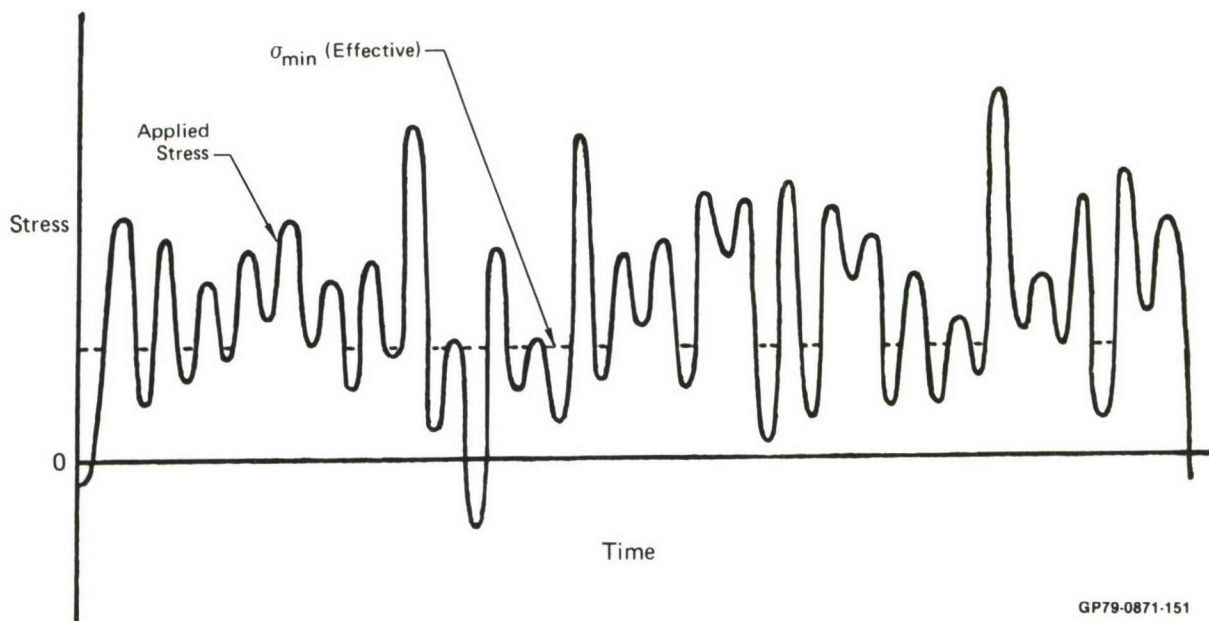


Figure 73. Relationship of Effective Minimum Stress Level to Applied Stress Levels

To determine the effect of sheet thickness on crack growth retardation, a series of constant amplitude and spectrum tests of center cracked panels of several thicknesses was performed as outlined in Table 12. Constant amplitude results for tests at 30 ksi, R = 0 are shown in Figure 74. The scatter shown is no more than would be expected for six tests of material from different lots in the same thickness.

TABLE 12. CONSTANT AMPLITUDE AND SPECTRUM TESTS TO INVESTIGATE SHEET THICKNESS EFFECTS

Stress Levels (ksi)	Sheet Thickness (in.)					
	0.02	0.04	0.08	0.15	0.25	0.50
15		X			X	
30	X	X	X	X	X	X
45		X			X	

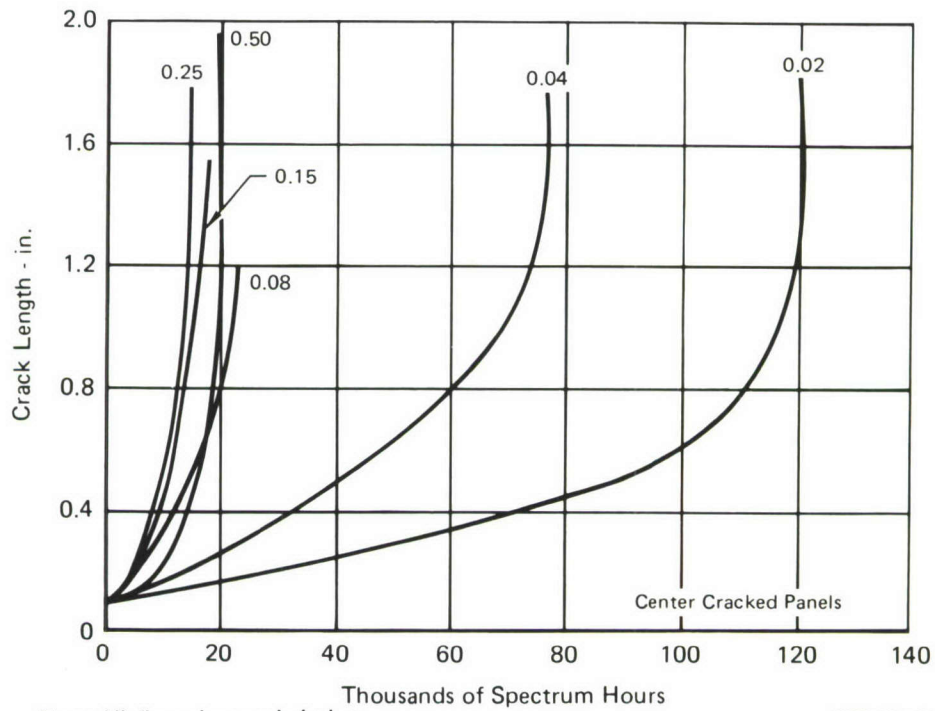
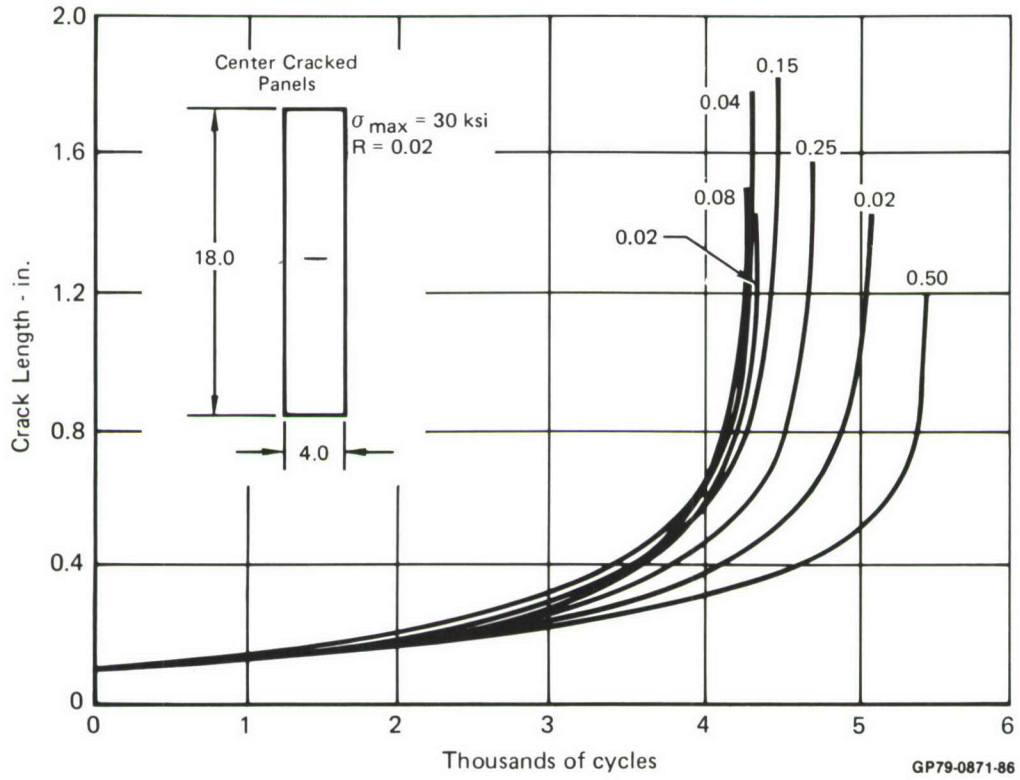
GP79-0871-85

Spectrum test results are shown in Figure 74 for the BL.44.5 stress spectrum applied at 30 ksi limit stress. Crack growth lives generally tend to increase with decreasing thickness. However, lives for thicknesses greater than 0.1 inches are within the scatter band of the constant amplitude results. Life for the 0.04 inch thick panel is four times those for thicker panels, for 0.02 inch thickness life is six times as long.

While previous investigations (References 13 and 14) have shown that thickness affects crack growth retardation following discrete high loads, the magnitude of this effect and its insensitivity to stress level were not anticipated. Hartranft and Sih, Reference 15, have postulated that a transition layer from plane strain exists which is a function of crack length and plate thickness.

$$\xi/t = \frac{1}{4 + \frac{16t}{a}} \quad (14)$$

Finite element results obtained by Raju and Newman, Reference 16, have provided support for this boundary effect, Figure 75.



Note: All dimensions are in inches

Figure 74. Sheet Thickness Tests - Constant Amplitude and Spectrum Test Results

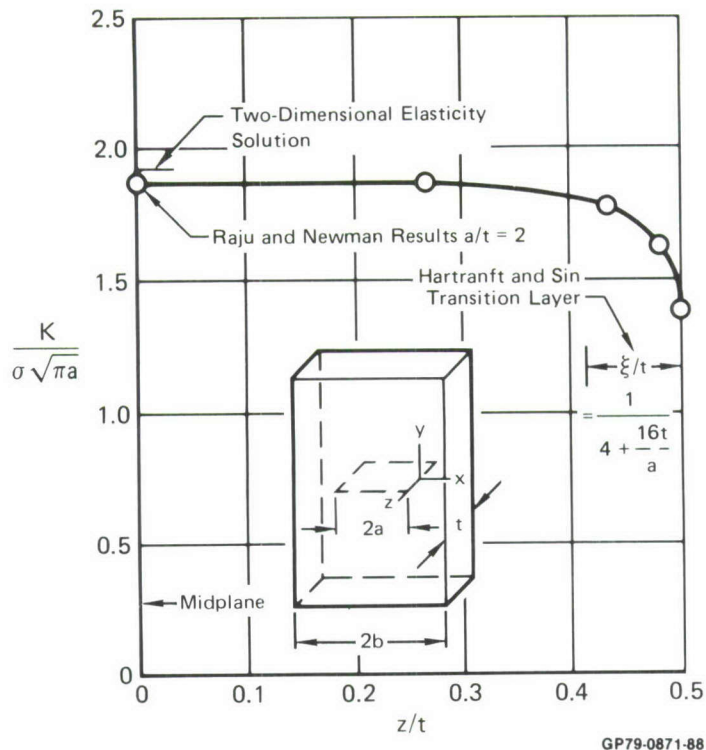


Figure 75. Comparison of Finite Element Analysis Results with Predicted Boundary Layer Depth

By selecting a minimum effective stress level (closure stress), assumed to be constant throughout the fatigue life as suggested by Elber, Reference 17, crack growth analyses were "tuned" to provide correlation with the spectrum test data. A plot of the minimum effective stress level used to match test data versus the boundary effect parameter, ξ/t , is shown in Figure 76.

Crack growth lives for all constant amplitude and spectrum tests are summarized as a function of specimen thickness in Figures 77 and 78, respectively. Also shown are the crack growth life predictions obtained from the Contact Stress model using the empirical relationship of Figure 76 to compute the minimum effective stress level. While the empirical relationship was developed from the results at 30 ksi, good correlation is found with lives at other stress levels. One constant amplitude test at 45 ksi appears to have an abnormally short life.

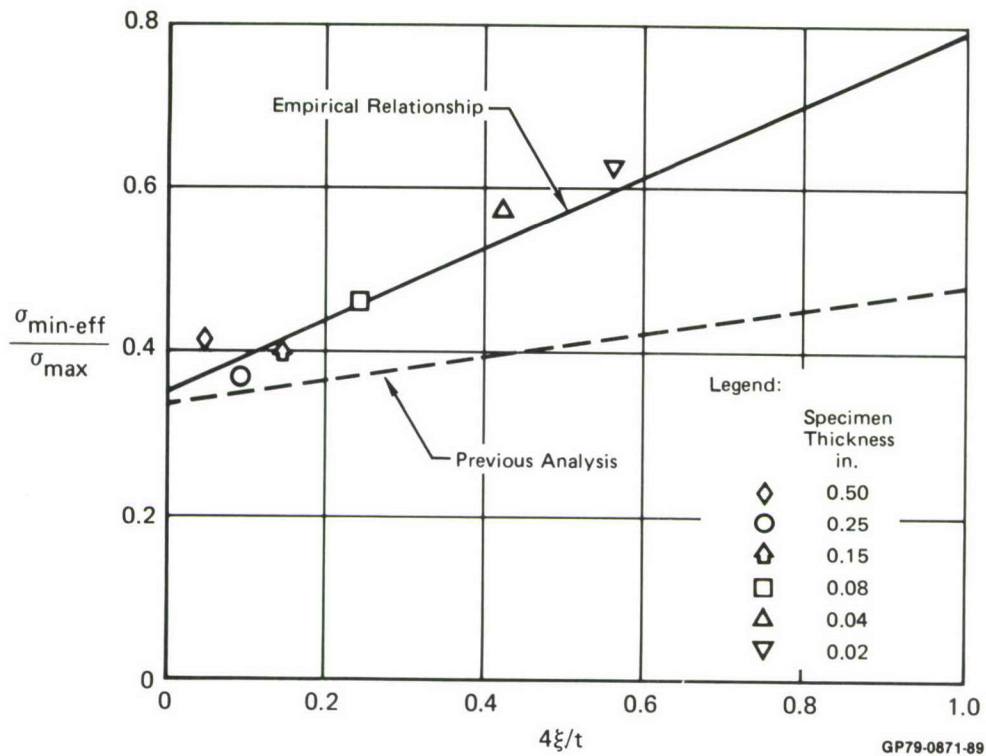


Figure 76. Relationship of Effective Minimum Stress Level to Boundary Layer Depth

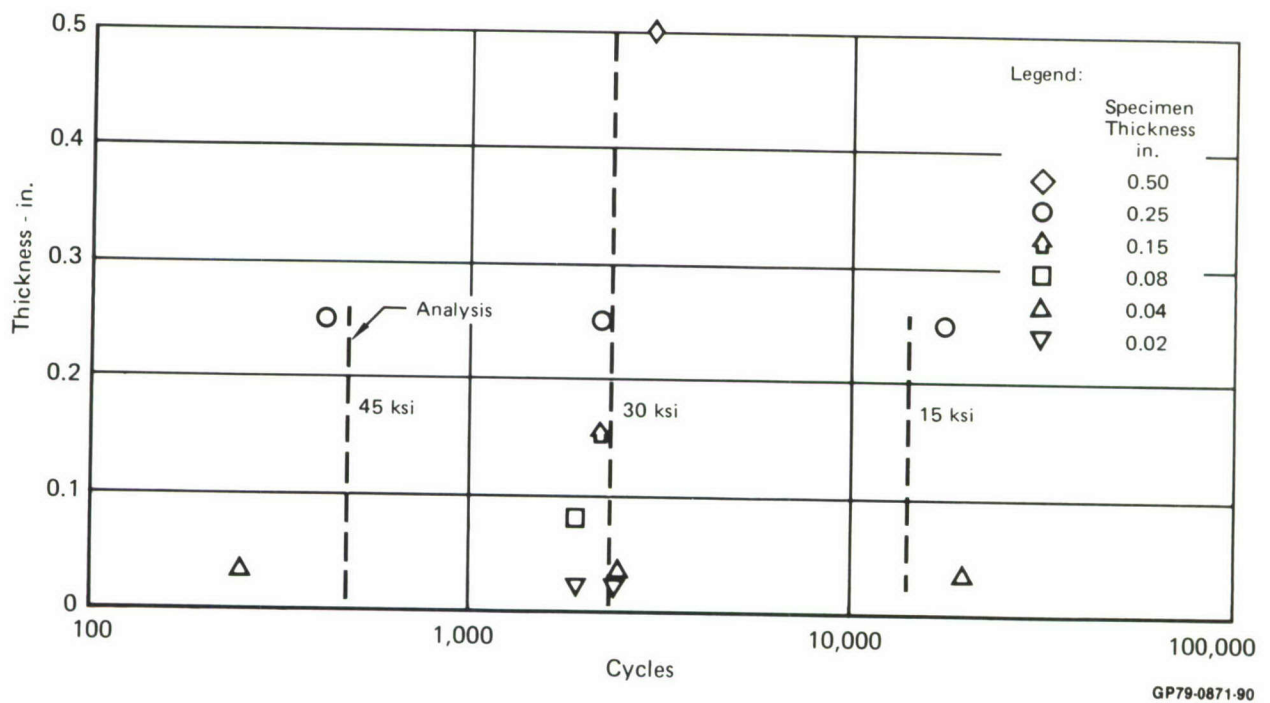


Figure 77. Effect of Thickness on Constant Amplitude Crack Growth Lives - Comparison of Analysis and Test Results

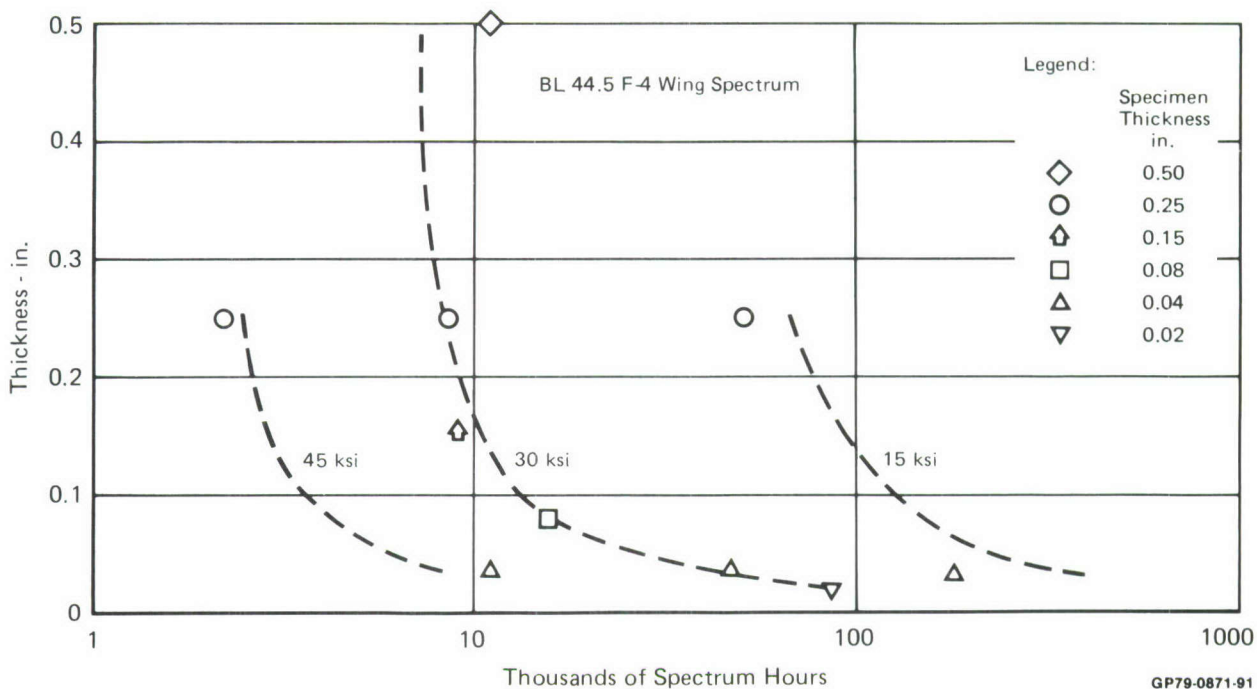


Figure 78. Effect of Thickness on Spectrum Crack Growth Lives - Comparison of Analysis and Test Results

5. GAGE CALIBRATION (SPECTRUM TESTS) - Using the Contact Stress model and the empirical relationship of Figure 76, good correlation was obtained with the majority of the gage calibration spectrum test results shown in Figures 79-89. One exception was Test 2 using the BL.132.5/LRS 183 spectrum, Figure 86. Data from this test does not agree with analysis or the duplicate test (Figure 87). This discrepancy has not been explained. It is interesting to note that, in those cases in which the gages separated from the specimen because of poor surface preparation, measured crack growth was close to that predicted until the gages separated.

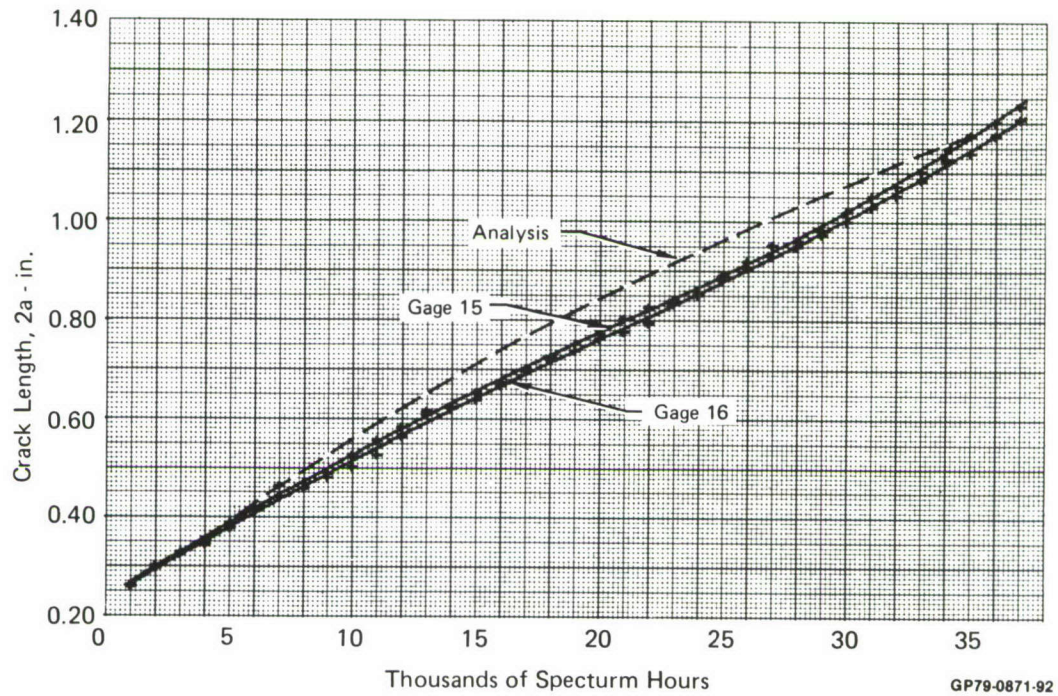


Figure 79. Comparison of Analysis and Test Results for Gage Calibration Test - BL 44.5 Spectrum - Test 1

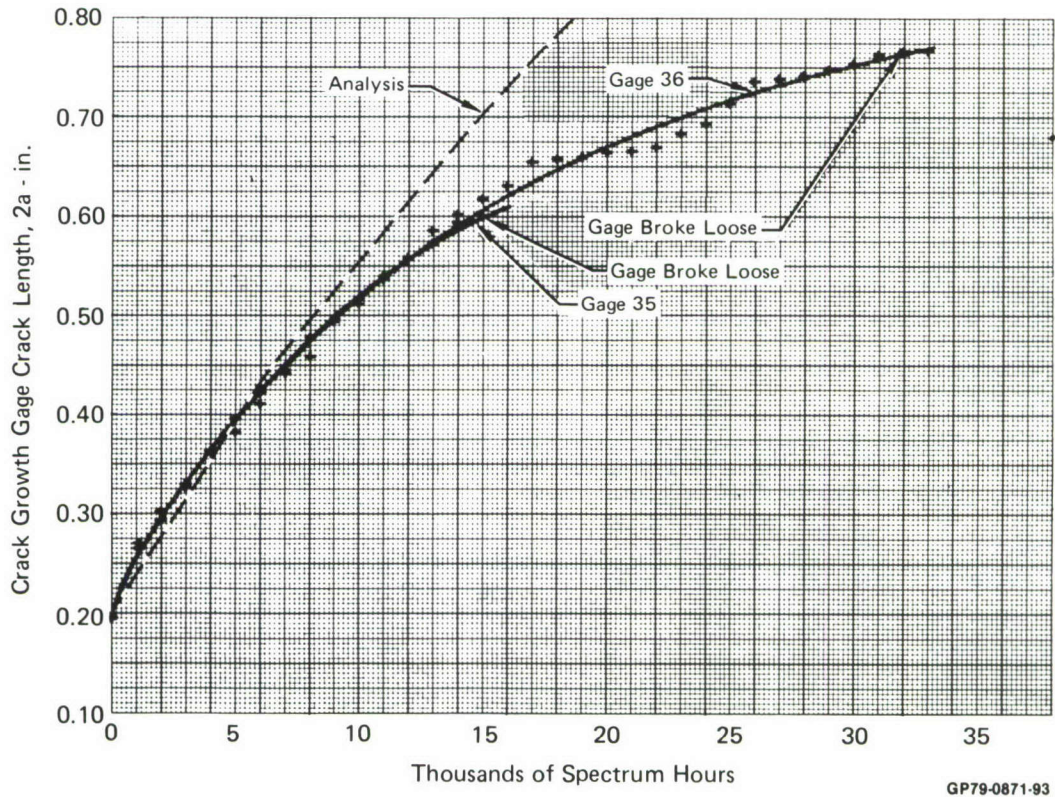


Figure 80. Comparison on Analysis and Test Results for Gage Calibration Test - BL 44.5 Spectrum - Test 2

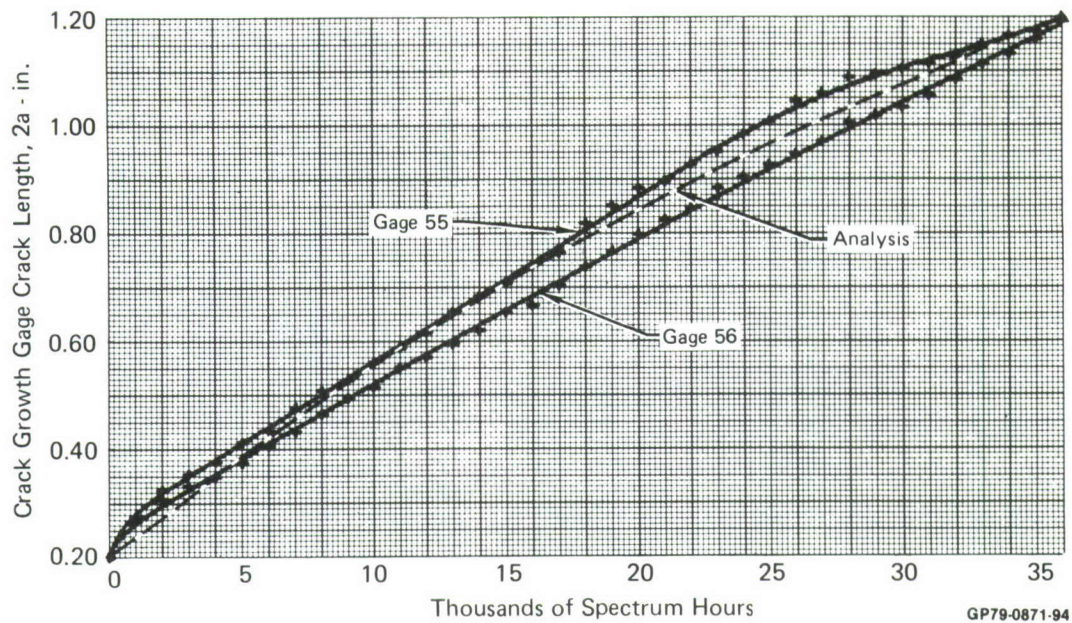


Figure 81. Comparison on Analysis and Test for Gage Calibration Test - BL 44.5 Spectrum - Test 3

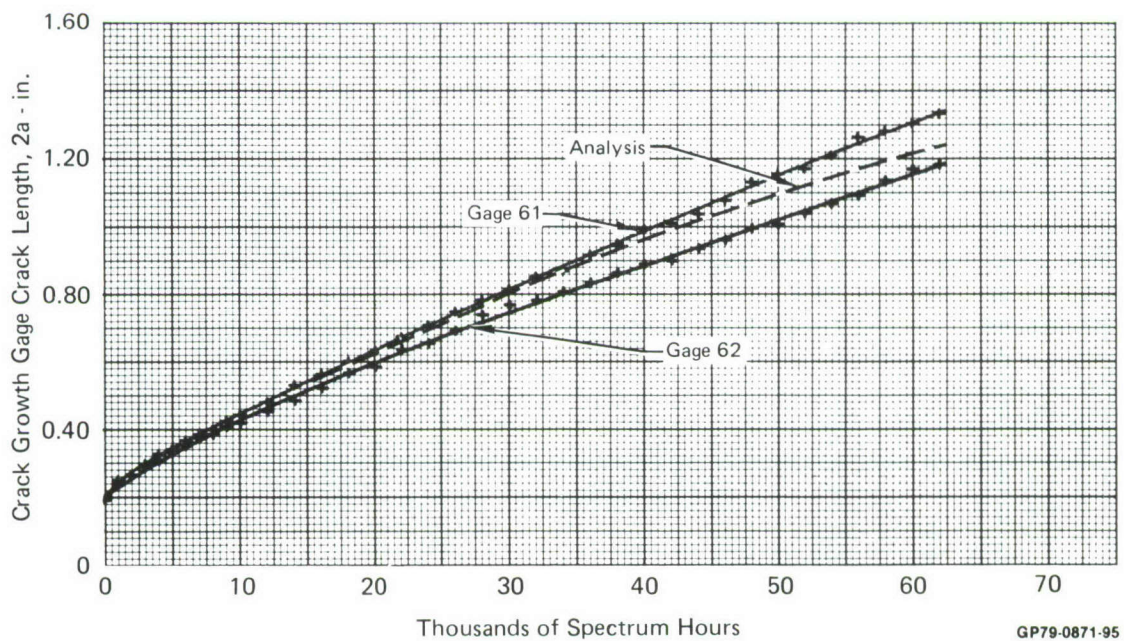


Figure 82. Comparison of Analysis and Test Results for Gage Calibration Test - BL 44.5 Spectrum - Test 4

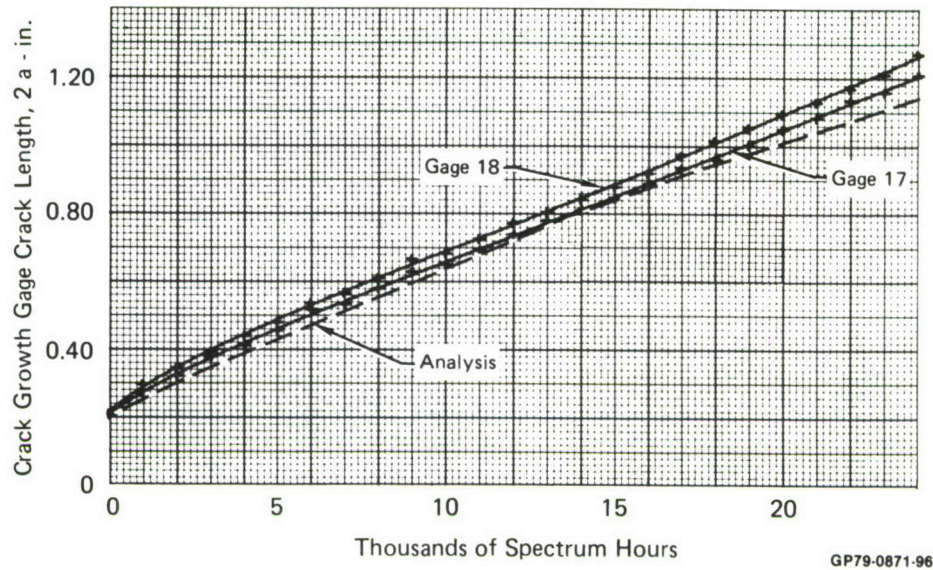


Figure 83. Comparison of Analysis and Test Results for Gage Calibration Tests - BL 100 Spectrum - Test 1

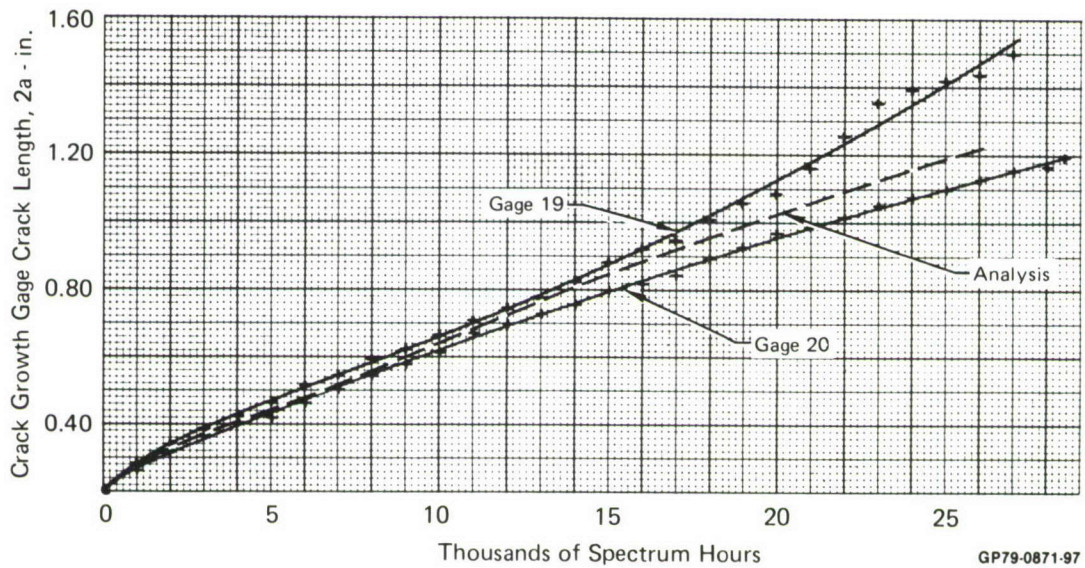


Figure 84. Comparison of Analysis and Test Results for Gage Calibration Tests - BL 100 Spectrum - Test 2

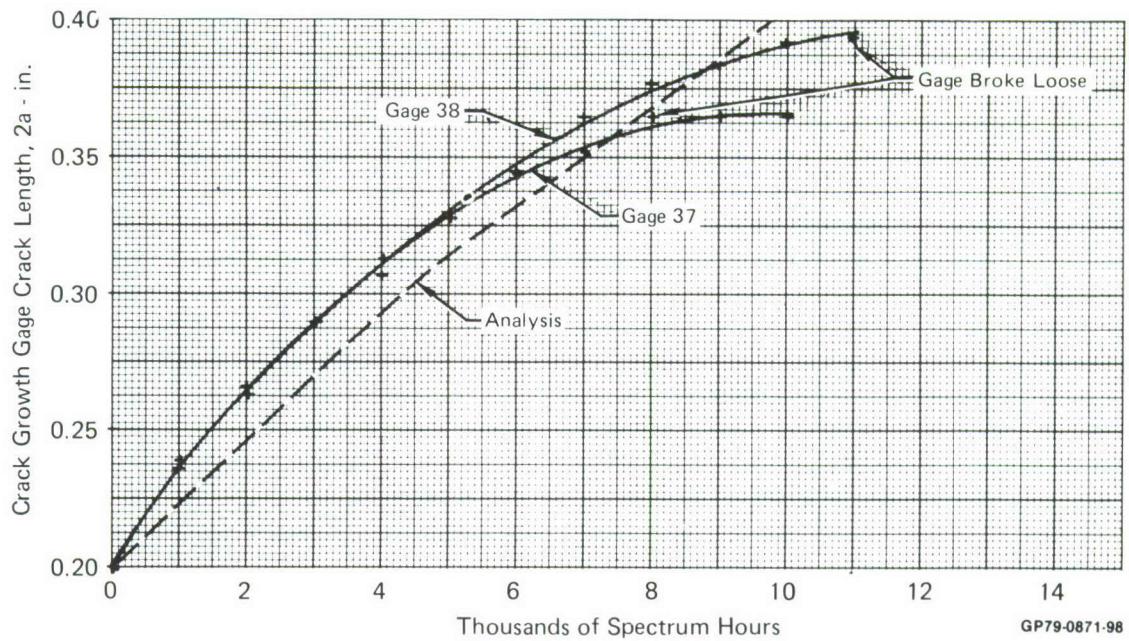


Figure 85. Comparison of Analysis and Test Results for Gage Calibration Test - BL 132.5 Spectrum - Test 1

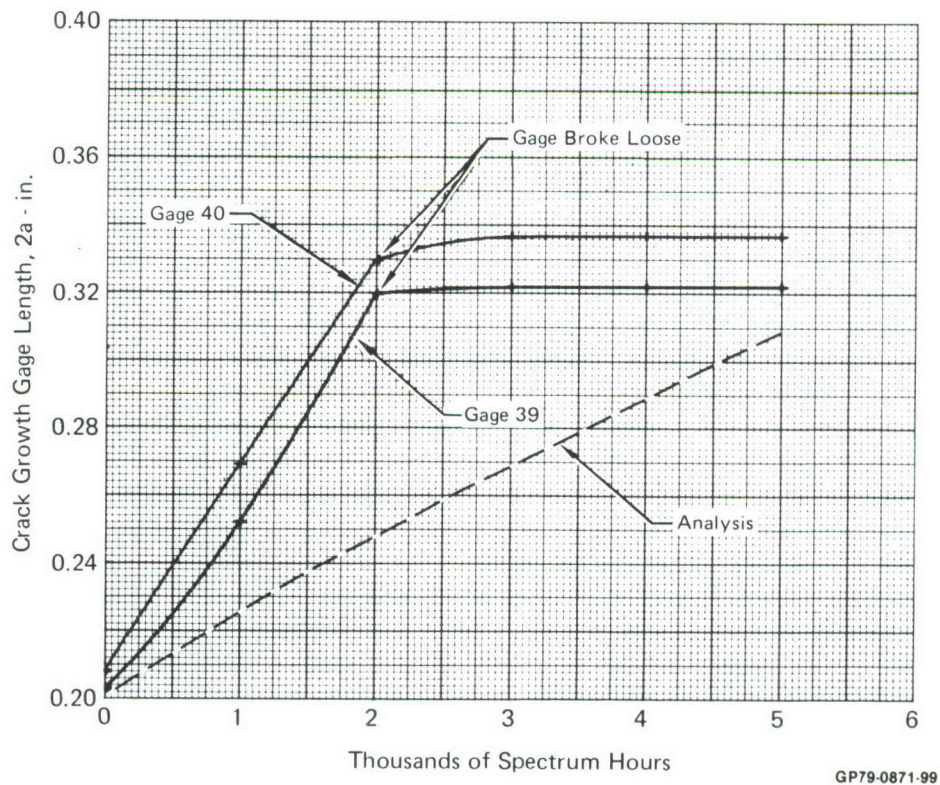


Figure 86. Comparison of Analysis and Test Results for Gage Calibration Test - BL 132.5 Spectrum - Test 2

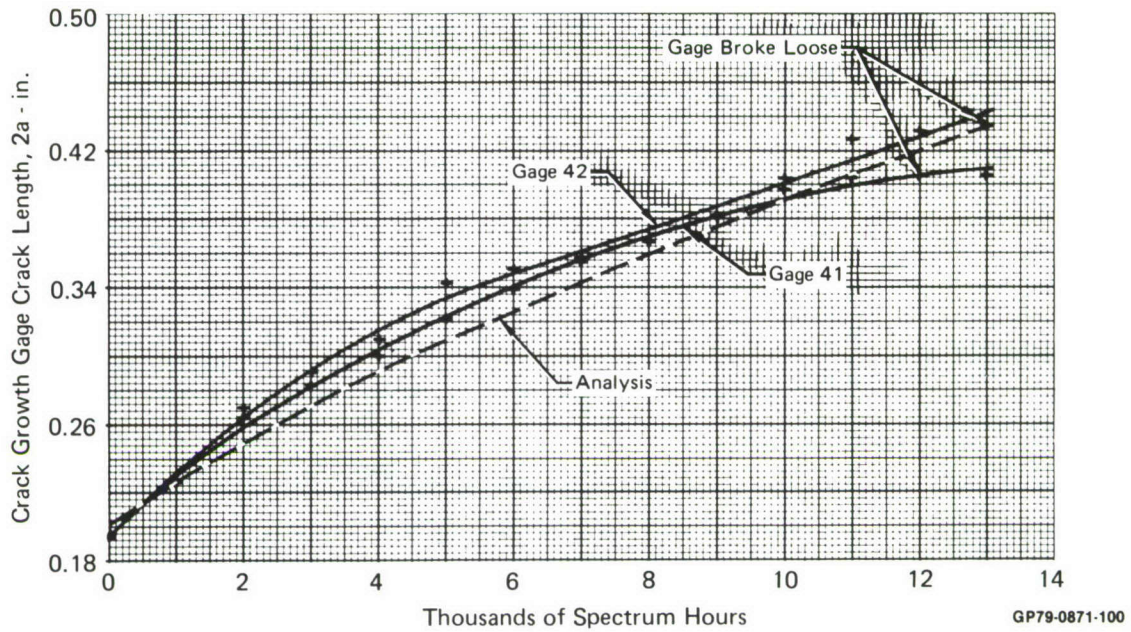


Figure 87. Comparison of Analysis and Test Results for Gage Calibration Test - BL 132.5 Spectrum - Test 3

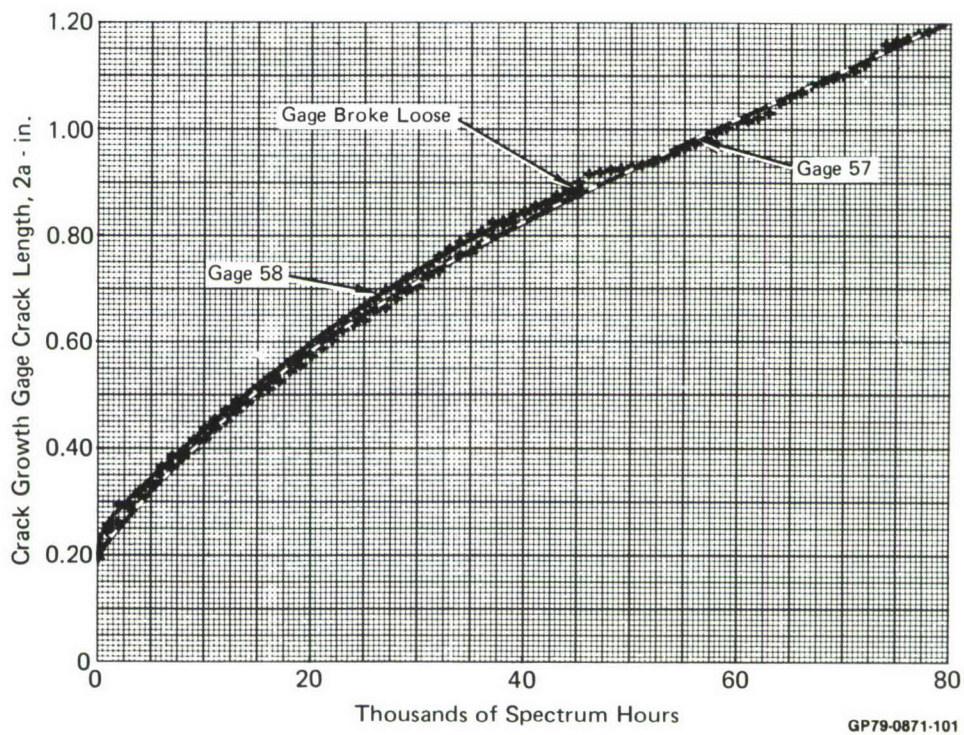


Figure 88. Comparison of Analysis and Test Results for Gage Calibration Test - BL 132.5 Spectrum - Test 4

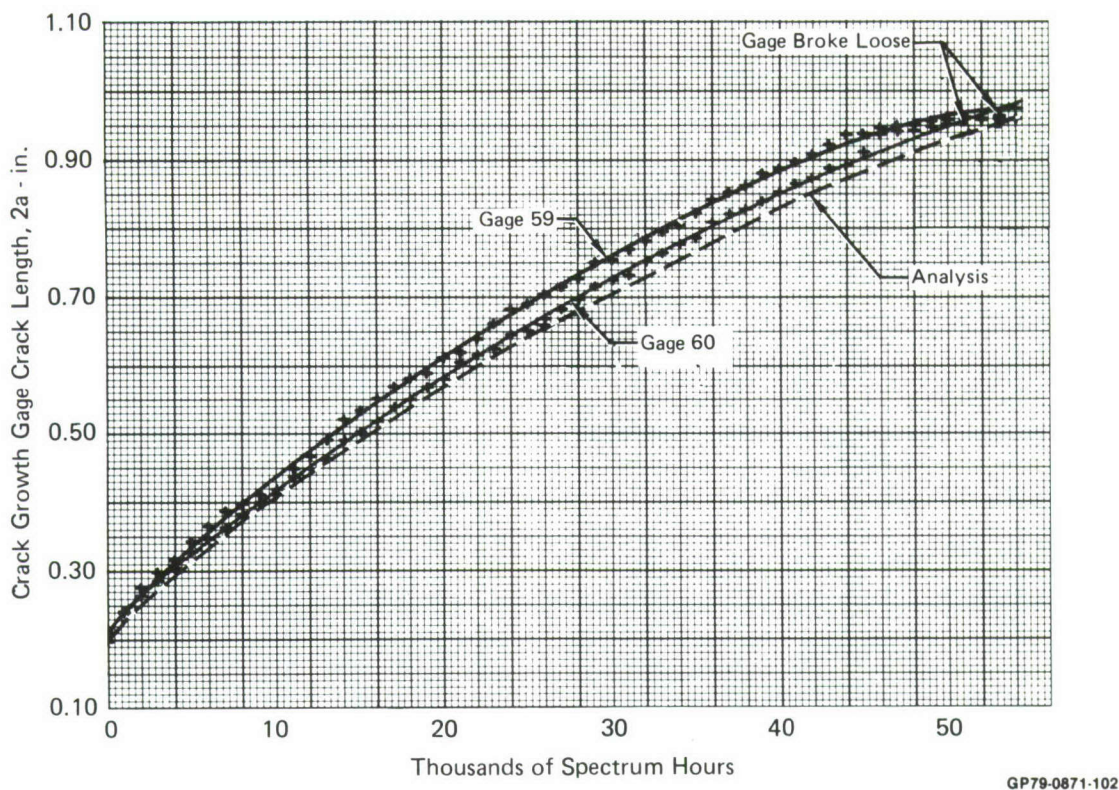


Figure 89. Comparison of Analysis and Test Results for Gage Calibration Test - BL 132.5 Spectrum - Test 5

6. GAGE VALIDATION TESTS - Gage validation tests were used to determine the relationship of crack length in a gage to that in a complex test coupon, Figure 57, under spectrum loadings. The test coupons simulated an area of the lower F-4 wing torque box skin at the intersection of the kick rib and main spar (BL.44.5/LRS 70). Corner flaws were introduced at the center hole on the surface opposite the countersink so that flaw growth could be easily monitored by removing the nut. A fastener was installed with clearance fit.

a. Analysis of Corner Flaw Growth from a Fastener Hole - Crack growth analyses for a corner flaw emanating from a fastener hole were performed using the Contact Stress model. Constant amplitude crack growth rate data was obtained from center cracked panel tests of the F-4 wing skin plate material from which the elements were fabricated, Figure 60.

Stress intensity factors were determined from Fujimoto's results, Reference 18. Effects of yielding near the hole edge were accounted for in these stress intensity factors, thus they are stress level dependent. Stress intensity factors for 30 and 33 ksi limit stress are shown in Figure 90 as a function of crack length. The solutions used to compute these stress intensity factors account for flaw shape change. Predicted flaw shapes are compared to striations on the specimen fracture surface in Figure 91.

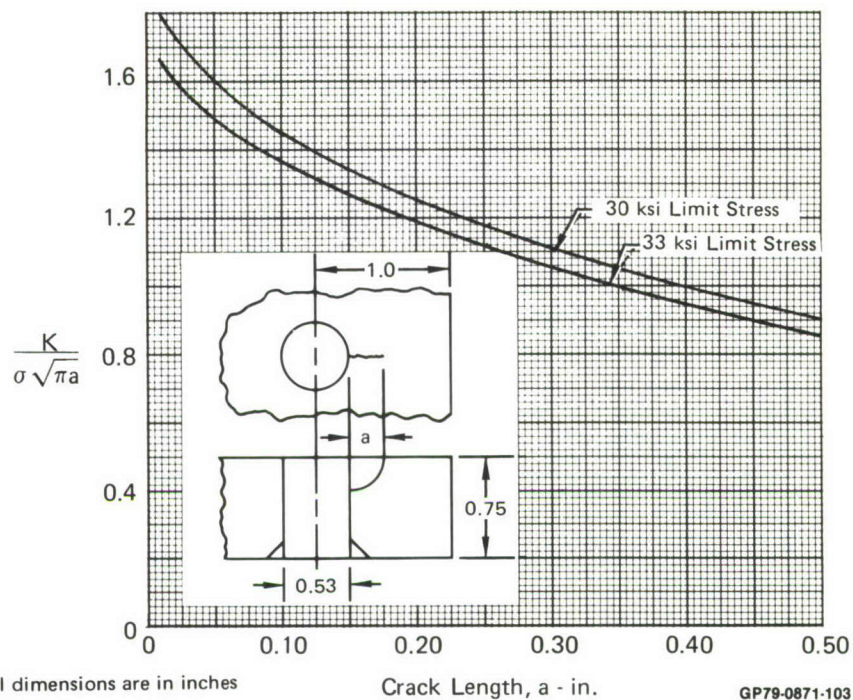


Figure 90. Stress Intensity Correction Factor Used for Analysis of Corner Flaw at Hole

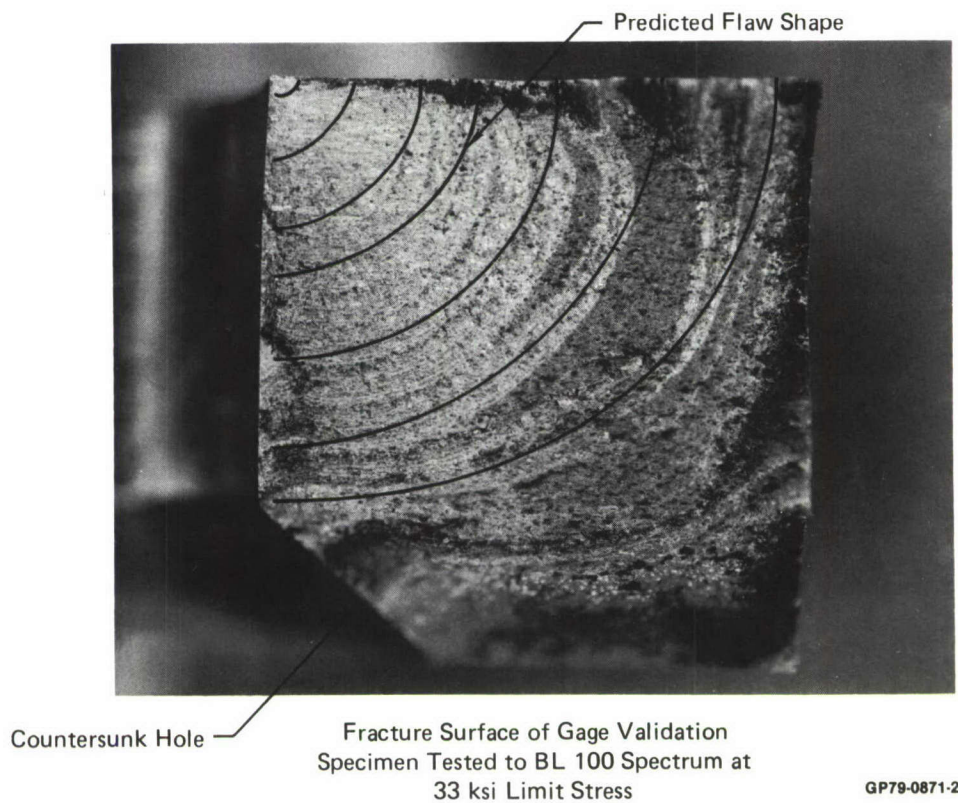


Figure 91. Predicted and Measured Flaw Shapes for Gage Validation Specimens

The minimum effective stress level was used to adjust the analysis to obtain correlation with corner crack growth results. The minimum effective stress level used for all analyses was 35 percent of maximum spectrum stress. Comparison of this stress level with those used in gage analysis indicates that thicker material exhibits less retardation.

Comparison of corner flaw analysis results with data from verification tests is shown in Figures 92-95. Correlation of both crack growth life and curve shape is good.

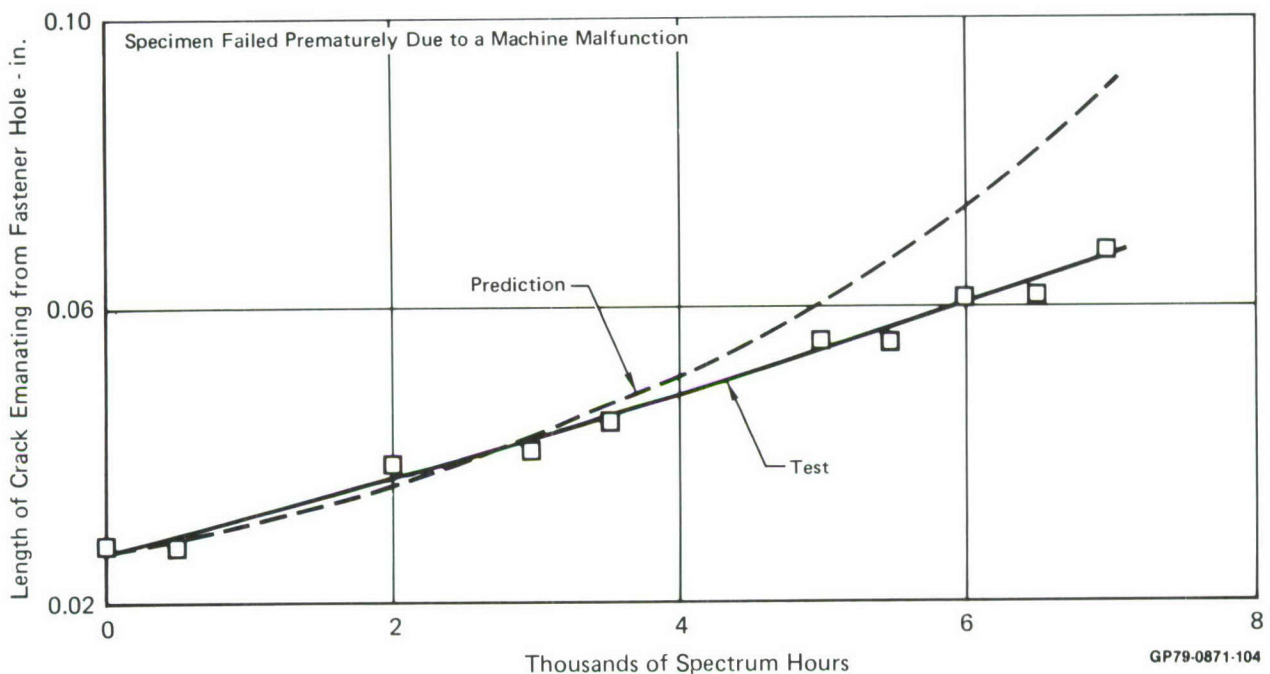


Figure 92. Crack Growth from Hole-Gage Validation Test Results - BL 44.5 Spectrum at 30 ksi Limit Stress (Test 1)

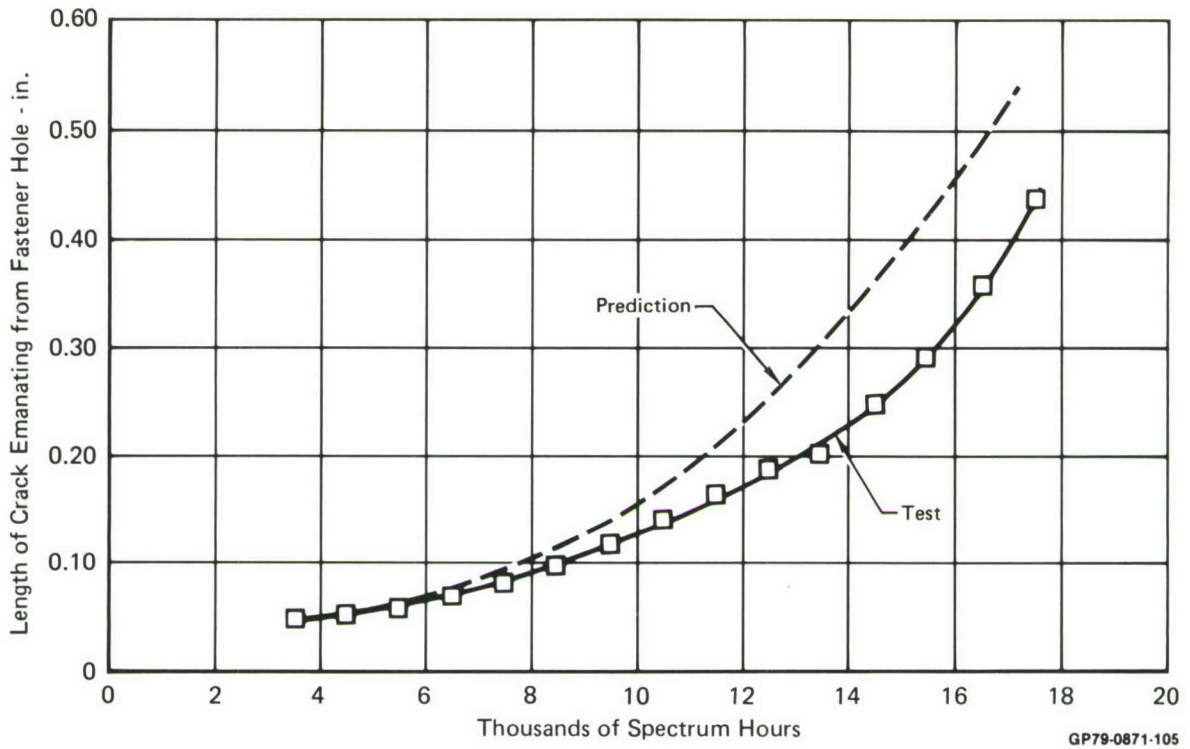


Figure 93. Crack Growth from Hole-Gage Validation Test Results - BL 44.5 Spectrum at 30 ksi Limit Stress (Test 2)

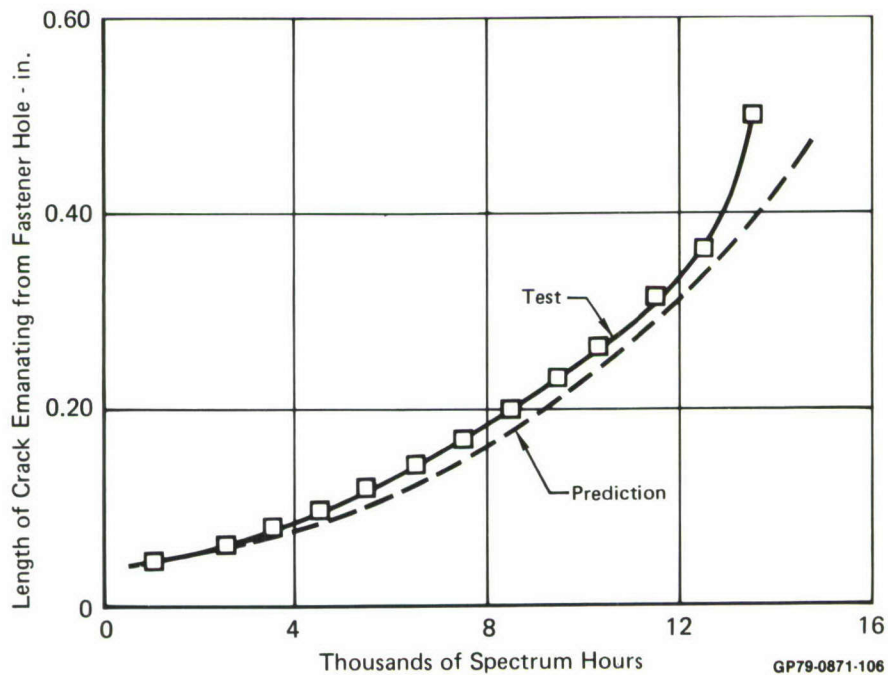


Figure 94. Crack Growth from Hole-Gage Validation Test Results - BL 100 Spectrum at 33 ksi Limit Stress

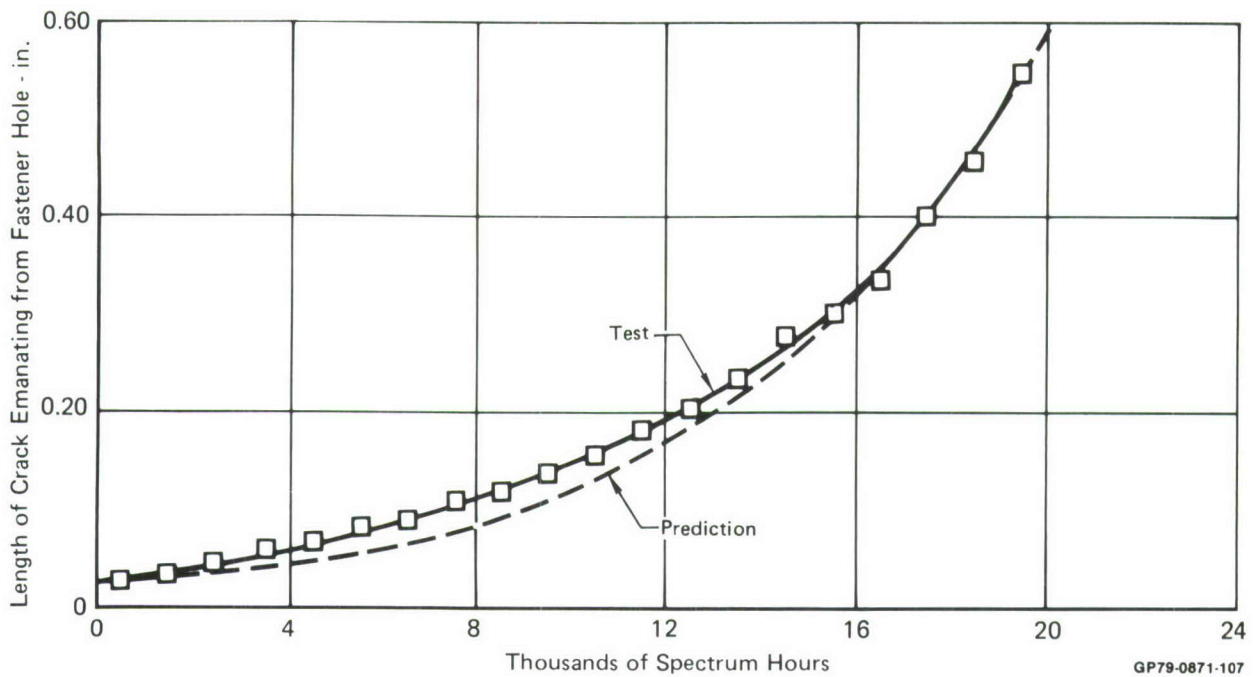


Figure 95. Crack Growth from Hole-Gage Validation Test Results - BL 132.5 Spectrum at 30 ksi Limit Stress

b. Gage Crack Growth Analysis for Verification Tests - Stress intensity factors for gages bonded to verification test coupons (Figure 56) were derived as described in Section 2. Gage stress and stress intensity factor are shown in Figures 96 and 97 as a function of crack length. Minimum effective stress levels for these analyses were the same as those used for gage calibration analyses.

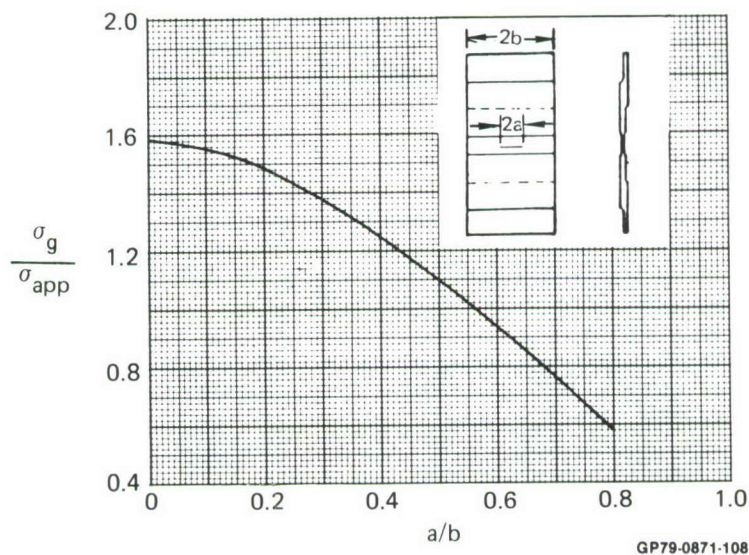


Figure 96. Relationship of Gage Stress to Gross Stress Applied to Gage Validation Specimen

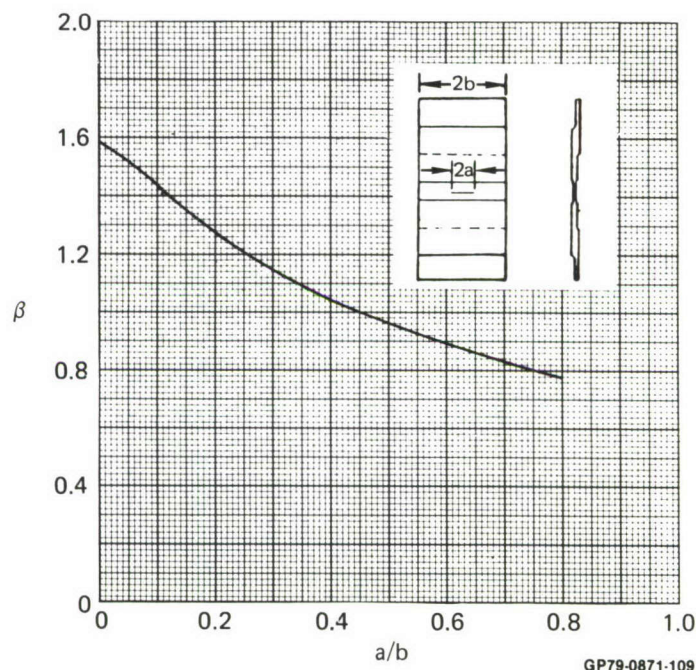


Figure 97. Stress Intensity Factor Correction for Gage Bonded to Gage Validation Specimen

Results of analyses and tests are presented in Figures 98-101. Good correlation is evident between analysis and test results for gages on the nut side of the specimen. Gage crack growth on the fastener head (countersunk) side of the specimen was usually somewhat slower than on the nut side. Analysis indicates that an 11 percent reduction in stress level would be required to produce this result.

c. Correlation of Gage Crack Growth and Corner Flaw Growth in Gage Validation Tests - Comparison of predicted and measured crack length relationship between gage and fastener hole is shown for each of the validation tests in Figures 102-105. Good correlation is evident and indicates that the relationship of gage crack growth to element crack growth can be predicted if the stress spectrum is known.

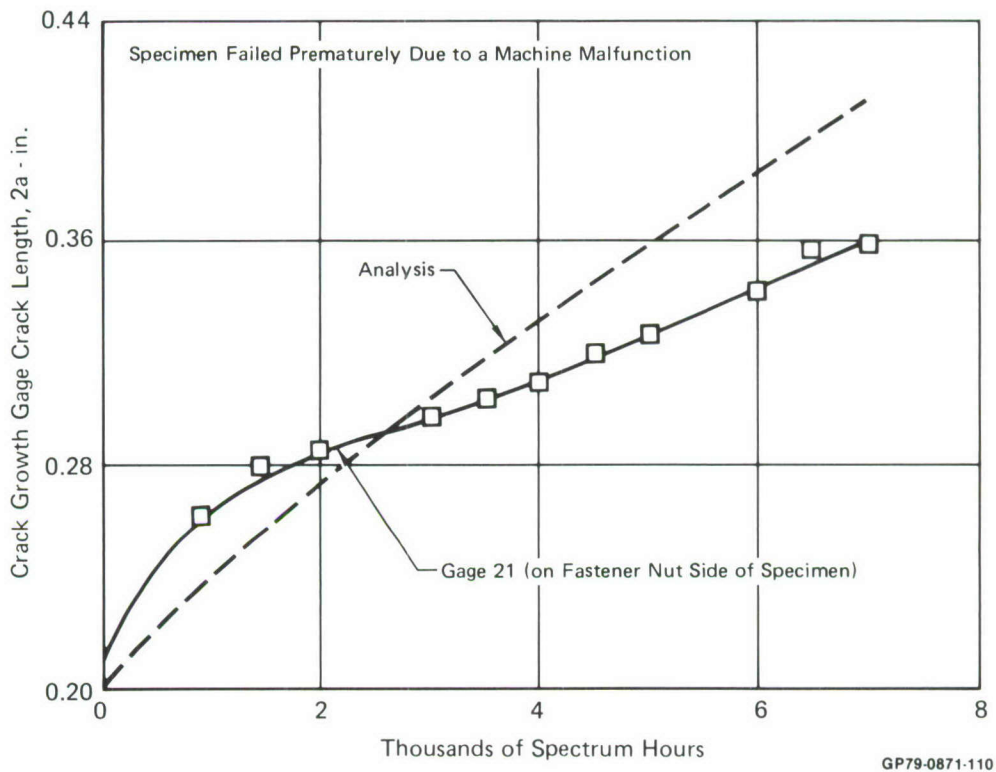


Figure 98. Gage Crack Growth - Gage Validation Test Results - BL 44.5 Spectrum at 30 ksi Limit Stress (Test 1)

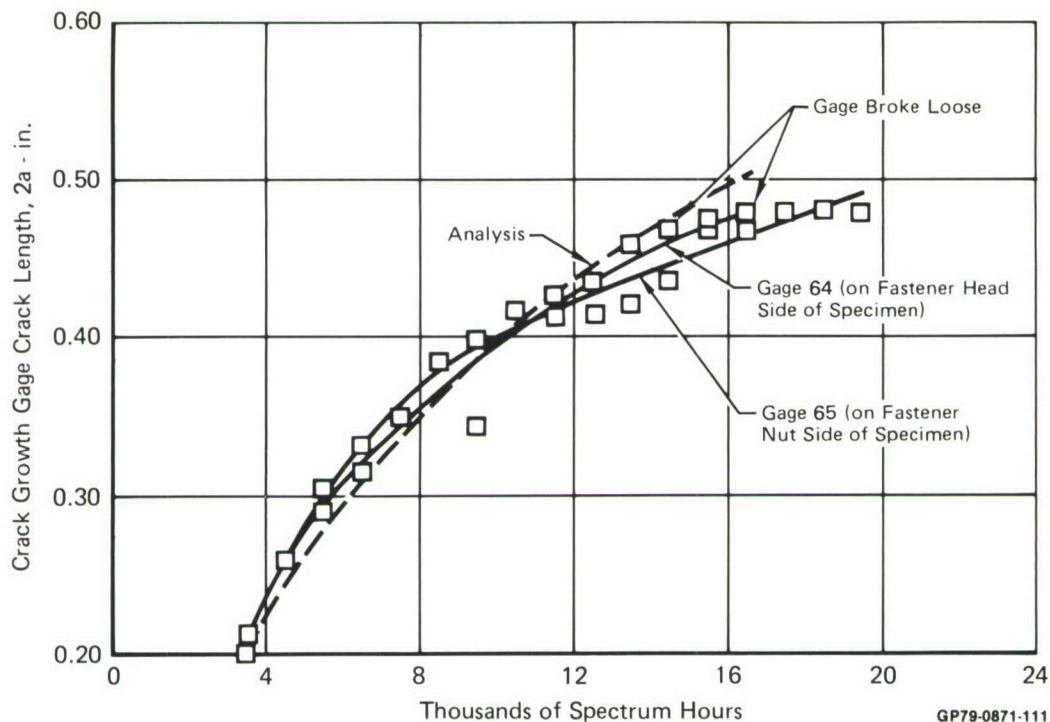


Figure 99. Gage Crack Growth - Gage Validation Test Results - BL 44.5 Spectrum at 30 ksi Limit Stress (Test 2)

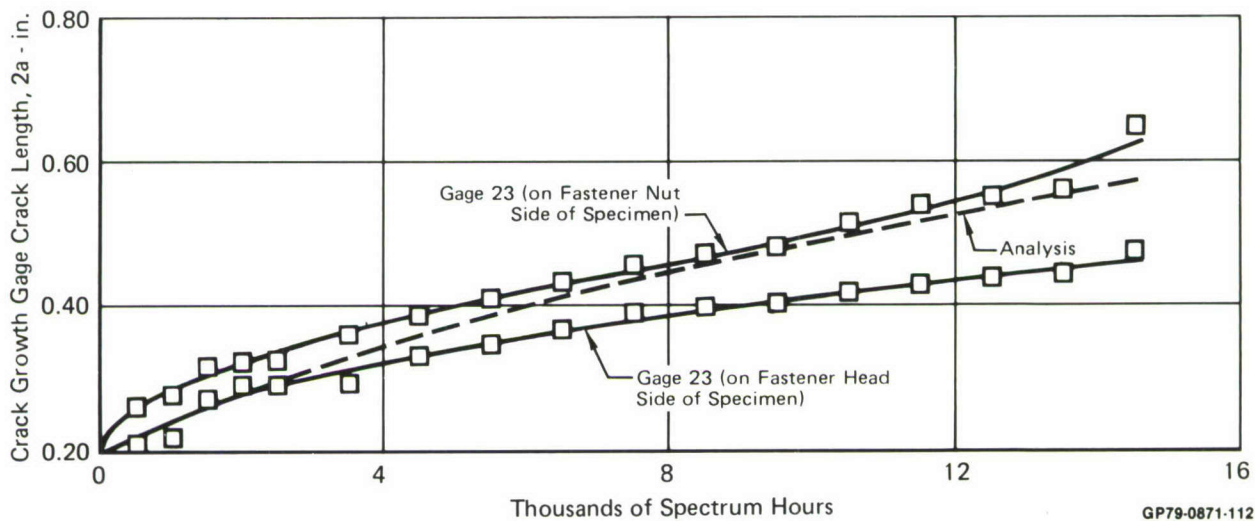


Figure 100. Gage Crack Growth - Gage Validation Test Results - BL 100 Spectrum at 33 ksi Limit Stress

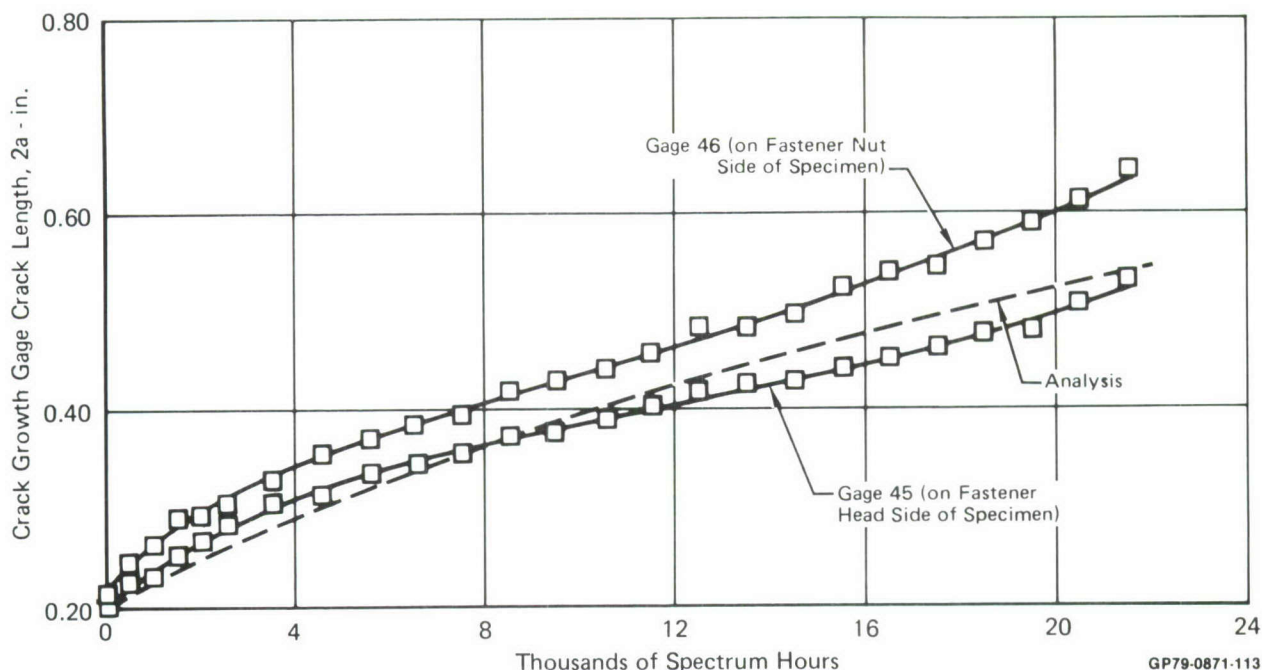


Figure 101. Gage Crack Growth - Gage Validation Test Results - BL 132.5 Spectrum at 30 ksi Limit Stress

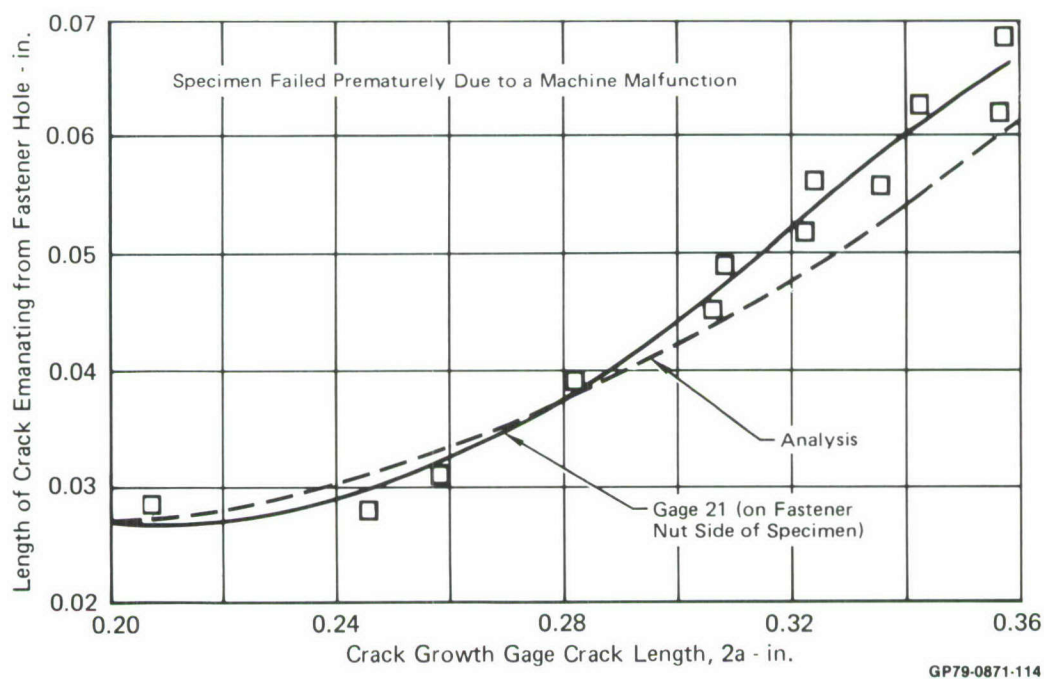
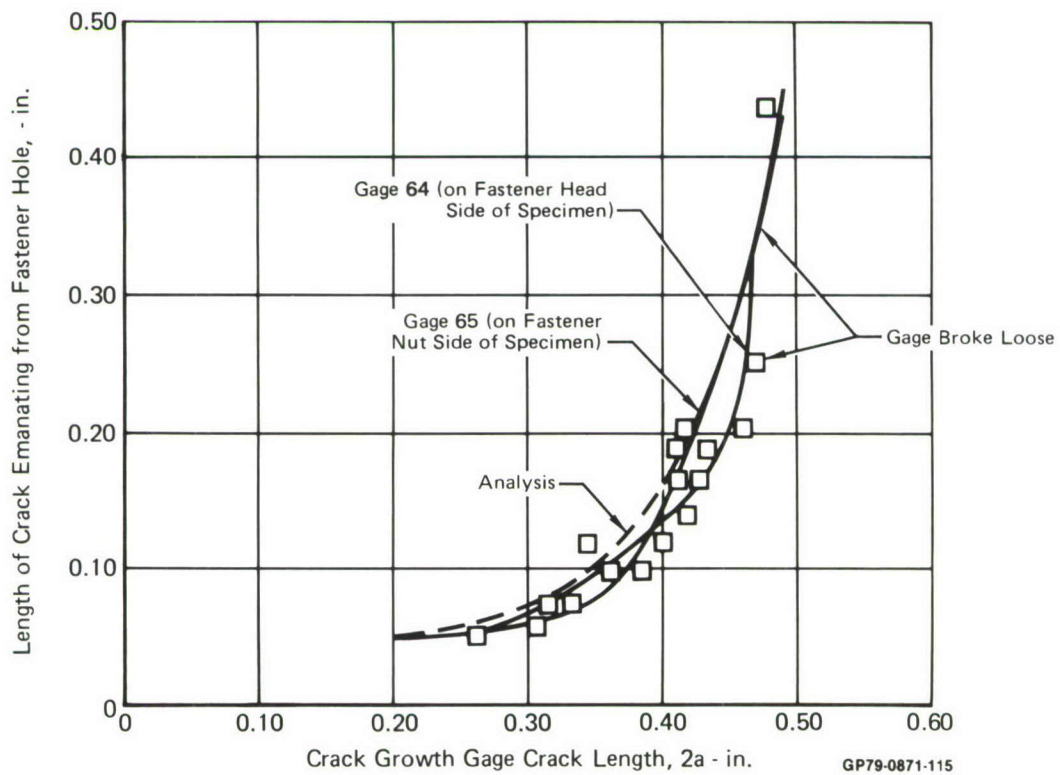


Figure 102. Gage Validation Test Results - BL 44.5 Spectrum at 30 ksi Limit Stress (Test 1)



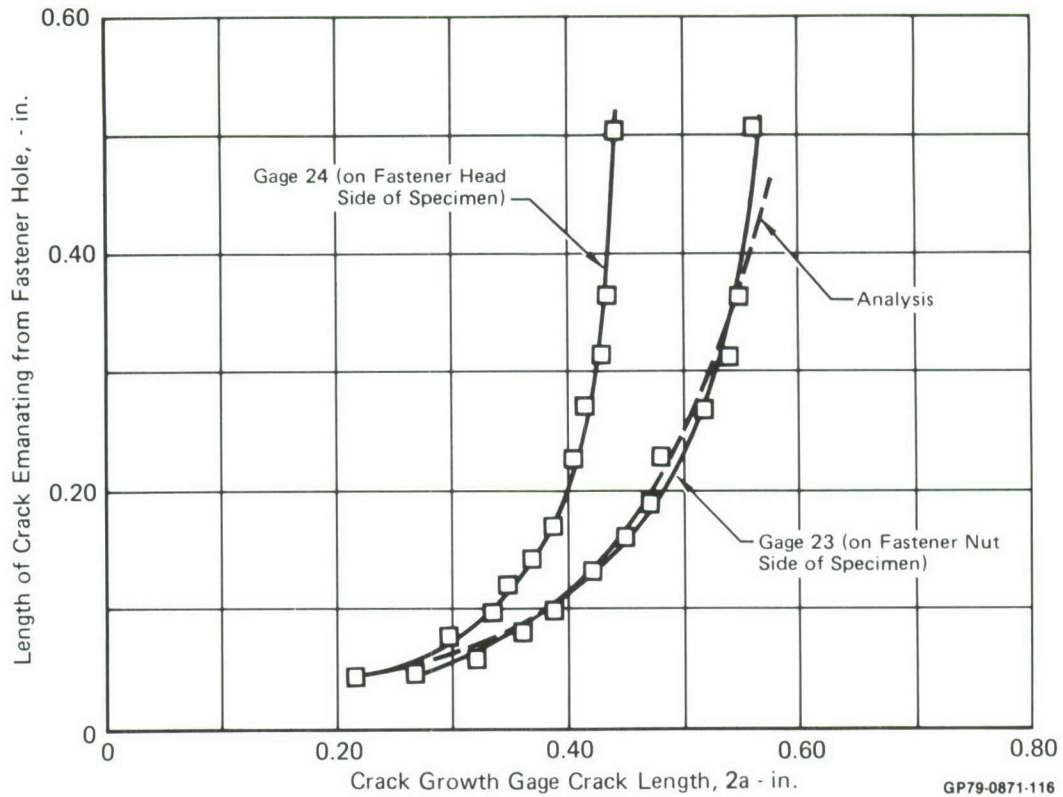


Figure 104. Gage Validation Test Results - BL 100 Spectrum at 33 ksi Limit Stress

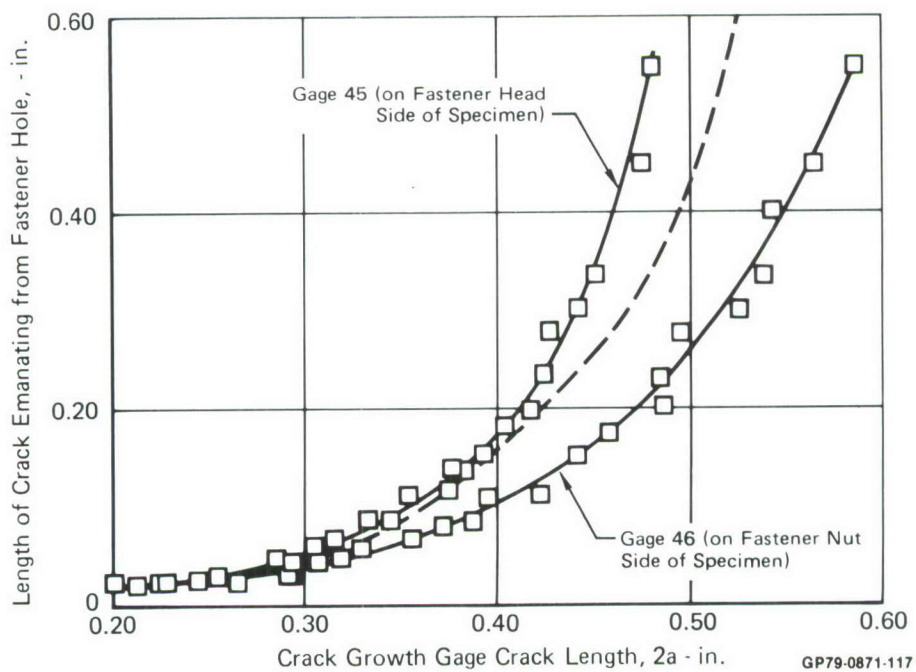


Figure 105. Gage Validation Test Results - BL 132.5 Spectrum at 30 ksi Limit Stress

SECTION VI

PREDICTED RESPONSE OF CRACK GROWTH GAGES ON F-4 FATIGUE TEST ARTICLE

The load-displacement characteristics, derived in Section III, for the crack growth gage were used to determine the relationship of stress in the gages to stress in three structural locations at which gages are applied to the F-4 fatigue test article at Wright-Patterson AFB. The three right wing structural locations considered were the three originally selected sites (Figure 44).

To predict crack growth in the gages mounted to the AFFDL fatigue test article, gage stress to structural stress relationships and stress intensity factors were derived for gages applied at the selected sites. Gage stresses and stress intensity factors were based on the analyses described in Section II. Crack growth predictions were based on the analyses of gage calibration and verification tests presented in Section V. Relationships of potential structural flaw growth to gage crack growth were determined.

1. RELATIONSHIP OF STRESS IN GAGE TO STRESS IN STRUCTURE - Analyses were performed to determine the gage stress. Equation 11 of Section II was used for all analyses of gage stress. Manufacturing and bonding tolerances shown to produce the maximum effect on gage stress were evaluated.

Results of these evaluations are presented for Sites 1 and 3 (Figure 44) which are the locations having the maximum and minimum skin thicknesses.

a. Effect of Wing Skin Thickness on Gage Stress - Wing skin thickness at the selected gage sites are 0.563 inch at Site 1 (BL 44.5/LRS 70), 0.381 inch at Site 2 (BL 100/LRS 140), and 0.178 inch at Site 3 (BL 132.5/LRS 183). The effective width of skin used in analysis was four inches, loads carried by the gage are assumed to reduce stresses in the skin two inches either side of the gage centerline. Gage stiffness was assumed to be the same as that used in the element coupon analysis (Section II).

Results of the analyses are shown in Figure 106. Gage stress levels are increased when applied in the areas having greater skin thicknesses. Gage stresses for Site 3 are closest to the gage stresses for calibration specimens. Results for Site 1 show up to ten percent greater stress in the gage than at Site 3. Site 2 stresses are up to seven percent greater than at Site 3. The greatest difference occurs at short crack lengths, when gage stiffness is greatest.

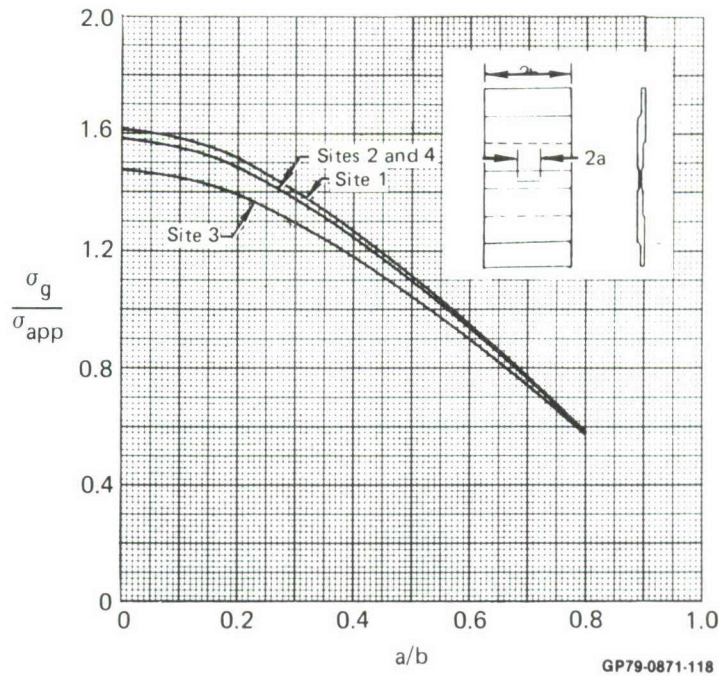
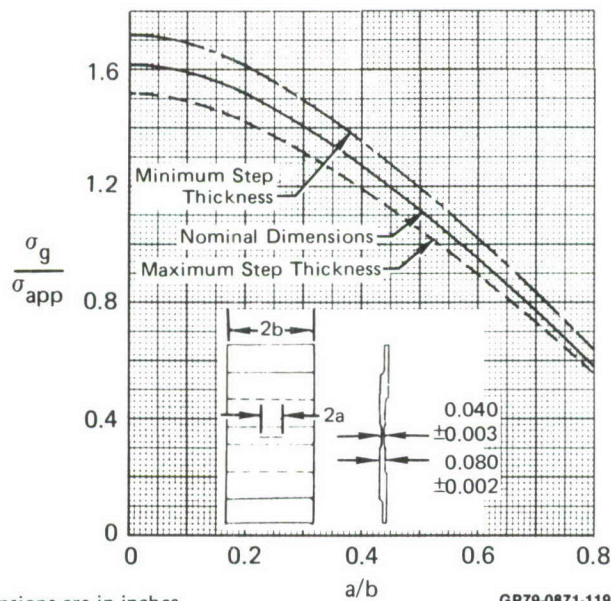


Figure 106. Nominal Relationships of Gage Stress to Stress in Wing Skin

b. Effect of Machining Tolerances on Gage Stress - The machining tolerance found to have greatest effect on gage stress was step thickness tolerance. The impact of gage step thickness variations on gage stress at Site 1 is shown in Figure 107. Maximum deviations from the nominal stress are less than eight percent. The reduction or magnification was found to be independent of crack length. These results are in good agreement with those found in the analysis of the calibration specimens (Section II.7.a.).



Note: All dimensions are in inches

Figure 107. Impact of Step Thickness Tolerances on Relationship of Gage Stress to Wing Skin Stress at Site 1

The impact of gage step thickness variations on gage stress at Site 3 is shown in Figure 108. Maximum deviations from nominal stresses are less than seven percent, independent of crack length, and in agreement with previous results summarized in Figure 32. Results for such variations at Site 2 are within seven to eight percent of nominal stress relationships.

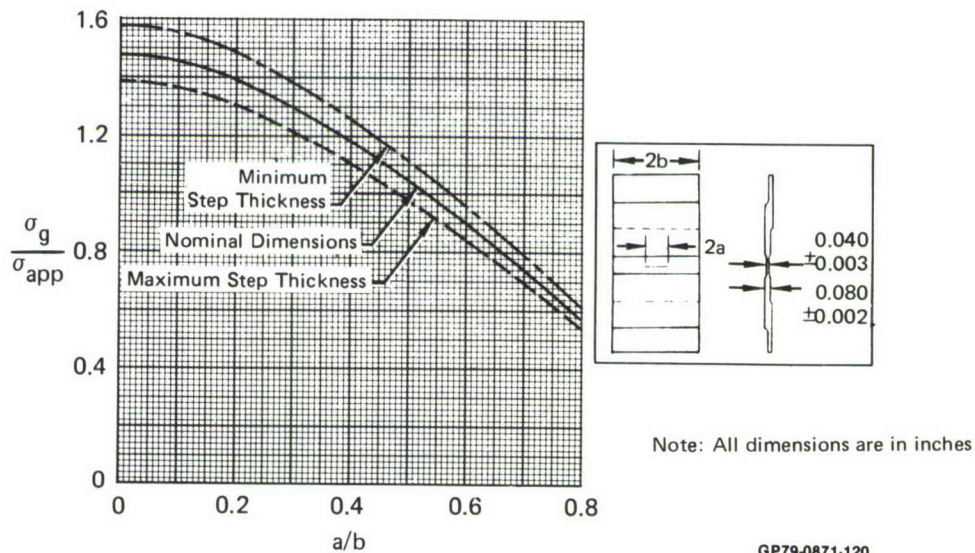


Figure 108. Impact of Step Thickness to Tolerances on Relationship of Gage Stress to Wing Skin Stress at Site 3

c. Effects of Adhesive Joint Variations on Gage Stress - Adhesive joint variations (step length and width, and bondline modulus) have little effect on gage stress. These variations cause less than one percent variation in the stress of gages mounted on gage calibration specimens. Similar results were found in this analysis for gages bonded to wing skins.

d. Effect of Gage Misalignment on Gage Stress - Gage alignment with principal stress direction is more difficult for application to a wing skin than to an element specimen. Therefore, the effect of misalignment could be greater for structural applications. The square of the cosine of the misalignment angle was used to estimate the reduction in gage axial stress. In complex structure such as a wing skin, gage misalignment could be as much as 20 degrees from the principal strain direction. This results in as much as a 13 percent reduction in gage stress at any crack length.

e. Effect of Temperature Differential Between Adherends During Bonding on Gage Stress - Heating blankets were used to bond gages to the F-4 fatigue test article at Wright-Patterson AFB. Thermocouples applied to another wing skin and gage during bonding tests showed that the surface of the gage can reach 360°F during bonding while the skin surface adjacent to the gage may only reach 250°F. At these temperatures the adhesive flows, however, as the adhesive cools after curing, it sets up. After the gage and wing skin have cooled, residual stresses exist in the gage and adhesive. The magnitudes of these residual stresses depend on temperatures of the gage and wing skin when the adhesive sets up, and ambient temperature.

Hart-Smith's adhesive analysis procedure, Reference 9, was used to estimate residual stresses caused by thermal mismatch. Analysis of the bondline stresses is complicated by uncertainty in adhesive set-up temperature and by the fact that thermal strains in the wing skin due to local heating are less than those for general heating, due to the elastic constraint of cooler surrounding structure.

Thermal strain mismatch between gage and wing skin has greater impact on the bondline strains than on stresses transmitted to the gage. Consequently temperature mismatch has greater impact on bond durability than on gage stress. Analyses showed that residual strains in the adhesive due to a 110°F temperature differential between gage and wing skin during bonding would produce considerable plastic strains under load, reducing the durability of the joint. Analyses to determine the effects of temperature differential on gage stresses assumed a 110°F temperature differential between gage and wing skin.

Gage stress, for gages bonded to the F-4 wing skin using heating blankets to cure the adhesive, has two components: that due to stresses in the wing skin, and that due to thermal strains. The magnitude of the first component is given by Equation 11 derived in Section II.4, repeated below

$$\frac{\sigma_g}{\sigma_s} = \frac{\sigma_{gh}}{E_v} \times \frac{v}{v_o} \times \frac{E v_o}{\sigma_{sh}} \quad (15)$$

where σ_s is the structural stress level. For the selected gage sites, values of this component are presented as a function of gage crack length in Figure 106, Section 1.a.

The component of gage stress caused by temperature differential between gage and skin at adhesive set up can be expressed as

$$\frac{\sigma_g}{\sigma_s} = \frac{\sigma_{gh}}{E_v} \frac{E v_{temp}}{\sigma_{sh}} \quad (16)$$

where v_{temp} is the gage displacement due to residual strains set up in the adhesive during bonding.

Combining the two components, the relationship of gage stress to structural stress can be expressed as

$$\frac{\sigma_g}{\sigma_s} = \frac{\sigma_{gh}}{Ev} \frac{v}{v_o} \frac{Ev_o}{\sigma_{sh}} + \frac{Ev_{temp}}{\sigma_{sh}} \quad (17)$$

Analyses of residual strains due to 110°F temperature differential between gage and skin show v_{temp} is 43.4 microinches at Site 1, 42.0 microinches at Sites 2 and 4, and 37.8 microinches at Site 3. The differences in residual strains are due to differences in skin thicknesses at the selected sites. Residual thermal strains in the adhesive were computed using Hart-Smith's analysis, Reference 9.

Results of gage stress analyses accounting for residual strains of the three gage locations are shown in Figure 109. The increases in gage stress level are about 3.5 percent at limit stress in the structure. These increases did not occur in the element test specimens since the specimens were cured in an autoclave so that gage and coupon were subjected to the same temperature. These increases did not occur in the gages finally bonded to the fatigue test article because a room temperature cure adhesive was used.

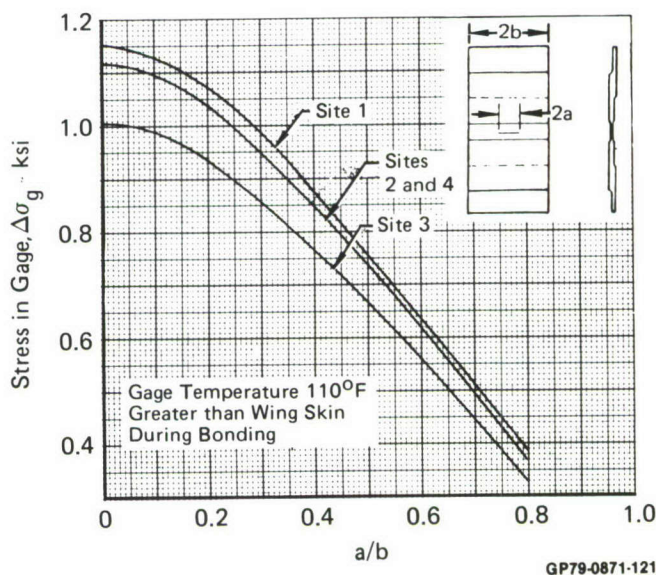


Figure 109. Stress in Gage Due to Bonding Thermal Strains

2. RELATIONSHIP OF GAGE STRESS TO STRUCTURAL STRESS USED TO PREDICT GAGE CRACK GROWTH - Gages selected for bonding to the fatigue test article were those gages having dimensions closest to the nominal dimensions. Nominal dimensions and the gage stress to structural stress relationships of Figure 106 were used for these analyses. Previous strain surveys of F-4 lower wing skins, Reference 19, showed that aligning the gages with the nearest spar caps and stiffeners produced axial stress levels at the selected sites slightly less than the principal stress levels shown in Section IV. Limit axial stress levels in the structure were determined to be those shown in Table 13. It was assumed that the temperature differential between gage and wing skin when the adhesive set-up after curing was negligible for the room temperature cure adhesive eventually used. Thermal strain differences between wing skin and gage would have to be considered were an elevated temperature cure adhesive such as FM-73 used. Thermal strain effects are discussed in Section 1.e. Without thermal strains the gage stress is given by Equation (11).

**TABLE 13. WING SKIN STRESSES
PARALLEL TO GAGE**

Gage Site	Limit Stress Level (ksi)
1	21.4
2	28.6
3	25.6
4	28.6
5	21.4
6	24.7
7	24.7
8	25.6

GP79-0871-152

3. STRESS INTENSITY FACTORS - Stress intensity factors for crack growth gages applied to the AFFDL fatigue test article were derived from the gage stress to structural stress relationship. As noted in Section II, the gage stress intensity factor can be expressed as

$$K = \sigma_g \beta_\sigma \sqrt{\pi a} \quad (18)$$

Consequently, the gage stress intensity factor, in terms of the structural stress is

$$K = \frac{\sigma_g h}{E v} \frac{v}{v_o} \frac{E v_o}{\sigma_s h} \sigma_s \beta_\sigma \sqrt{\pi a} \quad (19)$$

or

$$K = \frac{v}{v_o} \frac{E v_o}{\sigma_s h} \sigma_s \beta_v \sqrt{\pi a} \quad (20)$$

Equation (20) was used for computation of stress intensity factors in the crack growth analyses of gages bonded to the F-4 fatigue test article.

4. CRACK GROWTH ANALYSES - Crack growth analyses for gages applied to F-4 fatigue test article were performed using the Contact Stress model, References 6-8, modified to account for thickness effects. Predictions using this procedure were shown to correlate well with the gage calibration test results. The constant amplitude crack growth rate curve used for gage analysis was presented in Figure 58 of Section V. Predicted crack growth in the gages at the originally selected sites is shown in Figure 110.

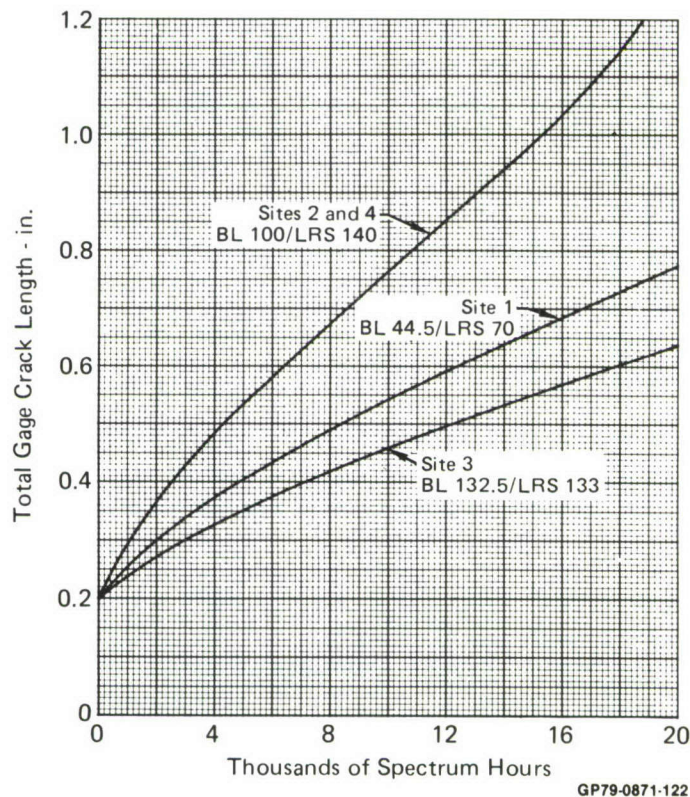


Figure 110. Predicted Crack Growth in Gages on F-4 Fatigue Test Article

5. RELATIONSHIP OF GAGE CRACK GROWTH TO POTENTIAL CRACK GROWTH IN STRUCTURE - The relationship of gage crack growth to flaw growth in the structure is determined by independent analyses of the gage crack and the structural flaw. Predicted crack growth of gages applied to the F-4 fatigue test article are presented in Figure 110. Model parameters for predictions of flaw growth in the fatigue test article were based on correlations with element test results reported in Reference 20. Relationships of gage crack growth to structural flaw growth were determined from these predictions.

a. Predicted Flaw Growth in Structure - Element test results were used to select model parameters for predictions of flaw growth at fastener holes in the F-4C/D fatigue test article. Test results were presented in Reference 19 for elements representing BL.44.5 at the main spar near gage Site 1 and the pylon hole at BL.132.5 (near gage Site 3) tested to the F-4C/D ASIP (FSCP 66 loads) baseline spectrum. Predicted crack growth curves for these locations using the F-4C/D full scale fatigue test spectrum are shown in Figures 111 and 112.

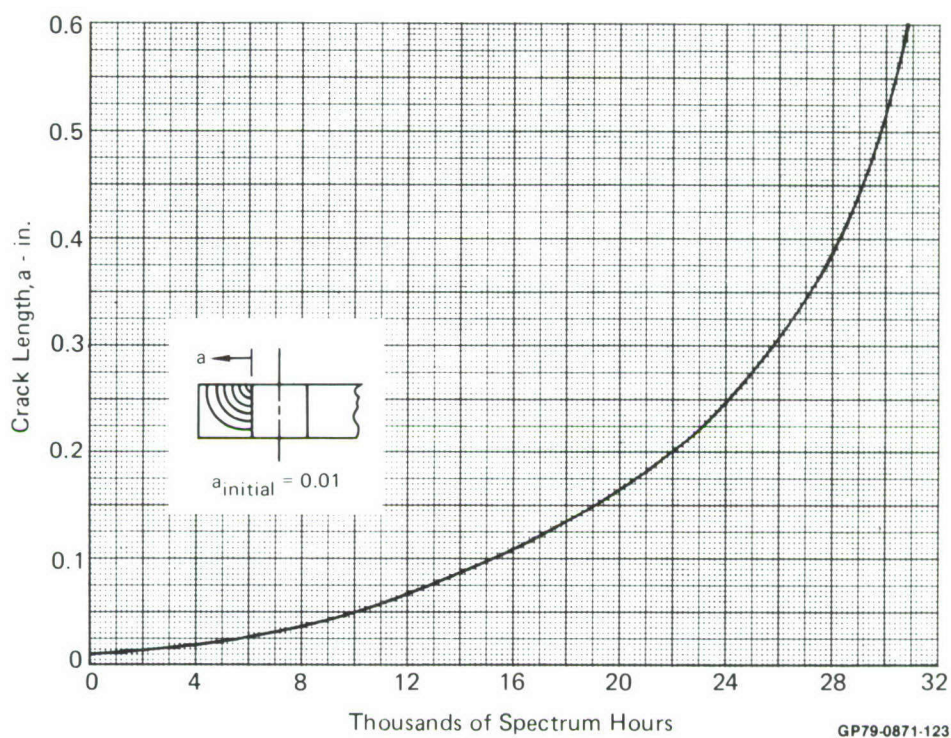


Figure 111. Predicted Crack Growth in Fatigue Test Article Lower Wing Skin - BL 44

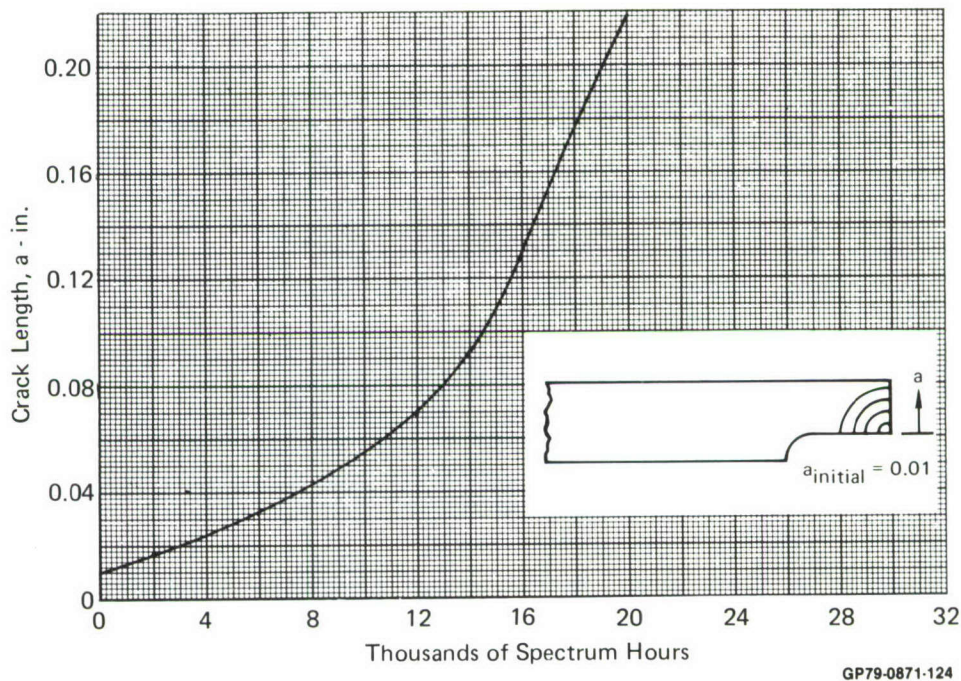


Figure 112. Predicted Crack Growth in Fatigue Test Article Lower Wing Skin at Pylon Hole

Flaw growth from fastener holes at BL.100 (near gage Sites 2 and 4) is expected to be very slow due to the taper-lok fasteners installed in that area. Test results show an average of 0.028 inch of growth from 0.042 inch precracks after 50,000 spectrum hours. For comparison with gage crack growth at Sites 2 and 4, crack growth at the main spar at BL.132.5 was predicted. Taper-loks are not used in the BL.132.5 area, and this area is predicted to be more fracture critical than the BL.100 area. Model parameters for these predictions were based on correlations with element test results presented in Reference 12 for the F-4 ASIP spectrum. Results of this analysis for the full scale fatigue test spectrum are presented in Figure 113.

b. Relationship of Gage Crack Growth to Structural Flaw Growth - Relationship of gage crack growth to structural flaw growth was determined from the above predictions. The relationships are shown in Figures 114-116. Crack growth in the gage at Site 2 (Figure 115) is fastest, making this the most sensitive location for tracking potential growth in the structure.

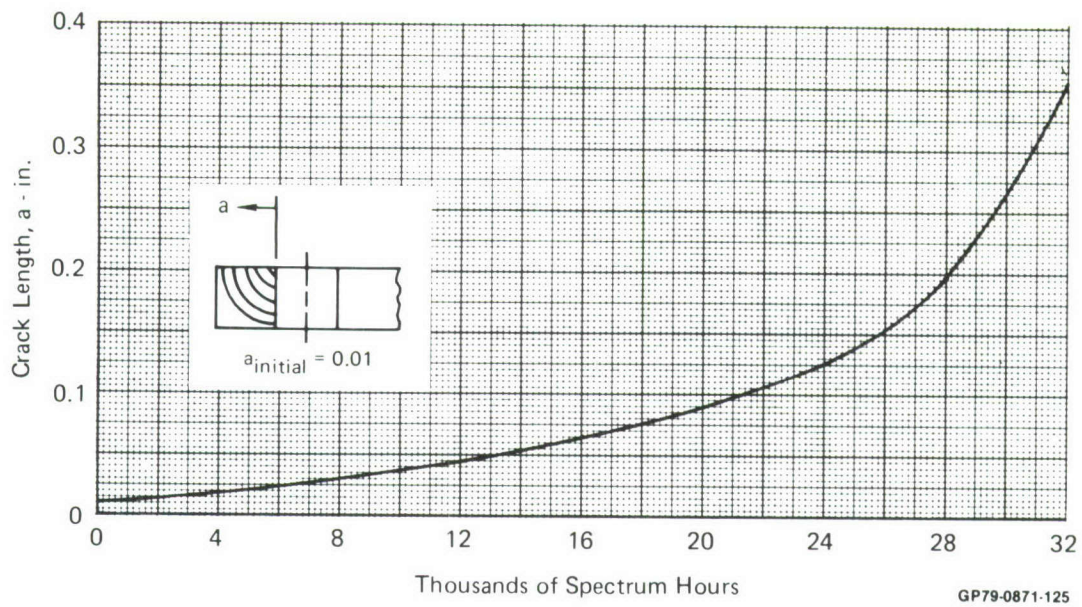


Figure 113. Predicted Crack Growth in Fatigue Test Article Lower Wing Skin at BL 132.5

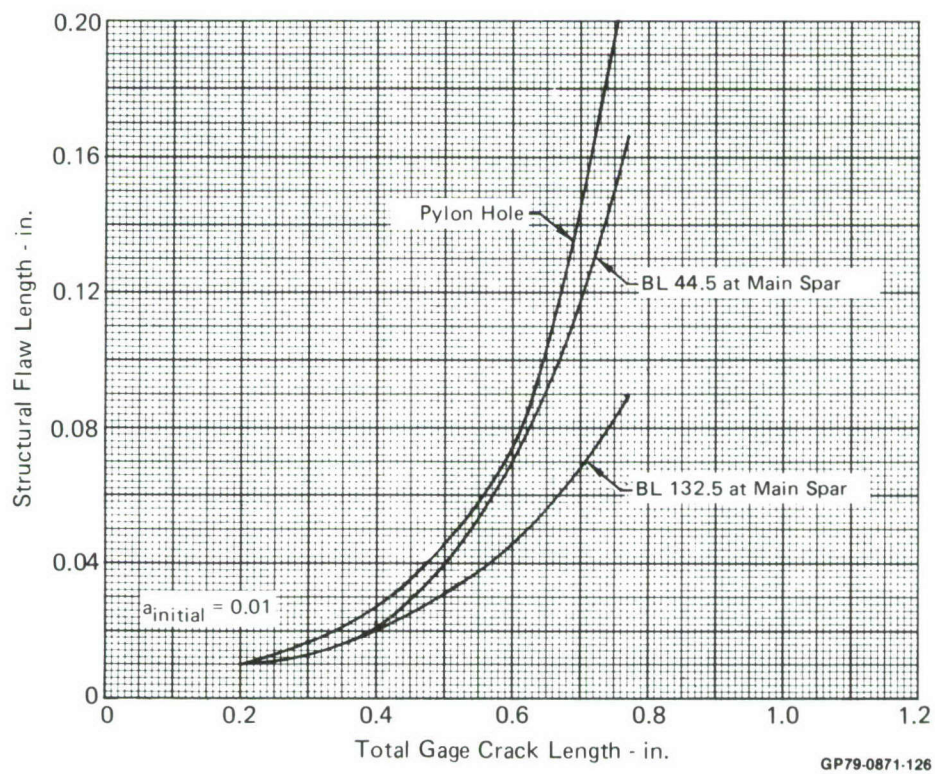


Figure 114. Predicted Relationship of Site 1 Gage Crack Length to Structural Flaw Length in Fatigue Test Article

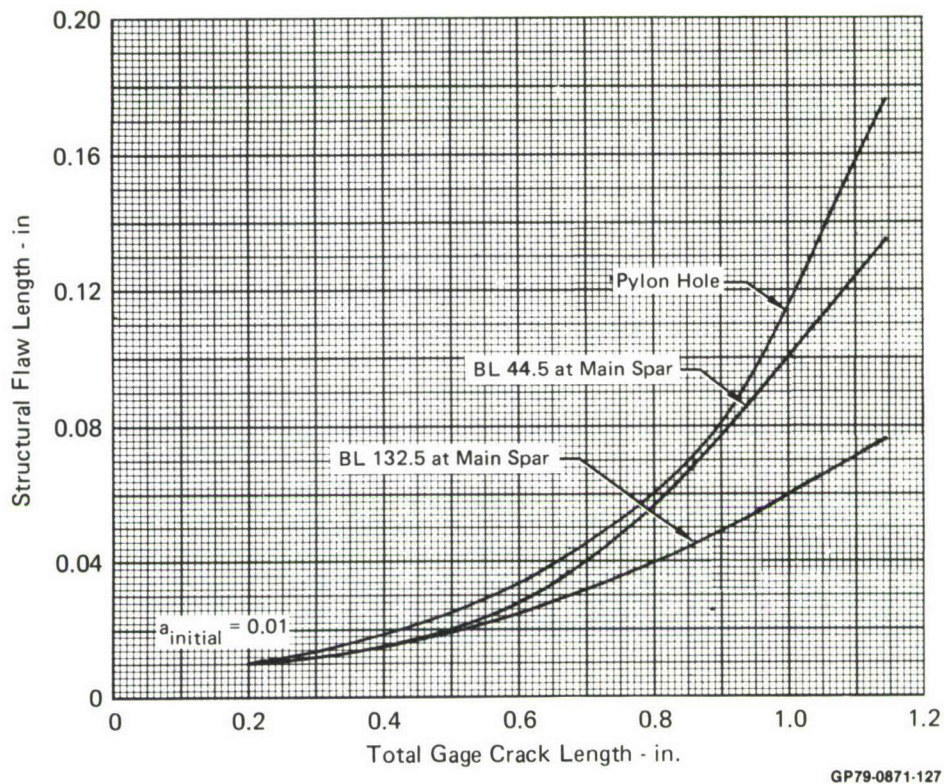


Figure 115. Predicted Relationship of Site 2 Gage Crack Length to Structural Flaw Lengths in Fatigue Test Article

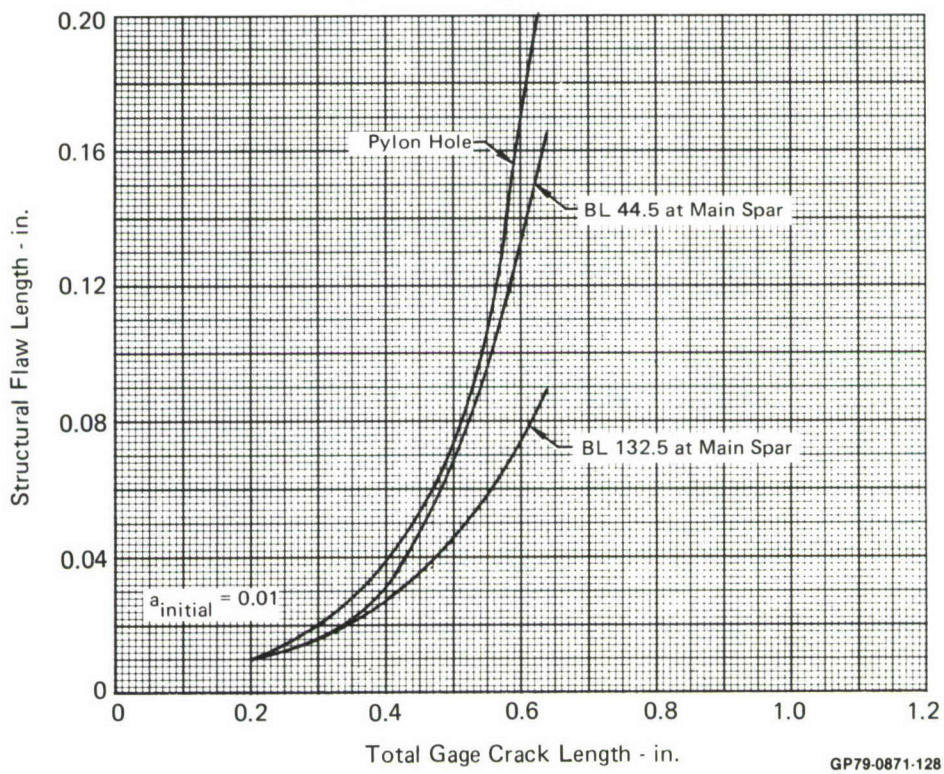


Figure 116. Predicted Relationship of Site 3 Gage Crack Length to Structural Flaw Lengths in Fatigue Test Article

SECTION VII

MONITORING POTENTIAL OF CRACK GROWTH GAGE

Assessment of the monitoring potential of this crack growth gage design accounted for prediction accuracy for crack growth in gages applied to the F-4 fatigue test article, potential uses of the gage as a fatigue life monitoring device, and the impact of gage design, adhesives, machining tolerances and inspection methods on life monitoring potential of the gage. From the data obtained from the full scale fatigue test article, gage crack growth predictions appear to be reasonably accurate. Because crack growth retardation in the gage differs markedly from that in the wing skin, due to the difference in thicknesses, correlation of gage crack growth with potential wing skin crack growth is complicated. One method of interpretation appears to give reasonable predictions of potential wing skin crack growth. The gage thickness significantly impacts the crack growth behavior and consequently the monitoring potential of the gage. The problems encountered during bonding with FM-73 adhesive indicate that the adhesive and bonding procedure selected for eventual gage attachment to fleet aircraft must be subjected to a comprehensive qualification test program before acceptance.

1. GAGE PERFORMANCE ON TEST ARTICLE - Gage crack growth predictions shown herein are based on the measured initial crack length in the gages rather than the nominal 0.2 inch crack length used in earlier predictions.

The predicted strains in the wing skins parallel to crack growth gages agree well with those measured (Figures 117-119). The trend of the ratio of measured and predicted strains is for the values at lower load levels to be greater than average and to approach an average asymptotically with increasing loads. The impact on crack growth caused by differences between measured and predicted strains is slight even for the location showing greatest difference, BL 100/LRS 140 (Figure 120).

Crack lengths in gages bonded to the fatigue test article were determined through microscopic examination of impressions of the crack made in Faxfilm replicating tape. The film was pressed onto the gage step containing the crack to obtain the impression. Measurements of the Faxfilm impressions could be made more accurately than direct measurement of gage crack length, and the Faxfilm impressions make a good record of measurements.

Comparisons of predicted and measured crack growth in the gages are shown in Figures 121-125. In general, the agreement between predicted and measured crack lengths is good unless the initial gage crack length exceeds 0.3 inch or the gage debonds. Gages having initial crack lengths greater than 0.3 inch (Figures 122 and 125) have shown somewhat faster growth than predicted. Perhaps this faster growth is due to acceleration

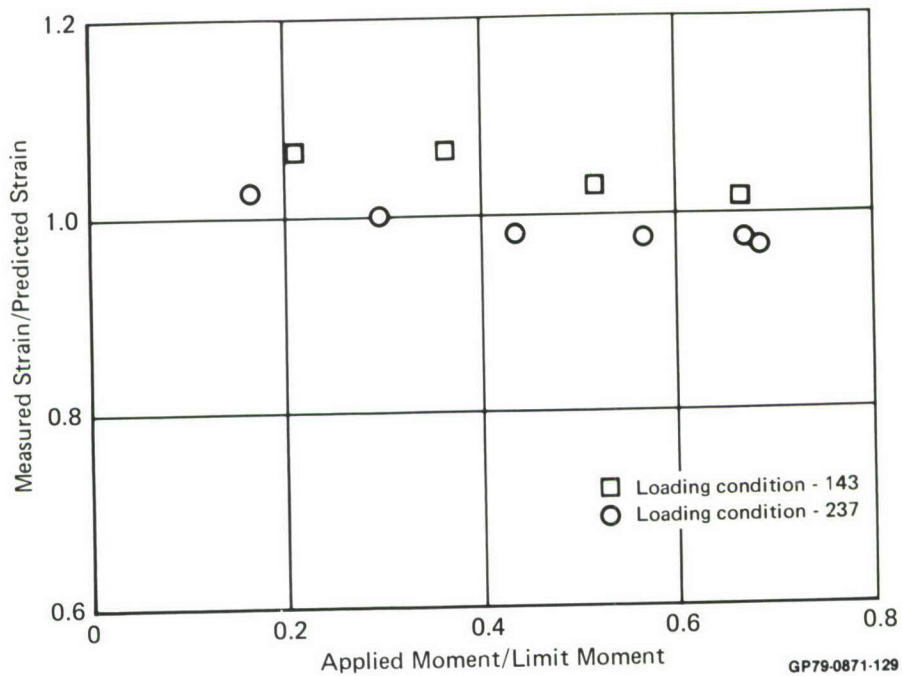


Figure 117. Comparison of Measured and Predicted Wing Skin Strain at BL 44.5

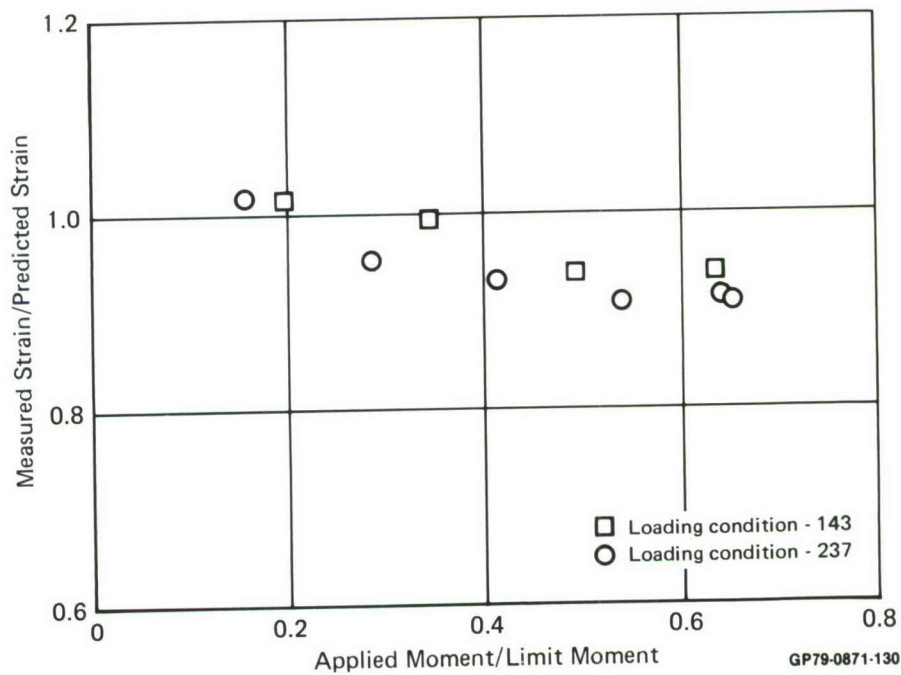
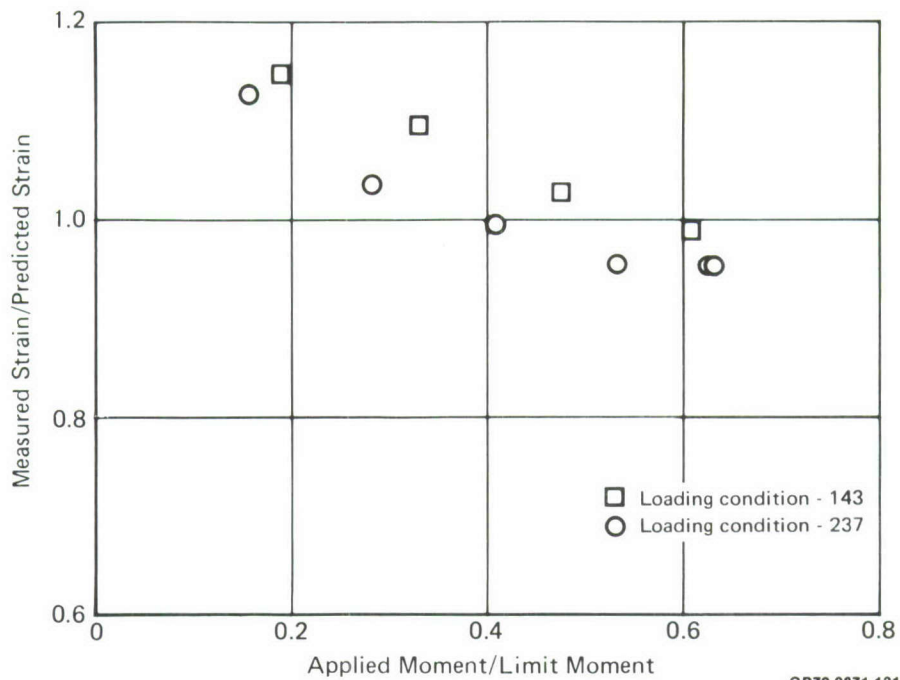
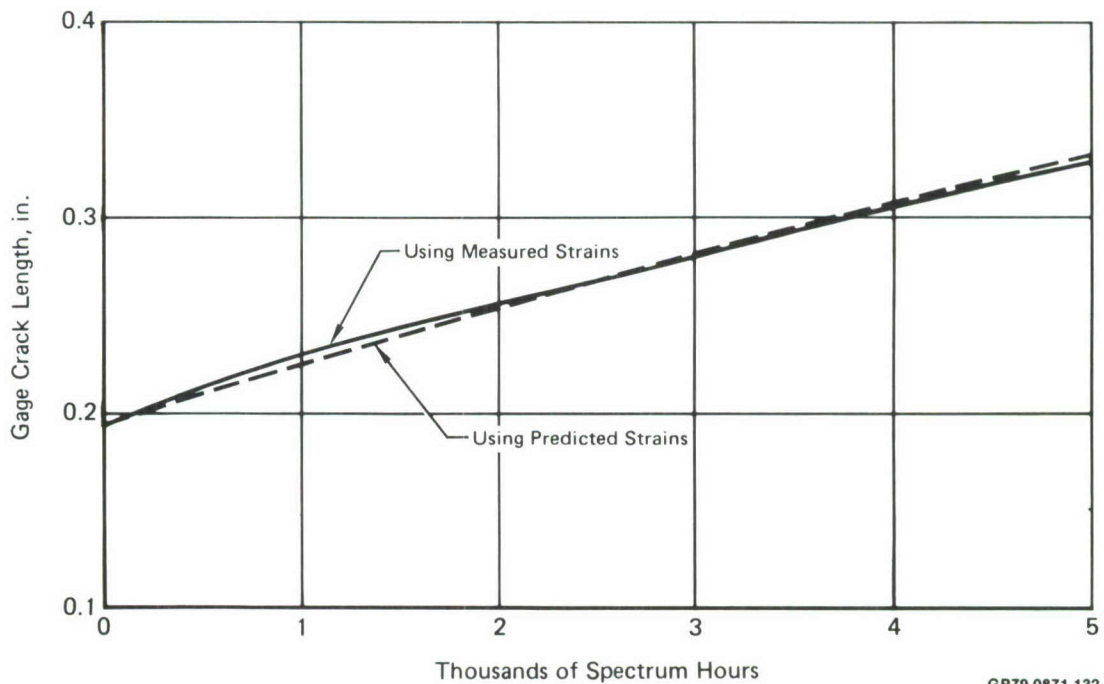


Figure 118. Comparison of Measured and Predicted Wing Skin Strain at BL 100



GP79-0871-131

Figure 119. Comparison of Measured and Predicted Strains in Wing Skin at BL 132.5



GP79-0871-132

Figure 120. Comparison of Predicted Gage Crack Lengths Using Predicted and Measured Strains

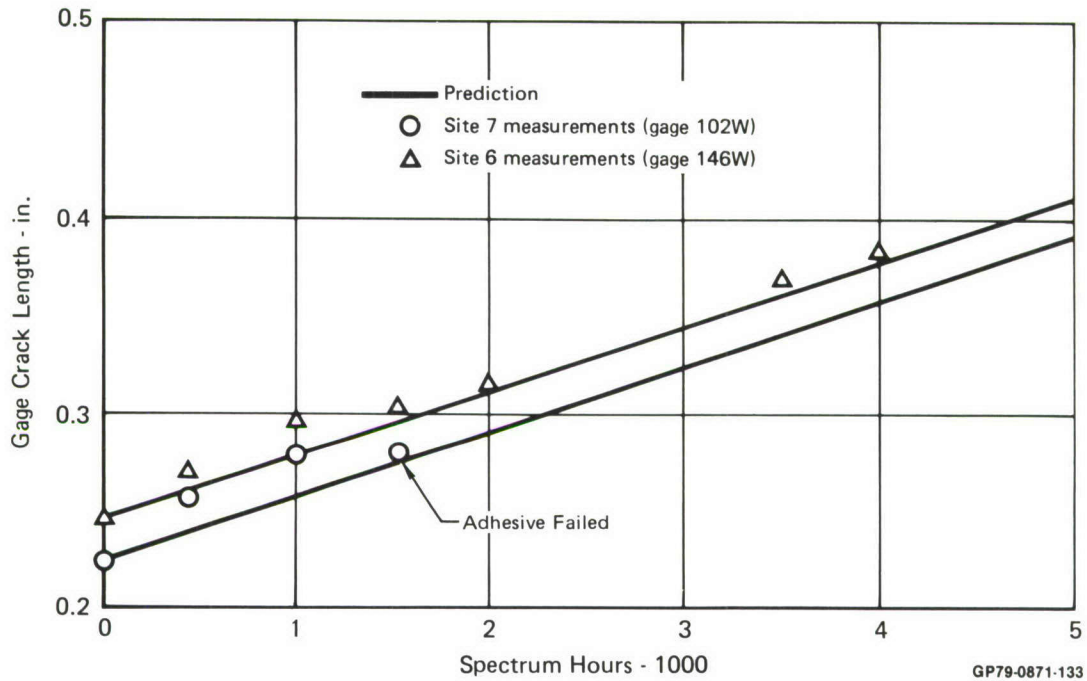


Figure 121. Comparison of Crack Length Measurements and Predictions for Sites 6 and 7

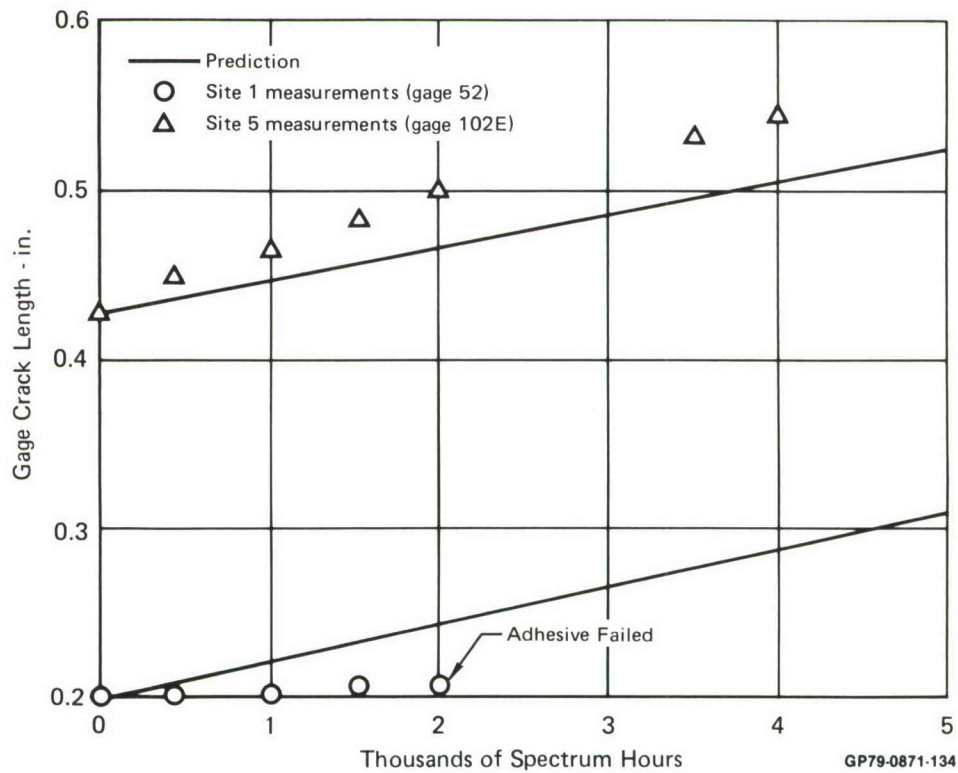


Figure 122. Comparison of Crack Length Measurements and Predictions for Sites 1 and 5

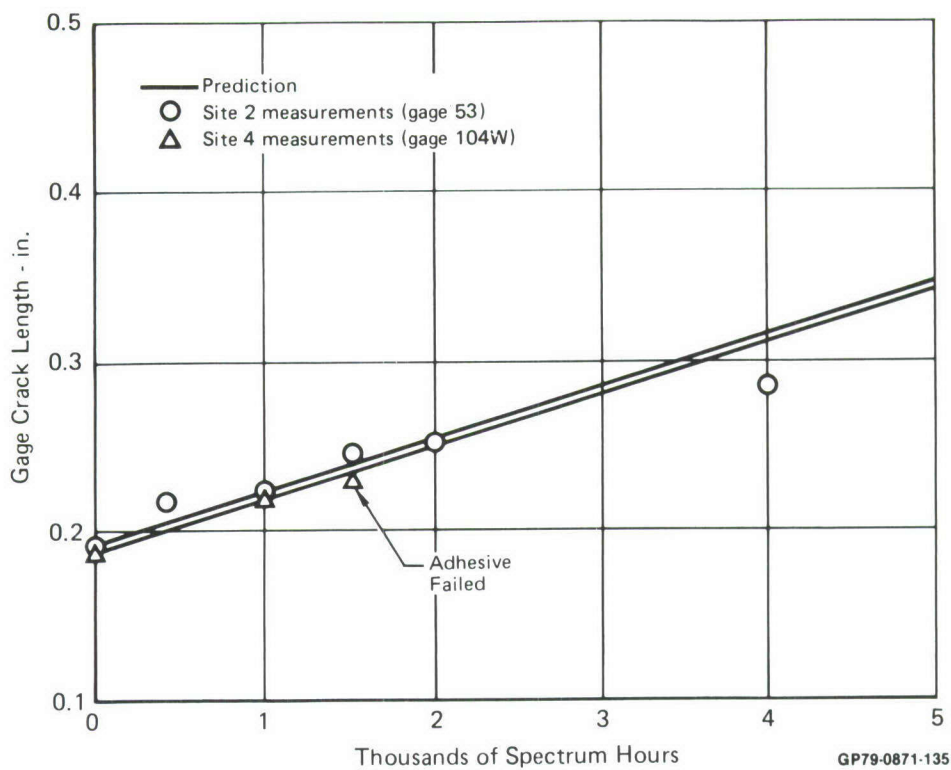


Figure 123. Comparison of Crack Length Measurements and Predictions for Sites 2 and 4

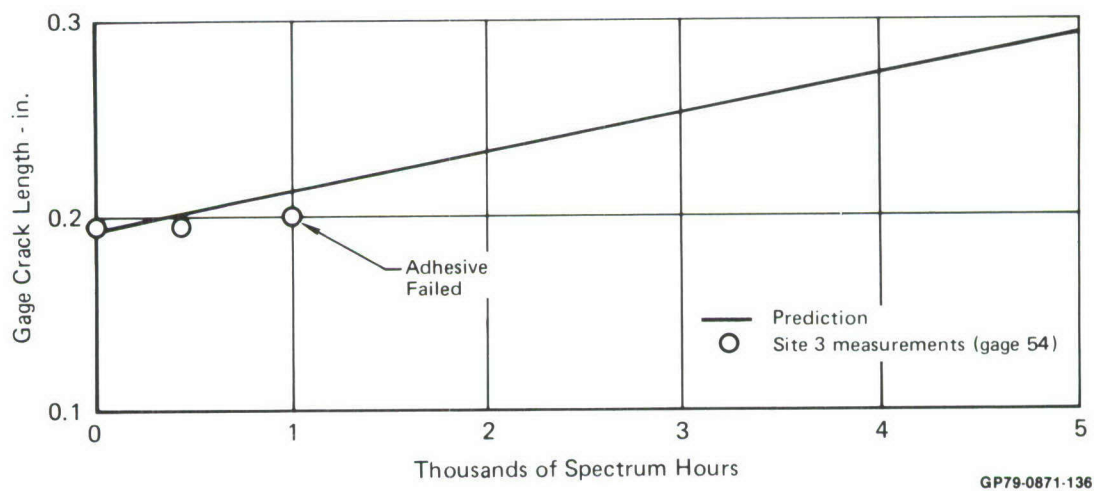


Figure 124. Comparison of Crack Length Measurements and Predictions for Site 3

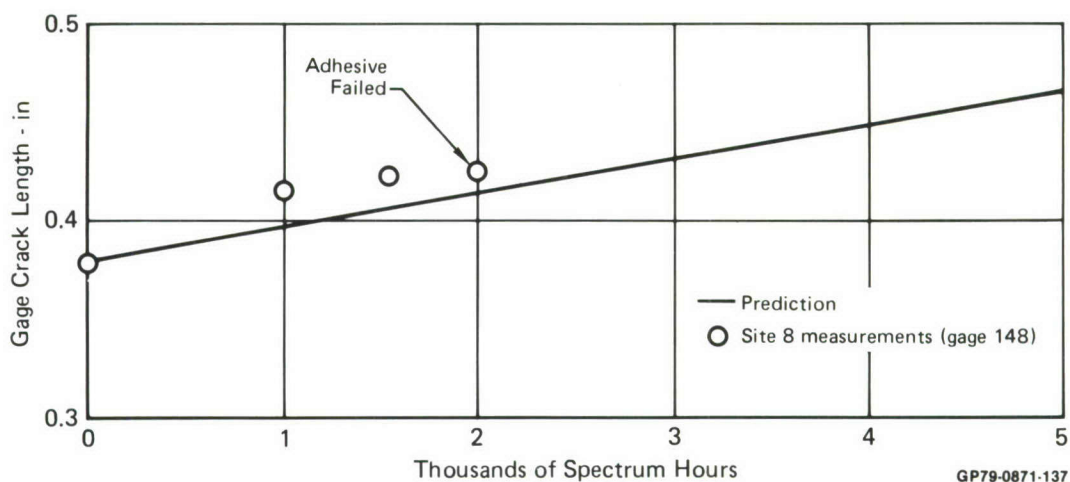


Figure 125. Comparison of Crack Length Measurements and Predictions for Site 8

caused by the initial stress intensity factors for gages mounted on the test article being greater than those used during pre-cracking. If this acceleration is due to the relationship between precracking stress intensities levels and service induced levels, initial gage crack growth behavior may be difficult to predict. The slow growth in gage 52 (Figure 122) may be due to bond failure. Measurements for the other gages agree well with predictions.

2. CRACK GROWTH GAGE AS USAGE MONITOR - Use of the crack growth gage as an aircraft fatigue life usage monitor is complicated by the fact that the relationship of potential crack growth in the structure to crack growth in the gage varies markedly (Figure 126) for mild variations in usage (Figure 127). The comparison shown herein is based on the assumed presence of an 0.01 inch initial semi-circular corner flaw at a hole. As shown in Figure 128, the variation in relationship occurs even when considering small flaws at the hole.

A procedure was developed to account for the variation in structure/gage flaw growth relationship based on predictions of crack growth in the gage (Figure 129) and in the structure (Figure 130) for a baseline spectrum under several limit stress levels. Measured gage crack length can be used to estimate potential crack growth from a hole as shown in Figure 131.

As an example of this technique for service life monitoring using the crack growth gage, five variations of the F-4 wing BL 44/LRS 70 load spectrum were considered: baseline, mild, and severe variations used in the earlier evaluations - the baseline with the maximum load per 1000 hours increased to 125 percent of limit and the baseline clipped at 80 percent of limit load (Figure 132). The latter spectrum variations were among the most severe of those reported in Reference 21.

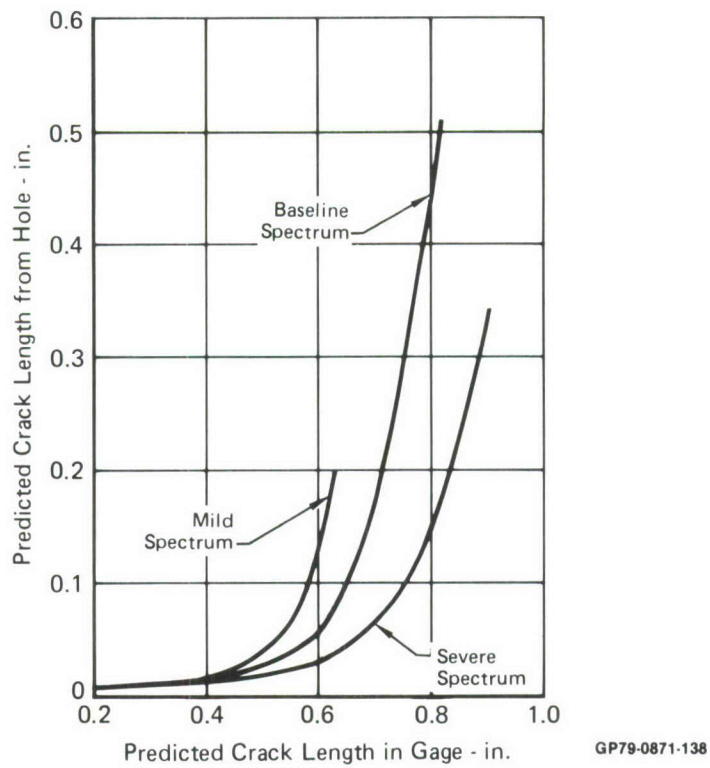


Figure 126. Relationship of Potential Crack Growth in Structure to Gage Crack Growth Varies with Aircraft Usage

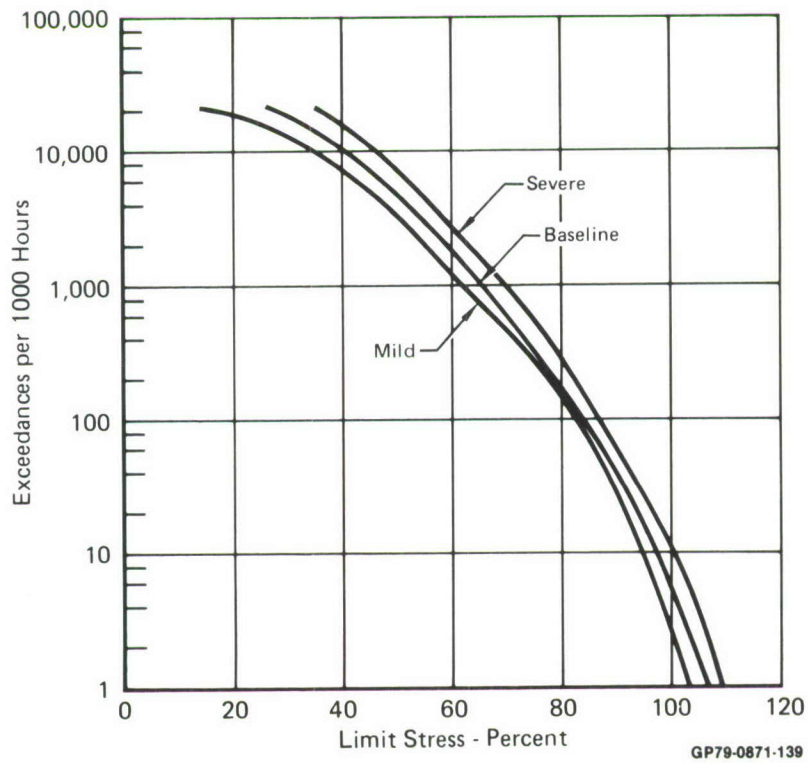


Figure 127. Usage Variations Examined

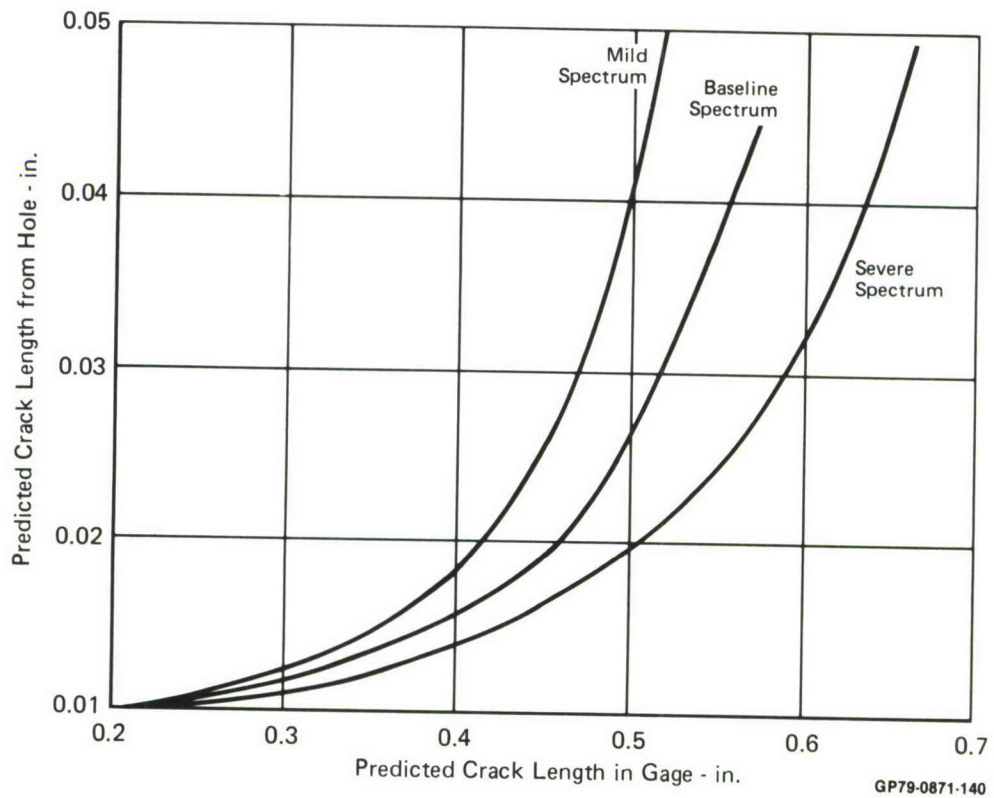


Figure 128. Variation of Structure/Gage Flaw Growth Relationship for Small Flaw Growing from Hole

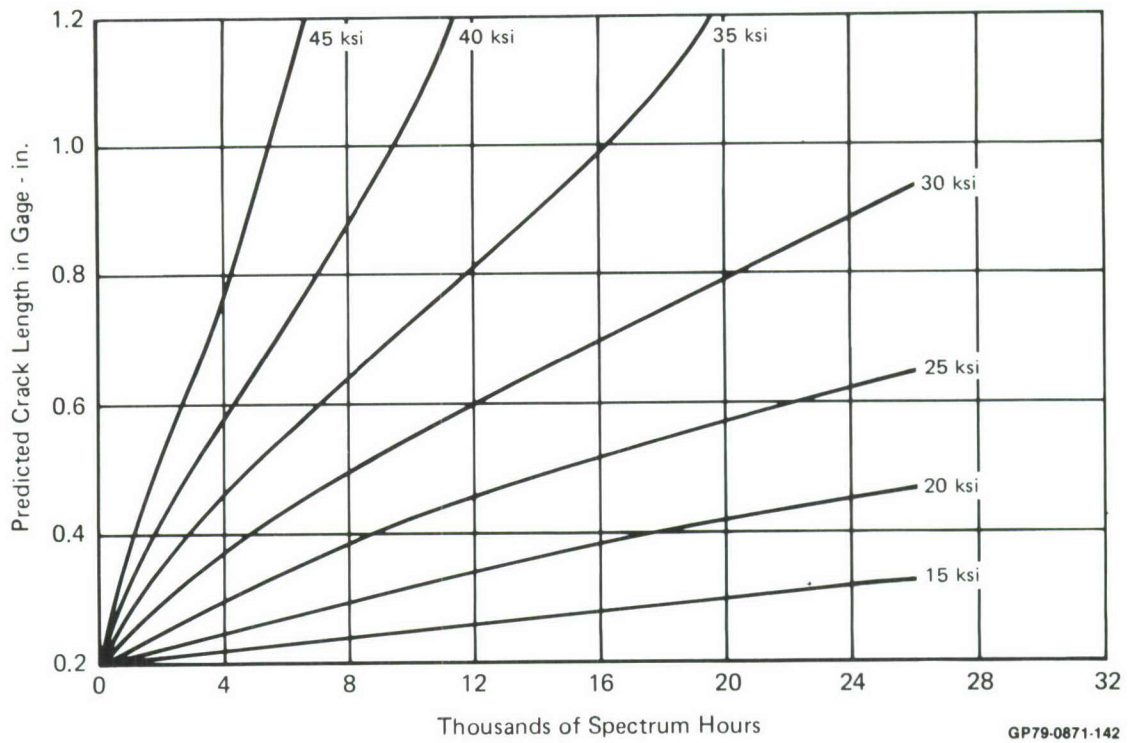


Figure 129. Predicted Gage Crack Growth for Several Stress Levels - Baseline Spectrum

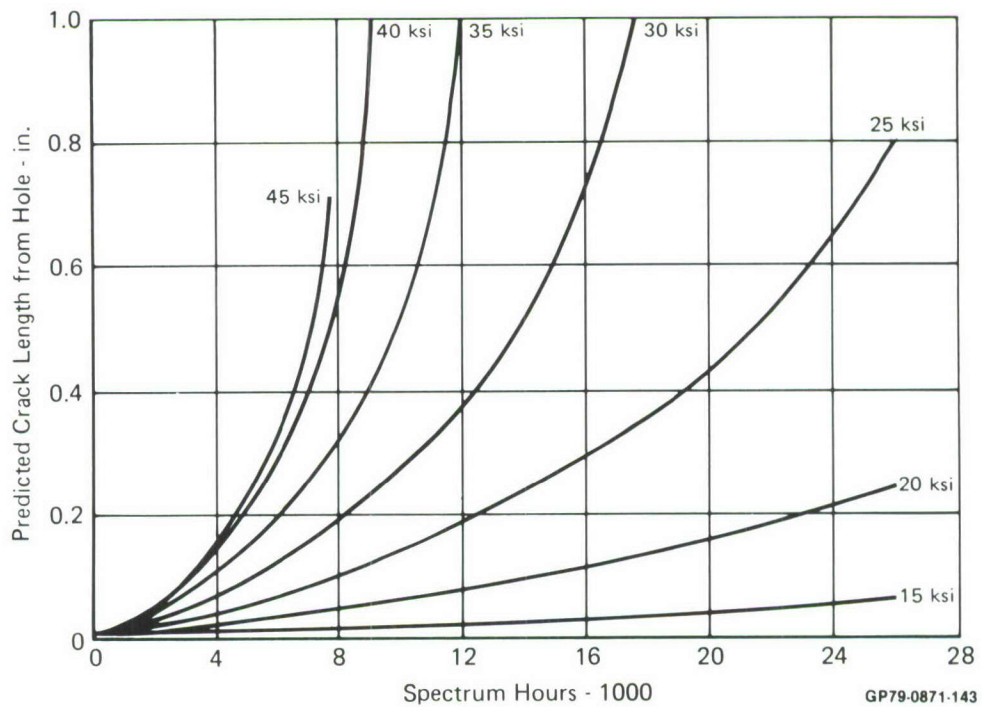


Figure 130. Crack Growth from Hole for Several Stress Levels - Baseline Spectrum

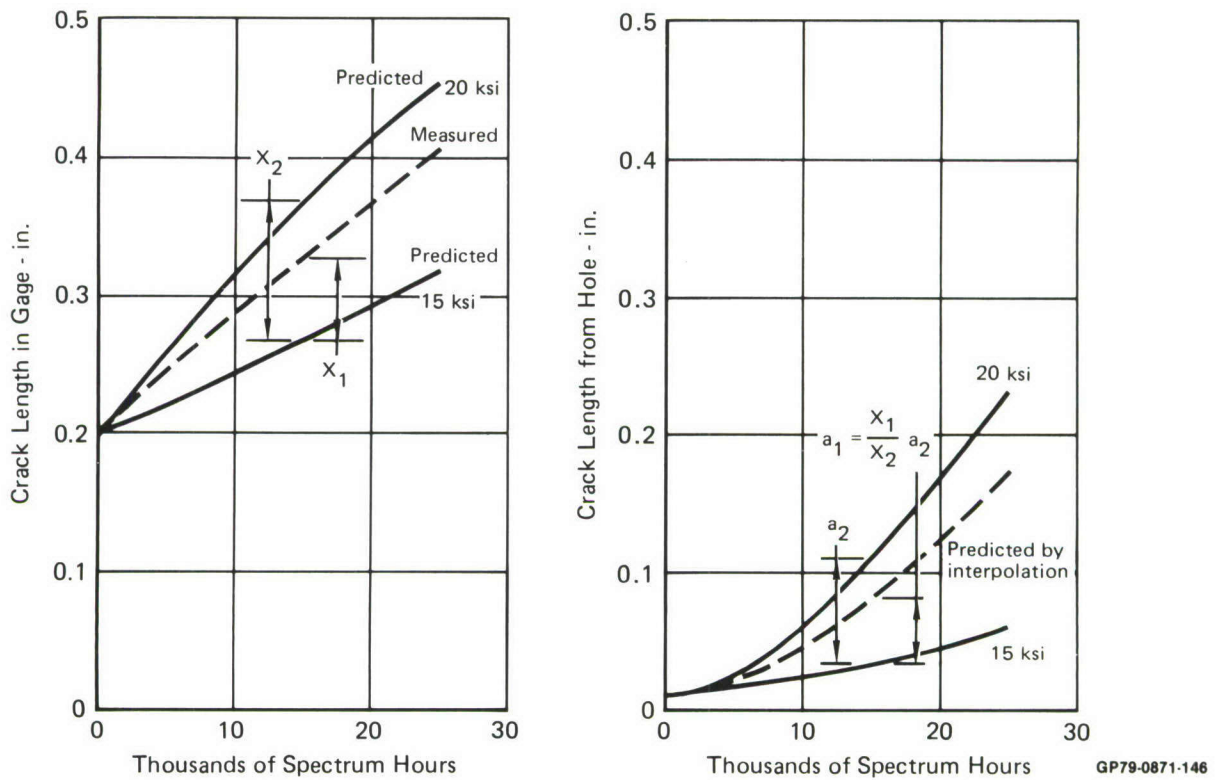


Figure 131. Crack Growth from Hole Prediction Interpolated from Gage Crack Growth

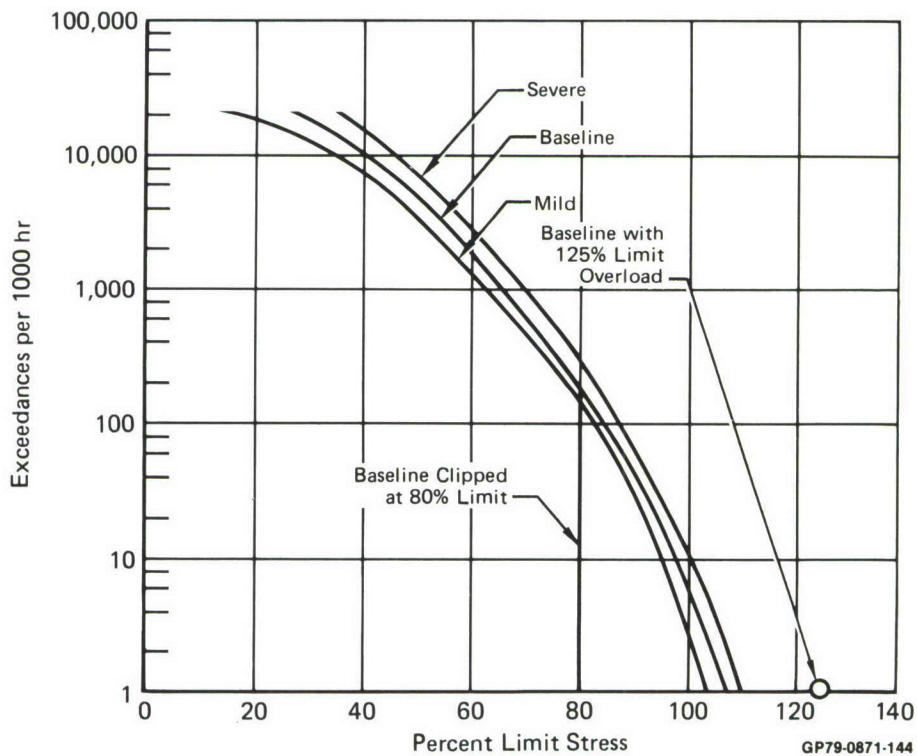


Figure 132. Spectrum Variations Examined

Gage crack growth predictions for these spectrum variations are compared in Figure 133 with predictions of gage crack growth under the baseline spectrum at various stress levels. Potential crack growth from the hole was estimated as shown in Figure 131. Predictions of potential crack growth from a hole for each of the spectrum variations are shown in Figure 134. The predictions based on gage analyses were compared with straightforward crack growth predictions using the Contact Stress model (Figure 135). Comparison of the two predictions is reasonably good and indicates that such gage crack growth interpretations will be consistent with the trends, at least, of potential crack growth in the structure.

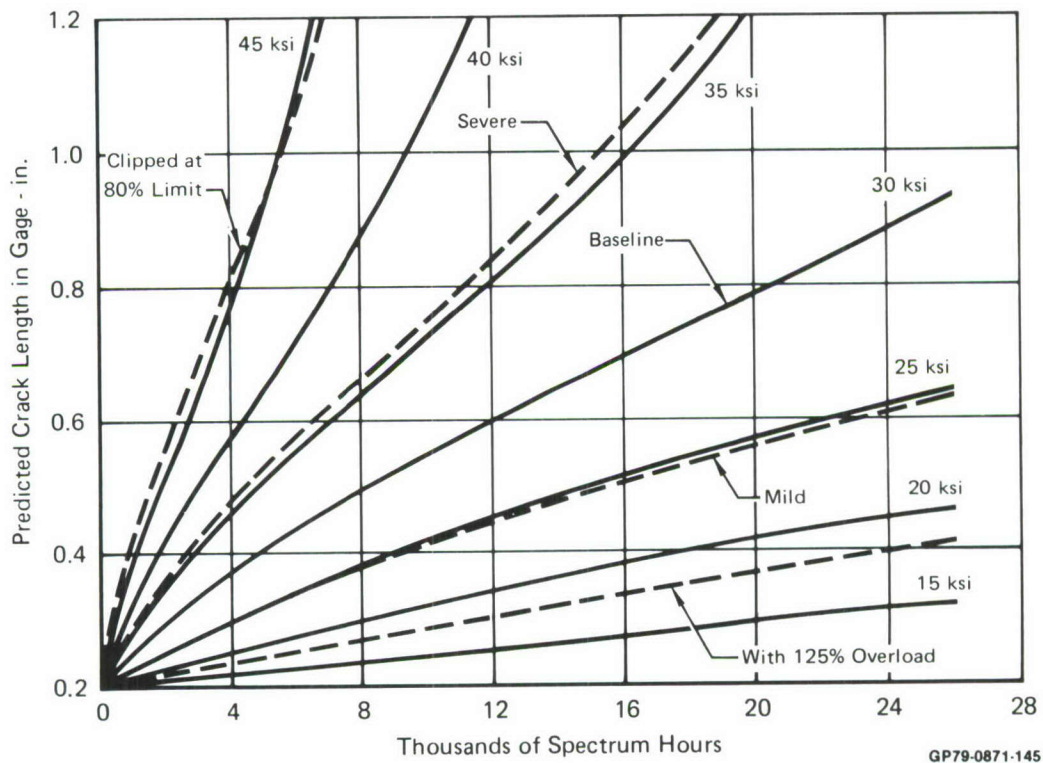


Figure 133. Predicted Crack Growth in Gage for Several Spectrum Variations

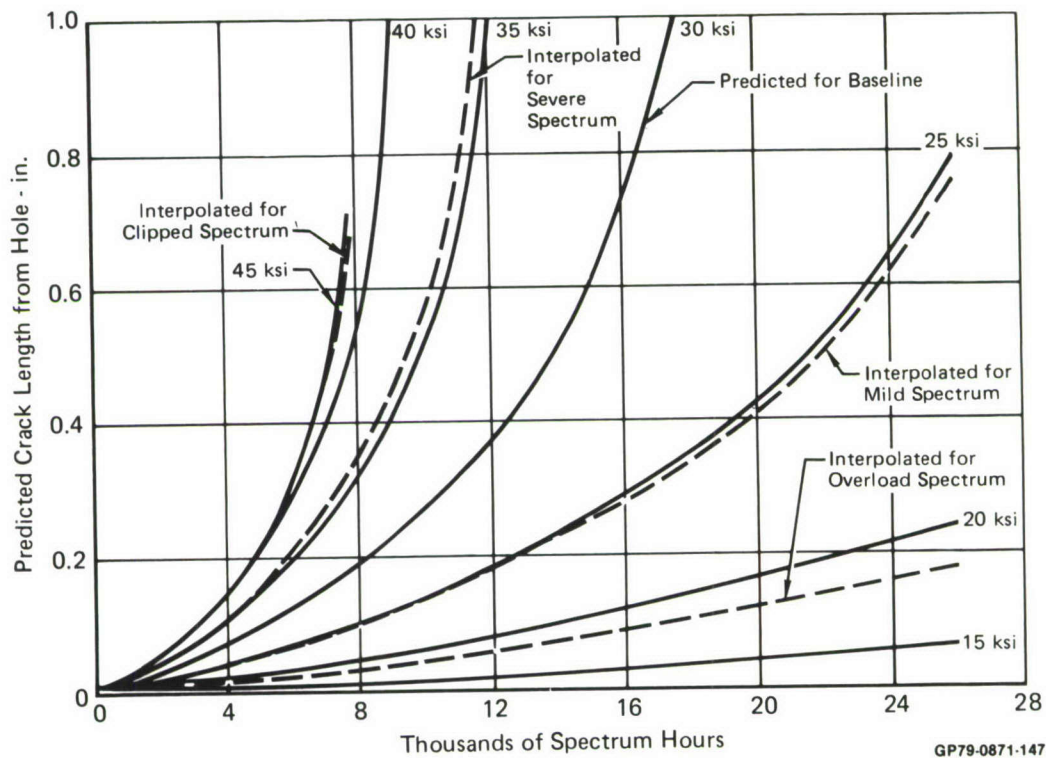


Figure 134. Predicted Crack Growth from Hole for Several Spectrum Variations

The comparison of predictions shown in Figure 135 is the only available measure of the ability of the gage to monitor service usage. The comparison must be substantiated by test before acceptance of the gage as a usage monitor. The predictions of crack growth from a hole are based on improved analyses of the test results reported in Reference 21. The predictions of gage response are based on test results for limit stress levels between 26 and 30 ksi and are subject to greater question at limit stress levels that are higher or lower.

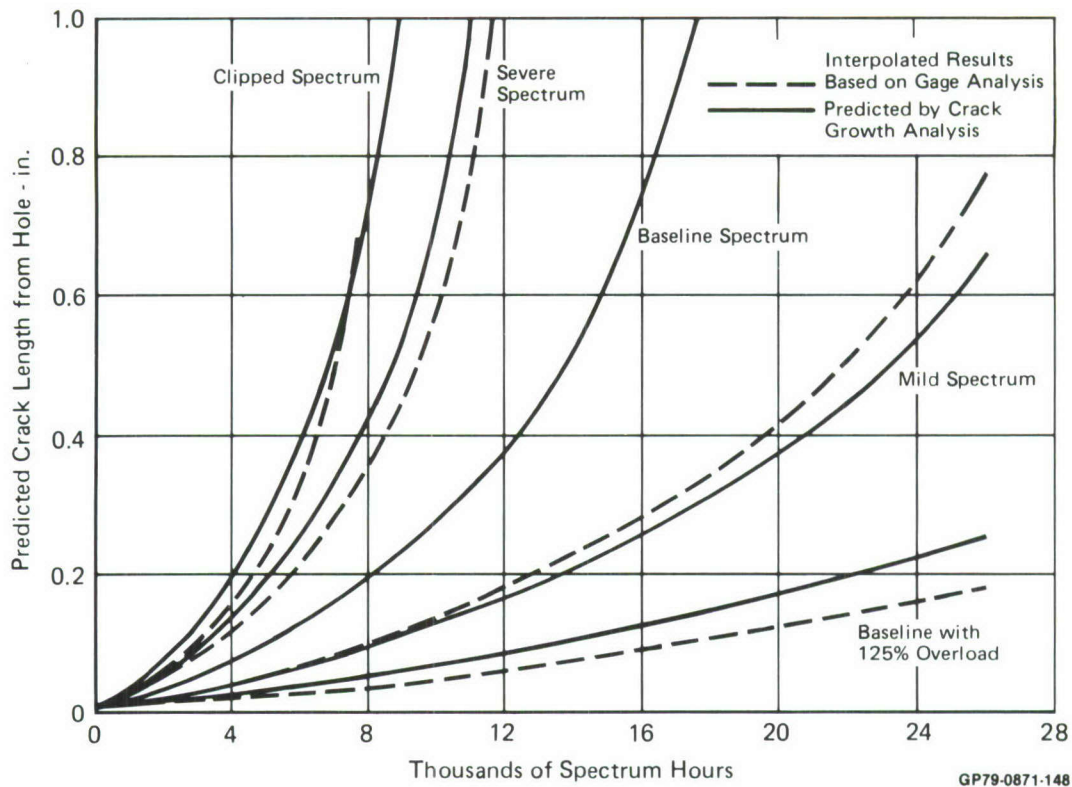


Figure 135. Comparison of Predictions for Crack Growth from Hole for Several Spectra

3. LIMITATIONS OF GAGE DESIGN, ADHESIVE BONDING, AND MANUFACTURING TOLERANCES ON MONITORING POTENTIAL - The effects of sheet thickness on crack growth retardation were found to complicate gage monitoring of potential crack growth in the structure, and reduced the crack growth obtained during the gage service life. Thickness effects could be reduced by increasing gage thickness to about 0.1 inch. However, to achieve the linear crack growth response, the overall gage thickness would be increased to about 0.22 inch. Aerodynamic smoothness requirements may prohibit the use of such a thick gage attached to the outer moldline.

Regardless of gage design, crack growth retardation will differ between gage and structure, unless the gage configuration is identical to that of the critical structural location monitored. Consequently, a technique such as that described in the previous section must be used to interpret gage crack growth and estimate potential structural flaw growth. The procedure must be substantiated by element tests to provide the confidence necessary for fleet management.

Attachment methods are a primary concern in gage development and use as a monitoring device. The attachment method must give adequate load transfer through the service life of the gage. Adhesive bonding, using an elevated temperature cure epoxy adhesive, is still the recommended attachment method although bondings to the test article using FM-73 were not successful due to circumstances peculiar to that application. Therefore, those bondings did not aid in qualifying such adhesives for fleet aircraft. A rigorous test program should be performed to qualify the selected adhesive for use on fleet aircraft.

Manufacturing tolerances were predicted to have little impact on gage response. This was confirmed by the element test program results.

The slow crack growth found in the gage under spectrum loadings requires accurate measurement of growth. The results obtained using the Faxfilm technique (Section 1) demonstrate the adequacy of this technique.

REFERENCES

1. Statement of Work, Appendix "A", Revision 1, Purchase Request FD2020-78-22232, Modification No. F42500-78-D-0014-000201, dated 18 April 1978.
2. Torvik, P.J., "Applications of the External Principles of Elasticity to the Determination of Stress Intensity Factors", AFIT TR-77-3, July 1977.
3. Isida, M., "Effect of Finite Width and Length on Stress Intensity Factors of Internally Cracked Plates Under Various Boundary Conditions", International Journal of Fracture Mechanics, Volume 7, No. 3, September 1971.
4. Rice, J.R., "Stresses in an Infinite Strip Containing a Semi-Infinite Crack" (Discussion to W. G. Krauss, Volume 33, p. 356, 1966) Transactions of the ASME, Series E, Journal of Applied Mechanics, Volume 34, p. 248, 1967.
5. Sih, G.C., Handbook of Stress Intensity Factors, Lehigh University, Bethlehem, Pa. 1973.
6. Dill, H.D., and Saff, C.R., "Spectrum Crack Growth Prediction Method Based on Crack Surface Displacement and Contact Analyses", Fatigue Crack Growth Under Spectrum Loads, ASTM 595, American Society for Testing and Materials, 1976, pp. 306-319.
7. Dill, H.D., and Saff, C.R., "Analysis of Crack Growth Following Compressive Analyses", Cyclic Stress-Strain and Plastic Deformation Aspects of Fatigue Crack Growth, ASTM 637, American Society for Testing and Materials, 1977, pp. 141-152.
8. Dill, H.D., and Saff, C.R., "Improved Methods for Predicting Spectrum Loading Effects", MCAIR MDC A4834, Volume I - Technical Proposal, dated 27 June 1977.
9. Hart-Smith, L.J., "Adhesive-Bonded Scarf and Stepped-Lap Joints", NASA CR 112237, 1973.
10. "Primary Adhesive Bonded Structure Technology (PABST), Phase 1b: Preliminary Design", AFFDL-TR-76-141; Douglas Aircraft Company, 1976.
11. Model F-4B (F4H-1) Thermodynamic and Structural Evaluation of Structural Temperature Data, McDonnell Aircraft Corp. Report 8130, 12 March 1963.
12. MCAIR Report MDC A2883, Vol. I, "F-4 Fatigue and Damage Tolerance Assessment Program", Contract No. AFSC F33657-73-A-0062, dated 28 June 1974.

REFERENCES (Continued)

13. Shih, T.T., and Wei, R.P., "Effect of Specimen Thickness on Delay in Fatigue Crack Growth", Journal of Testing and Evaluation, Vol. 3, No. 1, Jan 1975, pp. 46-47.
14. Mills, W.J., and Hertzberg, R.W., "The Effect of Sheet Thickness of Fatigue Crack Retardation in 2024-T3 Aluminum Alloy", Engineering Fracture Mechanics, Vol. 7, 1975, pp. 705-711.
15. Hartranft, R.J., and Sih, G.C., "An Approximate Three Dimensional Theory of Plates with Application to Crack Problems", International Journal of Engineering Science, Vol. 8, 1970, pp. 711-729.
16. Raju, I.S., and Newman, J.C., Jr., "Three-Dimensional Finite-Element Analysis of Finite-Thickness Fracture Specimens", NASA TN D-8414, May 1977.
17. Elber, Wolf, "Equivalent Constant Amplitude Concept for Crack Growth Under Spectrum Loading", Fatigue Crack Growth Under Spectrum Loads, ASTM STP 595, American Society for Testing and Materials, 1976, pp. 236-250.
18. Fujimoto, W.T., "Determination of Crack Growth and Fracture Toughness Parameters for Surface Flaws Emanating from Fastener Holes", AIAA Report 76-005, May 1976.
19. Hefti, N.B., "Results of Repeated Loads Test for ECP 613 - F-4B Wing Test", MCAIR Report F623, Vol. 2, April 1969.
20. Schaeffer, D.M., "Model F-4C/D Airplane Full Scale Test Loading Spectrum Development, Volume XI, Element Testing", MDC Report A3485, July 1975.
21. Dill, H.D. and Saff, C.R., "Effects of Fighter Attack Spectrum on Crack Growth", AFFDL-TR-76-112, March 1977.